Per Kristian Moe Garnes

Design and Optimization for Additive Manufacturing of Rear Footpeg Bracket

Master's thesis in Mechanical Engineering

Supervisor: Filippo Berto

June 2020

Master's thesis

NTNU
Norwegian University of
Science and Technology

Per Kristian Moe Garnes

Design and Optimization for Additive Manufacturing of Rear Footpeg Bracket

Master's thesis in Mechanical Engineering
Supervisor: Filippo Berto
June 2020

Norwegian University of Science and Technology
Faculty of Engineering
Department of Mechanical and Industrial Engineering

NTNU
Norwegian University of
Science and Technology

Summary

This master thesis is analyzing how topology optimization and additive manufacturing could be used on the Ducati Multistrada 1260's rear footpeg assembly. The main goal was to reduce the weight without compromising the structural integrity and stiffness of the component. The thesis presents the entire design process of the new footpeg bracket, from analyzing the current original equipment manufacturer (OEM) bracket to a final FEM validation of the new design.

The theory chapter of the thesis presents the main topics structural optimization and additive manufacturing with its pros and cons in accordance to the footpeg bracket. A design space was created based on the geometry and constraints of the OEM footpeg assembly given by Ducati. The main load case of 1700N at the footpeg was given by Ducati, and an extra load case of 200N luggage loads was added to ensure structural integrity in the accessory luggage mounts. This is due to these points being removed in the topology optmization without these loads. AlSi10Mg was chosen as the material for the bracket. The software used for the topology optimization was Siemens NX, based on a comparison against Abaqus Tosca and Fusion 360. NX' setup is presented in detail both for the topology optimization and the CAD redesign tools. Weight targets from 550g to 200g were utilized in the topology optimization. The results from the topology optimizations showed that the final component had a potential for weight reduction. Self-supporting constraints regarding print direction were added to the chosen weight target, and the resulting geometry was recreated to a solid in NX.

The first iteration of the final design did not fare well in benchmarking against the OEM component. It had several spots exceeding both yield strength and fatigue strength. The bracket's design was revised based on these results, by adjustment of cross-sections and other geometry. The final design iteration ended up with a weight of **382g**, resulting in a weight reduction of about **30%** to the OEM bracket's 536g. It also performed fine structurally when benchmarking against the OEM bracket, after the final tweaks of the design.

Samandrag

I denne masteroppgåva blir det sett på ein Ducati Multistrada 1260 sine bakre fotstøttar, og korleis desse kan bli optimalisert med bruk av topologioptimalisering og additiv tilverking. Hovudmålet var å redusere vekt utan at det gjekk utover den strukturelle stivleiken til komponenten. Oppgåva presenterar utviklingsprosessen frå analysering av det nåværeande fotstøtte oppsettet, til endeleg FEM validifisering av det nye designet.

Teori kapittelet tar for seg hovudtemaa strukturelloptimalisering og additiv tilverking, med deira fordelar og ulemper relatert til fotstøtte oppsettet. Eit design domene blei konstruert, basert på geometrien og innfestningane til det originale fotstøtte oppsettet gitt av Ducati. Hovudlasttilfellet på 1700N på fotstøtta gitt av Ducati blei kombinert med eit ekstra lasttilfelle, beståande av 200N laster i dei ekstra innfestningane til bagasje. Dette var for å forsikre at desse områda hadde tilstrekkeleg geometri, sida dei ville blitt fjerna av topologioptimaliseringa utan desse lastane. Programvara Siemens NX blei brukt til topologioptimaliseringa, basert på ei samanlikning med Fusion 360 og Abaqus Tosca. Oppsettet i NX er presentert i detalj for både topologioptimaliseringa og konstruksjonen av CAD solid model. Topologioptimaliseringa brukte vektmål frå 550g til 200g. Resultata som kom ut av dette var at den endelege komponenten har eit potensiale for vektreduksjon. Det endelge vektmålet blei bestemt å vere 350g, og blei køyrd med ein overhengsvinkel begrensing i forhold til printeretning. Ein solid model blei konstruert i NX, basert på resultata.

Den første iterasjonen av det endelege designet klarte seg dårleg i samanlikning med den originale braketten i FEM analyse. Den hadde fleire områdar som kryssa både flytegrensa og utmattingsgrensa. Braketten sitt design blei gått over basert på desse resultata, der geometrien blei endra med blant anna endring av diverse tverrsnitt for å redusere spenningane. Det endelge designet har ei vekt på **382g**, som er **30%** lågare enn original delen sin vekt på 536g. Den yter også tilstrekkeleg styrkemessig i forhold til original delen etter desse geometriske endringane.
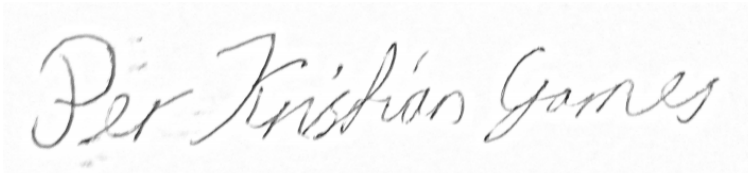
Preface

This master thesis has been written at The Department of Mechanical Engineering (MTP) at NTNU during spring 2020, as an answer to the course *TMM4960 - Engineering Design and Materials, Master's Thesis*. It is based on the preliminary work done in the pre-master specialization project with the same name from Autumn 2019. The project has been carried out with Prof. Filippo Berto as supervisor, and Prof. Terje Rølvåg as a co-supervisor. I want to thank for their guidance on this project.

The thesis is aiming to identify potential performance gains in a Ducati Multistrada 1260's rear footpeg assembly by the use of topology optimization and additive manufacturing. The task were provided by Bagnoli Leonardo, Head of Vehicle Simulation Dept. Ducati Motor Holding. A part of the task is investigating software used for topology optimization and the different settings that can be utilized. The next is utilizing the software on the rear footpeg bracket, and compare the results to the OEM bracket for evaluating potential performance gains. Personal motivation for the project is firstly a big interest in motorcycles in general, but also being able to learn more about topology optimization and additive manufacturing, and how they are used in the industry.

I would also like to thank the other two who are writing master's thesis on Ducati parts at NTNU this semester, Adrian Golten Eikevik and Kjetil Toft Ødegård, for collaboration and insightful discussions during the project.

Disclaimer: The Covid-19 pandemic outbreak happened during this thesis. Most of the thesis have therefore been carried out from a home office situation, which had its limitations.

Per Kristian Garnes
Trondheim, 09.06.20

Table of Contents

List of Tables

List of Figures

Abbreviations

AM	=	Additive Manufacturing
CAD	=	Computer Aided Design
CB	=	Condition-Based
CG	=	Center of Gravity
DfA	=	Design for Assembly
DfAM	=	Design for Additive Manufacturing
DfM	=	Design for Manufacturing
DfX	=	Design for X
DMLS	=	Direct Metal Laser Sintering
EBM	=	Electron Beam Melting
FDM	=	Fused Deposition Modelling
FE	=	Finite Element
FEM	=	Finite Element Model
FEA	=	Finite Element Analysis
LC	=	Load Cases
LENS	=	Laser Engineered Net Shaping
LMD	=	Laser Metal Deposition
MTP	=	The Department of Mechanical Engineering
OEM	=	Original Equipment Manufacturer
PBF	=	Powder Bed Fusion
RPM	=	Revolutions Per Minute
SB	=	Sensitivity-Based
SIMP	=	Solid Isotropic Material with Penalization
SLM	=	Selective Laser Melting
SLS	=	Selective Laser Sintering
STL	=	Stereolitography
TO	=	Topology Optimization
UTS	=	Ultimate Tensile Strength

Chapter 1

Introduction

1.1 Background and motivation

Ducati wants to create a concept for a high-performance electric racing bike. To do this they started an activity to bring some electrical vehicle knowledge in-house. The bike should be a concept bike to avoid problems related to processes and regulations around homologation for road bikes. It is also needed to build up a new internal unit and develop partnerships with universities and suppliers to support and follow the company on the challenge. One of the tasks sent out as a part of this was chosen for this project, and that is the task of finding an optimal shape for the rear footpegs suitable for additive manufacturing. The bike chosen for the project by the group of students writing projects for Ducati at NTNU, in collaboration with co-supervisor Terje Rølvåg, is the Ducati Multistrada 1260, shown in Figure 1.1.

Figure 1.1: 2020 model Ducati Multistrada 1260, Pikes Peak edition [Eker-Performance (2019)]

1.2 Problem description and objectives

A big part of high-performance bikes, both electric and combustion engine powered, is to have as low weight as possible without compromising stiffness and structural integrity. There might be an opportunity to achieve this, due to improvements in production technologies. The focus of this project will therefore be to see how topology optimization coupled up with additive manufacturing could improve the rear footpeg asembly and its production. The current footpeg assembly will be used as a base, mainly focusing on the footpeg bracket. By utilizing additive manufacturing, it is also necessary to look into how the part is going to be produced, and what advantages and limitations one can get with additive manufacturing.

The following objectives were given by co-supervisor Terje Rølvåg:

1. Evaluate and select tools and methods for topology optimization, e.g. weight reduction without compromising the strength requirements.

2. Identify load cases, constraints, weight and stiffness targets for the footpegs.

3. Study the selected software tool and methods for footpeg optimization based on outputs from task 1 and 2.

4. Optimize the footpegs and benchmark the new design versus the original equipment manufacturer (OEM) design.

5. Reverse engineer the optimized design solution (create a CAD model).

6. Mesh and evaluate the structural performance of the final CAD design.

7. If time and money permits: Manufacture the new footpegs

1.3 Summary of pre-master project report

A pre-master project with the same name was done Autumn 2019 as preliminary work for this master thesis. This thesis is a continuation of that project report, hence several sections of the main theory part are identical. The pre-master project focused mainly on acquiring general knowledge about how topology optimization and additive manufacturing could be utilized to improve the rear footpeg brackets compared to traditional manufacturing methods.

The pieces of software that were utilized in the pre-master was Autodesk Inventor for creating the design space and it was also planned to be utilized for reverse engineering a final CAD design of the part. For the topology optimization task Abaqus Tosca was chosen and tested. This worked rather smoothly until the project met a wall at objective five from the previously mentioned task list. The outputted STL file from the optimization was not the easiest model to continue working on. The result of this was to reevaluate the task list, resulting in only objective one to four being the focus area of the pre-master. The last design iteration from last semester is shown in Figure 1.2.
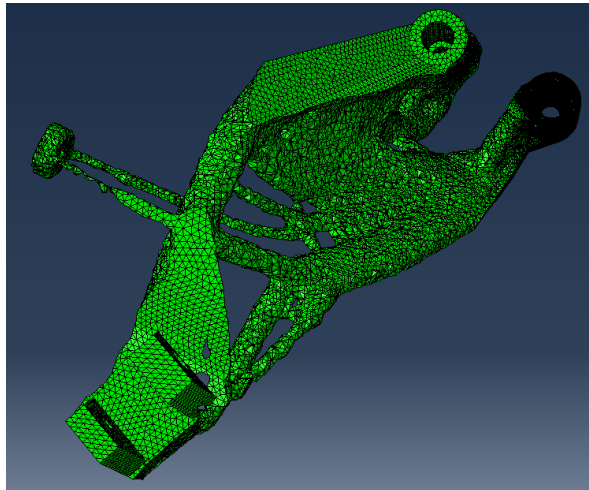
(a) The results directly from the TO task in Tosca.
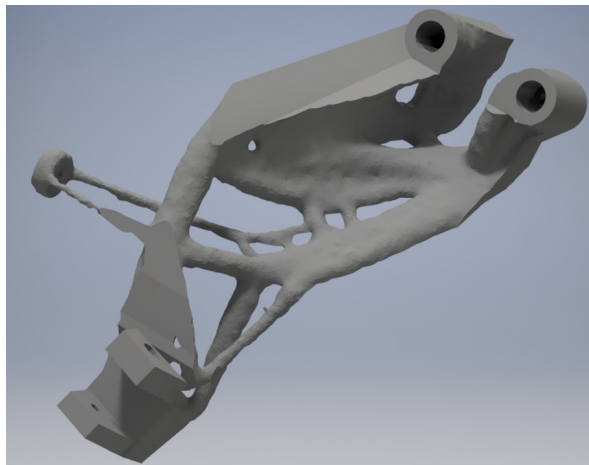
(b) Final STL export from Abaqus Tosca in the pre-master project.

Figure 1.2: The final results from the pre-master project.

Based on these results it was decided to start the master thesis at objective one again, and do a more thorough evaluation of topology optimization tools. The first step was therefore to compare the experiences from Abaqus Tosca last semester with new tools. The chosen ones to look deeper into were Siemens NX' topology optimization for designers and Autodesk Fusion 360's generative design features, as these had potential solutions to the problems that were met in the pre-master. This comparison will be done in Chapter 3.

Chapter 2

Theory and Literature Review

In this chapter theory and literature reviews are presented on the different topics at hand. At first the main ones, topology optimization and additive manufacturing, then some info regarding design methodologies for the project, the current footpeg assembly and motorcycle regulations in the later sections.

2.1 Structural Optimization

2.1.1 Topology optimization

Topology optimization is the method of trying to find an optimal lay-out of the geometry of a part within a given space. The given space is typically defined as a design space, which consists of the area where the part can exist without interfering with any other parts or functions. Known variables can be loads, connections, the volume of the space and potential voids. The voids are for example places where the part would interfere with other structure or cable channels. The geometrical shape of the final component is unknown. [Bendsoe (2004)]

Christensen (2009) used a function and two variables to describe topology optimization analytically, these goes as follows:

- Objective function (f): This function classifies the different designs, and f is a number used to describe how good the design is. Typically one looks at minimization problems, which means that the smaller the f, the better it is. An example would be weight reduction, where f then would be the weight.

- Design variable (x): This is the variables of the design space, which describes the merits of the design. It can also be a variable that changes throughout the process. Examples could be the geometry limitations or the choice of materials.

- State Variable (*y*): This is the response of the structure that is being optimized, which means that for a given design *x*, one can expect to get a response *y*. Examples of different responses is the values of stress, strain and displacement.

These three are combined with the equilibrium constraint, consisting of the stiffness matrix **K**, the displacement vector **u** and the force vector **F**, shown in Equation 2.1. This creates a formulation of the topology optimization, as shown in Equation 2.2 [Christensen (2009)]:

$$\mathbf{K}(x)\mathbf{u} = \mathbf{F}(x) \tag{2.1}$$

$$\mathbb{TO} = \begin{cases} \text{minimize } f(x,y) \text{ with respect to } x \text{ and } y \\ \text{subject to } \begin{cases} \text{behavioral constraints on } y \\ \text{design constraints on } x \\ \text{equilibrium constraint} \end{cases} \end{cases} \tag{2.2}$$

In Equation 2.2 the function *f* and the variables *x* and *y* are the same as those described in the analytical approach, meaning the behavioral constraints are based on the state variable, the design constraints are based on the design variable and *f* being the objective function.

One could also set up an optimization with multiple objective functions, as shown in Equation 2.3 where n is the number of objective functions [Christensen (2009)]:

$$\text{minimize } (f_1(x,y),\ f_2(x.y),\ ...,\ f_n(x,y)) \tag{2.3}$$

The different objective functions might not be minimized based on the same x and y. Instead one could find the design solution that is meeting all the objective functions better than no other for given x and y, called a Pareto optimal. To obtain a Pareto optimal one can use weight factors, w, to each of the objective functions [Christensen (2009)]. This means that different weighting of the different objective functions will give different Pareto optimal solutions. As this weighting can be a difficult task, a single-term objective function is widely used. An example could be to instead of trying to optimize for both stiffness and weight at the same time, one is optimizing for one of them based on specific targets of the other one. This could be to minimize strain energy (U), shown in Equation 2.4, in combination with specific weight targets below the original weight. The results from the optimization can then show how the strain energy is minimized, as the different weight targets are met.

$$U = \frac{1}{2}V\sigma\epsilon \tag{2.4}$$

2.1.2 Minimum Compliance Optimization

Minimum compliance is one of the most used optimization methods, and it is based on the inverse of the stiffness matrix ($\mathbb{K}^{-1}$). Minimizing compliance is in other words maximizing global stiffness [Bendsoe (2004)]. A method commonly used here is the solid isotropic

material with penalization (SIMP) model. SIMP is a density-based interpolation model, used in combination with a penalization factor, to make a clearer difference between what should be material and voids [Huang and Xie (2010)].

2.1.3 Other Types of Structural Optimization

Topology optimization is one of the three main types of structural optimization, together with sizing optimization and shape optimization [Christensen (2009)]. Sizing optimization is when the actual size, for example structural thickness or cross-sectional areas, are defined as the design variable x. Shape optimization is when the design variable x is defined as being the shape or form of the part. An example can be to define some of the shape to cope with machining constraints, compared to if the part were created freely of these constraints. It is also a subclass of topology optimization on paper, but the way they are implemented in practice makes them treated like two separate methods. A comparison of the three structural optimization methods is shown in Figure 2.1. This project will focus mainly on topology optimization.
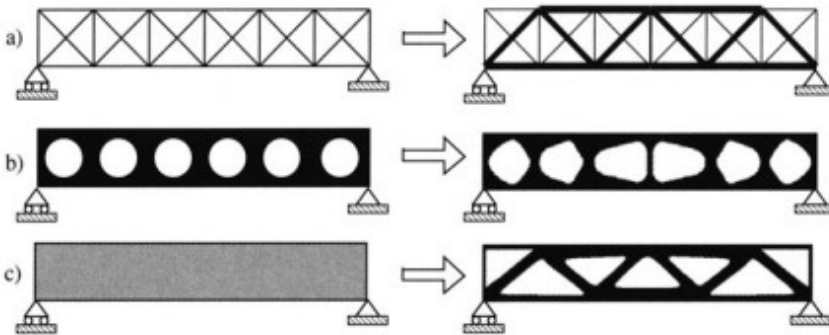
Figure 2.1: Comparison of topology optimization methods: a) Sizing optimization of struss structure, b) Shape optimization of structure with holes, c) Topology optimization of a rectangular beam. [Bendsoe (2004)]

2.1.4 Generative Design

Generative design is a process using algorithms to get several different design proposals compared to with a more traditional process [McKnight (2017)]. The main thing with generative design is to try to create designs similar to the evolution processes that exists in nature. Several criteria and goals for the study are set. The study then iterates through several design proposals, while trying to optimize towards convergence for the proposed goals. This is similar to what is done in topology optimization, which in itself is one of the tools that can be used in a generative design study.

According to McKnight (2017), one would typically divide a generative design process into 4 steps:

1. The input parameter and goal stage where the study's optimization criteria is applied. This could for example be properties such as mass and strength, or external cases such as loads and constraints. Defining a volume/design space could also be an option, but it is not always needed. Typical goals could be weight or stiffness targets.

2. The generative design study calculates design proposals and performance analysis by the use of its algorithms and goals. For more complex studies cloud computing is often utilized.

3. The results are presented to the user, which then has to examine them to find the optimal of the proposed solutions. This could be done by the use of filters sorting the solutions after which respective criteria they meet the best.

4. The manufacturing process often end up being additive manufacturing, due to complex results. Generative studies could also be set up to optimize for other manufacturing processes, by limiting the study to create designs within the frame of the proposed manufacturing method.

Typical results to achieve in a product with a generative design study is reduced weight, improved performance, increased creativity and efficiency [McKnight (2017)]. Currently this is mostly used in the aerospace industry, where reduction of a couple of kg's can result in big gains in fuel economy over time.

2.2 Additive manufacturing

Additive manufacturing (AM) is a production technology that has been rapidly evolving over the last years. It is well used in rapid prototyping, and with the market of 3D printers for home use it is increasingly commercially available. The concept is that one can create a part/prototype directly from a CAD file using only the AM machine. This happens through a step wise layer by layer production, where several layers are built on a two dimensional plane (X-Y) after another in the direction of the third dimension (Z). [Bandyopadhyay (2015)]

CAD has made it so that people can iterate on each others designs from all over the world, and with the inclusion of AM can these designs be manufactured and tested as well. The advantages of AM have caught the industry's eyes over traditional methods, but it also has its challenges. A summary of both is shown in Figure 2.2. The main advantages is the design freedom and versatility of creating complex parts, which is a good combination with the organic structures typically created by TO. Another point is the ability to use less material compared to subtractive manufacturing methods like machining. It is also possible to create complete parts, instead of using an assembly of machined parts. The challenges are for example the need to still have post processing and the high cost of the printers. It would be safe to assume that these challenges will most likely be overcome, as printers of higher quality are developed and available at a lower price.
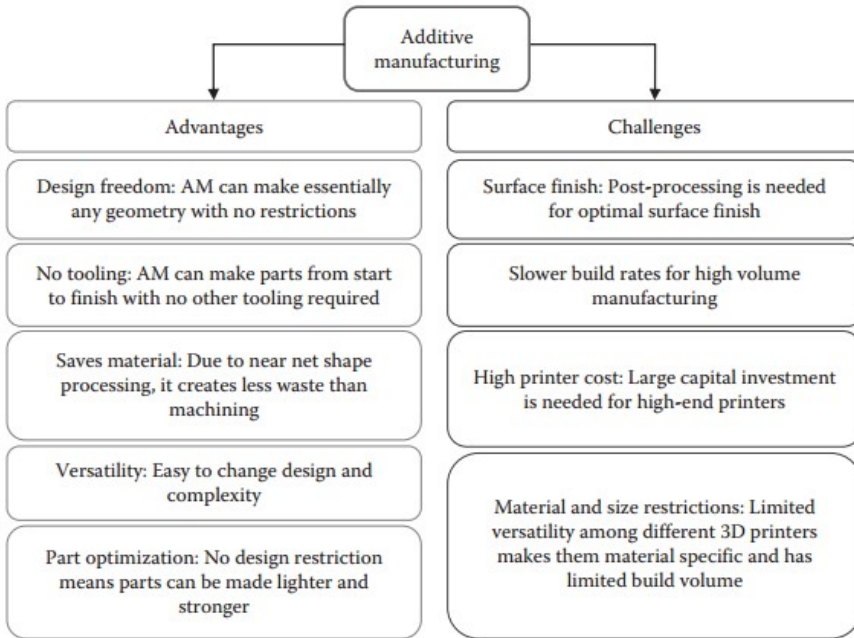
Figure 2.2: Advantages and challenges with AM [Bandyopadhyay (2015)]
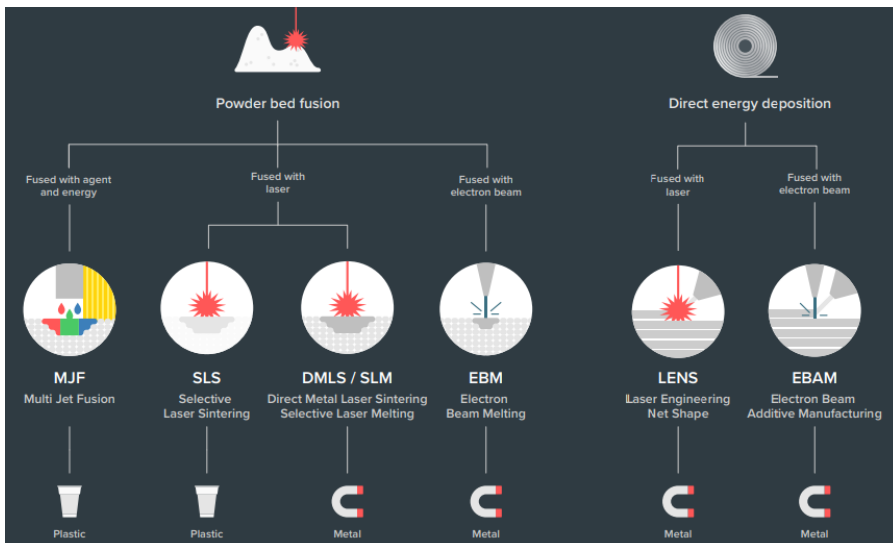
Figure 2.3: Map of the AM categories looked into in this project [Redwood (2019)]

2.2.1 Selective Laser Sintering

Selective Laser Sintering (SLS) was a proposed AM method from Ducati for the project. It is a form of Powder Bed Fusion (PBF), as shown in Figure 2.3. SLS is a method where a CO_2 laser beam is applied to a powder, which in turn is sintered to create a three dimensional part. The chamber in the machine has a heat level close to the melting point of the material used. A given design is used as a guide for the laser to know at which locations it is going to fuse the powder. New layers of powder are distributed over the current layer and then lasered to form the next layer [Bandyopadhyay (2015)]. An example of a way the powder can be distributed is by having the build plate controlled by a piston that moves downwards with the height of a layer after each layer is produced. Afterwards a new layer of powder is added on the top. This method is shown in Figure 2.4.
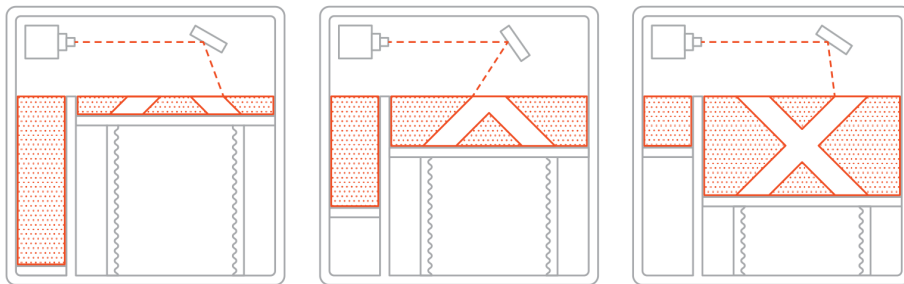
Figure 2.4: The SLS manufacturing method. The red dashed line is the laser and the dotted red areas are the powder [Varotsis (2019)].

According to Wong (2012), the main advantage with SLS is that it offers a great variety of materials and combinations of these. It is also material efficient due to unused powder having a possibility of being reused. Disadvantages of this technique is that accuracy is limited to the size of the powder particle, risk of oxidation from gases in the surrounding atmosphere and the challenge of holding the temperature constant near the melting temperature [Wong (2012)].

2.2.2 Selective Laser Melting

A subcategory of SLS is Selective Laser Melting (SLM). The main difference being, as the name implies, that it fully melts the material instead of sintering it. It is also known as Direct Metal laser Sintering (DMLS) which is a somewhat misleading term, since it does melt and not sinter the metal [Bandyopadhyay (2015)]. In the paper "Review of selective laser melting: materials and applications", Yap et al. (2015) notes that this leads to a part that is denser and stronger than what is acquired with sintering. SLM does have limitations when it comes to use of materials, and it is currently mostly used with metals like steel, titanium and aluminium. It is a high energy demanding process. The temperature from heating each layer up to above its melting point can lead to dislocations and stresses, which

in turn can compromise physical properties [Yap et al. (2015)]. An important advantage to note with this technique is the possibility of building parts that are complex on both the inside and the outside. This includes combining several parts into one, and still keep features such as hinges and joints [Crucible-Design-Ltd (2015)]. This will be followed up in Section 2.2.5 - Design for Additive Manufacturing.

2.2.3 Electron Beam Melting

Electron beam melting (EBM) is also a method of PBF, as shown in Figure 2.3, and it is rather similar to SLM. The main difference being that an electron beam is used to melt the powder instead of a laser. To avoid oxidation the process is typically performed in a high vacuum chamber. This is a process that is seeing rapid growth, but it has not been around for as long as SLM. [Wong (2012)]

2.2.4 Laser Metal Deposition
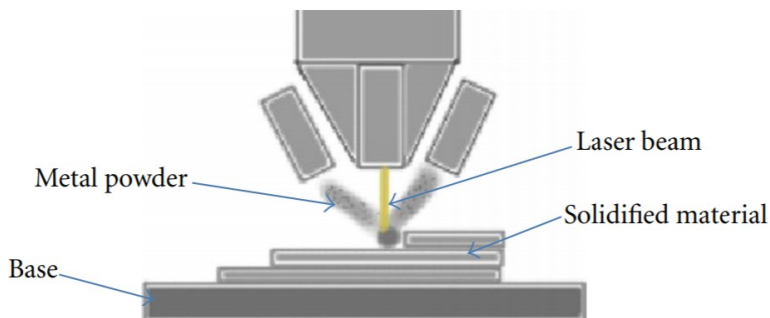
Figure 2.5: Laser metal deposition also known as laser engineered net shaping [Wong (2012)].

A different additive manufacturing process used with metal is laser metal deposition (LMD), also known as laser engineered net shaping (LENS). It is a method of direct energy deposition as shown in Figure 2.3. A laser is used in combination with a nozzle to create the layers that become the material, as shown in Figure 2.5. In the figure we see the metal powder coming out of the nozzles and intersecting with the laser. The metal solidifies on the base plate at the intersection point after being cooled. The advantage of this method is the possibility of using several different metals [Wong (2012), Mahamood (2018)]. By tilting the build plate one can also overcome some of the overhang constraints of more traditional additive manufacturing techniques [TWI-Ltd (2014)].

2.2.5 Design for Additive Manufacturing (DfAM)

Additive manufacturing is a manufacturing method with small limitations when it comes to how complex the design and geometry can be, but some work is needed to connect the topology optimization to the production. [Zegard and Paulino (2016)].

Overhang is one of the main constraints for AM, and a lot of printers typically have a limitation of a minimum angle of 45° [Langelaar (2017)]. This accounts especially for aluminium, but steel and titanium can overcome angles as low as 30° and 20° respectively with DMLS [Crucible-Design-Ltd (2015)]. To overcome this one can use support structures on angles below the minimum limitation, as shown in Figure 2.6. Support structure is a material that will support the product at needed locations under production and then be removed afterwards, hence resulting in it being wasted material. A solution is to create structures with overhang angles that is within the limit of where the structure is self supporting. The angles should still not be too close to the limit, as this can cause rougher surfaces that need machining anyway [Crucible-Design-Ltd (2015)].
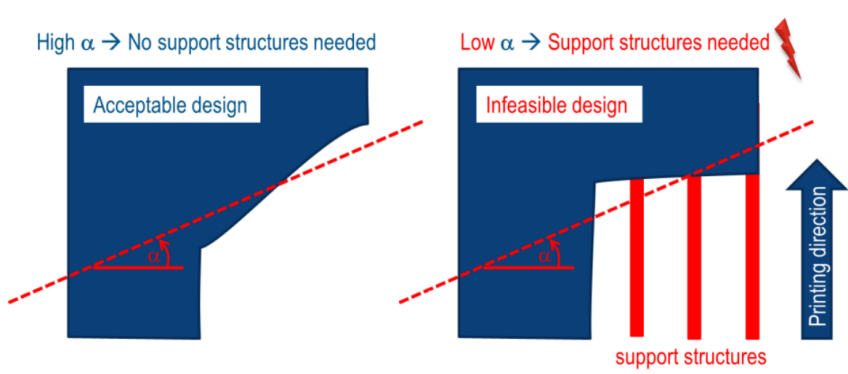
Figure 2.6: Visualization of overhang angle (α) and support structure [Hoffarth et al. (2017)].

Several **filter techniques** for overhang constraints have been implemented into topology optimization processes in recent years, some notable ones by Gaynor and Guest (2016), and by Langelaar (2017). The last one has been implemented into Tosca Structure and further looked into by Hoffarth, Gerzen and Pedersen [Hoffarth et al. (2017)]. This filter is in its current state able to detect overhang angles, and add changes to the optimization to overcome these. However, it might also add support structure and is not a bulletproof feature at this point. It has the possibilities of reducing the amount of support material overall, hence reducing print time. Hoffarth et al. (2017) also notes that one has to choose the printing direction manually, which can be challenging if one does not know the result of an optimization without the filter. Figure 2.7 shows an optimized bike stem with different printing directions assigned, where one can see the change in structure to overcome the different overhang angles.

Crucible-Design-Ltd (2015) mentions in their design guidelines for DMLS that small **holes** can be accommodated for in the AM process. Typical sizes are below 6mm in diameter. Any holes above this size would require to be supported by support structure to avoid collapsing. There is also a potential for rough surfaces on larger circular holes [Crucible-Design-Ltd (2015)].
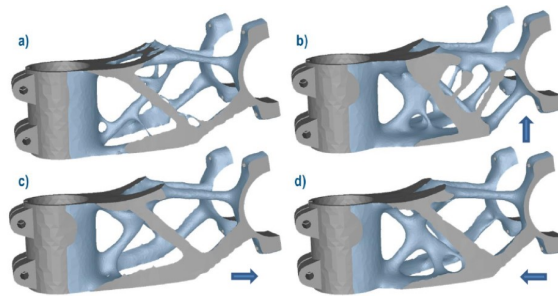
Figure 2.7: An optimized bike stem where a) is without overhang constraint, and b), c) and d) show with overhang constraint of 45° in different print directions shown by the arrows [Hoffarth et al. (2017)].

Hinges can be produced by AM as one component instead of producing several parts and assemble them together [Crucible-Design-Ltd (2015)]. In the book "Understanding Additive Manufacturing: Rapid Prototyping - Rapid Tooling - Rapid Manufacturing", Gebhardt (2012) explains some key points around hinge design for AM. The hinge can be designed as a barrel and rod style design, and be produced already assembled with laser based processes such as sintering. For the hinge to work one would need a certain level of movability in the joint. To achieve this one need to assure that there are enough clearance between the inner diameter of the bore and the outer diameter of the rod. Recommended clearances are, as shown in Figure 2.8, A from 0.3 to 0.5mm and B from 0.5 to 0.6mm. C is the total length of the hinge. Gebhardt (2012) notes that many sources claim one or two free layers is enough, but that one in practice should have at least twice as many to create a functional hinge.
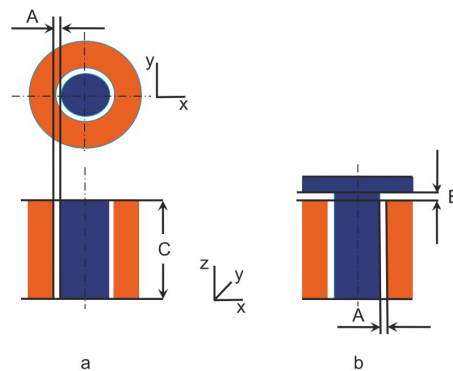
Figure 2.8: Clearings of bores and rods in AM laser process hinge design. *a* shows a regular joint, while *b* shows a bullhead rivet-type joint. [Gebhardt (2012)]

2.2.6 Defects in AM

Surface Roughness is one of the defects in AM, and it can for example come from the staircase effect shown in Figure 2.9 [Lim et al. (2016)]. A triangle of error will be created on the curved surfaces, due to layers being printed stepwise on horizontal planes. These triangles are affected by layer height. Lower layer height results in smaller triangles, but this will increase print time. Surface roughness is also affected by the overhang angles as mentioned in Section 2.2.5. The level of surface roughness is dependent on the AM process used as well, and some typical values for the processes looked into in this project is 7-20 μm for SLM and EBM, and 4-10 μm for LMD [DebRoy et al. (2018)].
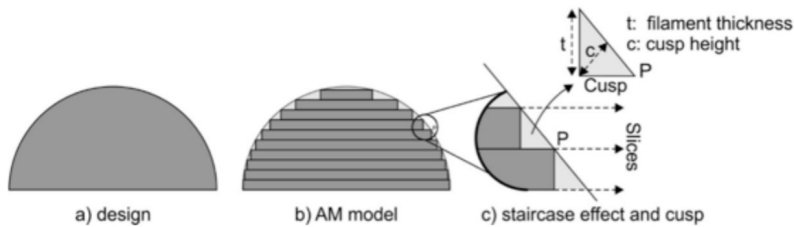
Figure 2.9: Staircase effect in AM, a) shows the original design, b) shows the staircase effect by the layers and c) shows the triangle of error in the effect [Lim et al. (2016)].

Fusion Defects and **Porosity** are defects that are closely related. They can occur from for example gases entrapped in the powder particles, or the layers not melting properly together due to the molten pool depth being too low. These effects can be reduced by the use of AM in vacuum or by using shielding gases. [DebRoy et al. (2018)]

2.2.7 Material

The materials used would preferably be metal due to required stiffness. Potential metals that are already used in the automotive industry in additive manufacturing are [DebRoy et al. (2018)]:

- Aluminium (AlSi10Mg): A low weight alloy with good hardness and strength. It has a good combination of mechanical and thermal properties compared to weight.

- Titanium (Ti6Al4V): Used in motorsports and aerospace and has excellent mechanical properties with low weight. It has high corrosion resistance and has the ability to be heat treated to improve properties.

- Stainless Steel (SS316): It has good corrosion resistance and is used due to its decent properties compared to low price.

Some properties of these metals are shown in Table 2.1. The assembly itself would preferably be one of these, with the potential add of a rubber pad on the footpeg itself to reduce vibrations and increase passenger comfort. The bracket are currently made out of aluminium, so it would be interesting to compare it with additive manufactured aluminium.

Then one could identify the potential improvements that come from the topology optimization itself, and not from a change in material. AlSi10Mg also has potential due to low weight with good hardness and strength. The two others are both good contenders as well. Especially, Ti6Al4V with its high strength to density ratio. The decision for this project is that AlSi10Mg will be used in the TO task, mainly to compare how the optimized part compares to the OEM part structurally.

Table 2.1: Material properties of typically AM metals used in automotive industry [Zare (2019), DebRoy et al. (2018)]

Material:	AlSi10MG	Ti6Al4V	SS316
Young's modulus [MPa]	70 000	110 000	167 000
Density [tonne/mm^3]	2.67e-9	4.00e-9	7.85e-9
Poisson's ratio [ ]	0.33	0.31	0.27
Yield Strength [MPa]	260	1100	464

Another point in favor of AlSi10Mg is that it also has the possibility to allocate more material in the design space, compared to Ti6Al4V with identical weight criteria. This is due to the lower density shown in Table 2.1, where AlSi10Mg has a density of 2.67 g/cm^3 and Ti6Al4V has a density of 4.00 g/cm^3. This can result in parts having bigger cross sections when utilizing AlSi10Mg. If one where to look at the footpeg bracket as a simple cantilever beam with a load on the end as in Figure 2.10, one would get the formula for maximum deflection as shown in Equation 2.5 [Irgens (1992)].
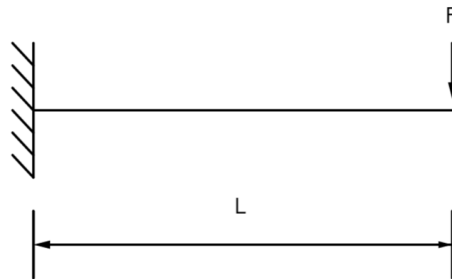
Figure 2.10: Cantilever beam with a length L and subjected to a load F

$$u_{max} = \frac{FL^3}{3EI} \tag{2.5}$$

The second moment of inertia (I) and the modulus of elasticity (E) are reducing the deflection the higher they are. Meaning if I or E increases, the stiffness increases. The second moment of inertia for a simple rod is given in Equation 2.6 [Irgens (1992)]. The radius

(r) of the specimen is affecting the stiffness with a power of four, while the E-modulus is only affecting with a power of one. Meaning that AlSi10Mg's 36% lower density could have a bigger impact on the stiffness than the 37% lower E-modulus, when comparing with Ti6Al4V.

$$I = \frac{\pi r^4}{4} \tag{2.6}$$

The part will consist of several layers of material when additive manufacturing it. These layers can lead to the part not having isotropic material properties [EOS (2014)]. Values for AlSi10Mg are shown in Table 2.2. Conventionally casted components of AlSi10Mg would typically be heat treated afterwards to improve the mechanical properties. Similar properties to these can however be gained from the rapid melting and solidification process of laser melting, and a stress relieving process at 300°C is often used instead [EOS (2014)].

Table 2.2: Material properties of anisotropic AlSi10Mg from AM [EOS (2014)]

Material:	AlSi10Mg	
	As Built	Heat Treated
Young's Modulus XY [MPa]	75 000	70 000
Young's Modulus Z [MPa]	70 000	60 000
Yield Strength XY [MPa]	270	230
Yield Strength Z [MPa]	240	230
Ultimate tensile Strength XY [MPa]	460	345
Ultimate tensile Strength Z [MPa]	460	350
Density [tonne/mm^3]	2.67e-9	
Poisson's Ratio [ ]	0.33	
Fatigue Strength [MPa]	97	

2.3 Design Methodologies

2.3.1 Design for X

A product development methodology relevant for design and optimization is Design for X (DfX). DfX is a method within concurrent engineering comparing several key elements of the product at the same time, being the different X's. They are then evaluated to find out which to focus your resources on to create the optimal product [Eastman (2012)]. Some of the main points to take from this are DfAM as presented previously, but also the more general design for manufacturing (DfM) and design for assembly (DfA). DfM is about reducing the costs and time of the manufacturing process. In the task given by Ducati a goal of 10 000 units per year where set as a pointer. Here one would have to look into how complex the part is and if it justifies the cost of producing it in AM vs traditional methods.

Figure 2.11 illustrates a case of manufacturing cost against geometry complexity for AM vs traditional methods. The cost of AM produced parts increase slowly with complexity compared to traditional methods like machining. The TO designed bracket will most likely lay in the zones where AM has its advantage, as this project is not adding restriction to optimize for other manufacturing methods. If compared to casting the situation could however end up being different. The main cost of casting is the creation of the mold. The mold cost would be high for 10 parts, but not if one produced 1000 parts instead with the same mold. For a number of 10 000 parts a year, it could potentially be cheaper to use casting if the complexity is within the limits of casting the component. A complete analysis of this is beyond the scope of this project, as one of the main goals is to optimize for additive manufacturing. This project will therefore mainly focus on the previously mentioned DfAM category.
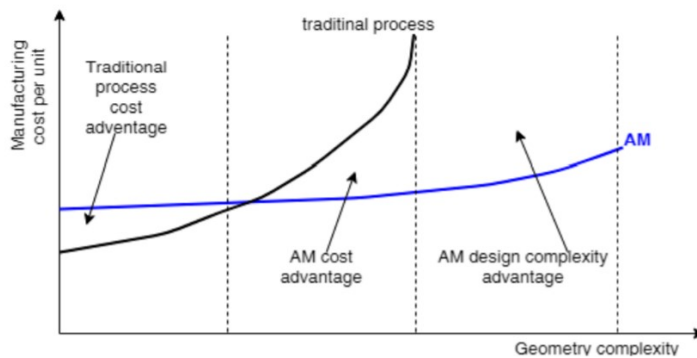
Figure 2.11: Cost vs complexity for AM vs traditional manufacturing processes [Durakovic (2018)].

DfA on the other hand is when the main goal is to ease the assembly of the product and reduce costs and assembly time [Ulrich and Eppinger (2011)]. It is linked to the part about potentially creating the entire footpeg assembly in process. By combining several parts and features into one, the time used for assembling the part could be reduced.

How the part is designed by for example use of symmetry, different types of bolts and other features is something that also can influence the assembly time. Currently the mounting bolts used are of the same dimension, meaning one could not use the wrong bolt. Another thing is the shape of the bracket as it is mounted on both the left and the right side. One side is a mirrored version of the other. They should either have distinct enough differences to easily see which goes where, or be interchangeable in a new solution.

Boothroyd and Dewhurst proposed a method to keep score of the cost of assembly in chapter 1 of "Design for X: Concurrent engineering imperatives" Eastman (2012). Their method is presented in the equation for DFA index:

$$\text{DFA index} = \frac{(\text{Theoretical minimum number of parts}) * (3 \text{ seconds})}{\text{Estimated total assembly time}} \qquad (2.7)$$

In Equation 2.7 the theoretical minimum number of parts times 3 seconds, the average time to assemble a perfect fit part, is divided by the total assembly time. This ratio shows how close the theoretical ideal assembly would be compared to the estimated time of the actual assembly. The closer these values are, the better the index. The printing of the footpeg hinge in one go would for example reduce the number of parts from seven, with the footpeg, bracket, rubber pad, two bolts, pivot pin and a retaining ting, to four. This is due to the bracket, footpeg, pivot pin and retaining ring could potentially already be assembled from the print. It would also reduce the total assembly time, but the most complex part of fitting the actual footpeg is now gone.

Reducing the number of parts could be done by integrating parts in this sort of matter. To see if this is possible one can ask if the part is theoretically necessary. The component that will be created instead of creating several parts, will be able to avoid problems around assemblies. A problem could for example be the interface between two parts mounted together, if they are mounted with a bad fit the product might not achieve its desired values. It is however not always the best option as you could also end up with having a component that is hard to repair or maintenance. A problem could be if a part of the component is easily broken and it is required to replace the entire component instead of just the part that is broken. This could be more expensive than to have it as two components, where the easily damaged part could be replaced by itself. Having the footpeg printed together with the bracket, could potentially make it harder to change out just the footpeg if it was damaged, or if the user wanted a different footpeg.

2.3.2 Design Thinking

Design thinking is a methodology based on the five stages shown in Figure 2.12. The first stage is to emphasize with the user to find their needs, and was used as a tool in the early stages of the project. A trip to a demo day at the local Ducati dealership in Trondheim was therefore part of the preliminary work. It was a good starting point to get a feel of the fit and finish of the bikes created by Ducati, and also to get a sense of the culture surrounding these bikes. A common theme was a high level of fit and finish throughout the products, from general mechanical components to cable management and other finer details. This is to be expected as Ducati bikes are generally regarded as high end motorcycles. The final solution should preferably be up to par with the fit and finish found in current Ducati bikes.
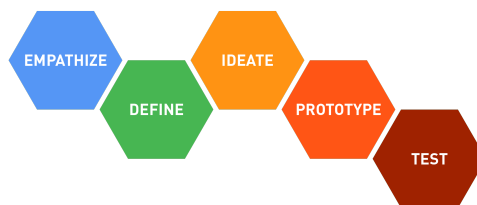
Figure 2.12: The five stages of design thinking [Plattner (2018)].

2.4 Current Rear Footpeg Assembly

(a) Outer side.

(b) Inner side.
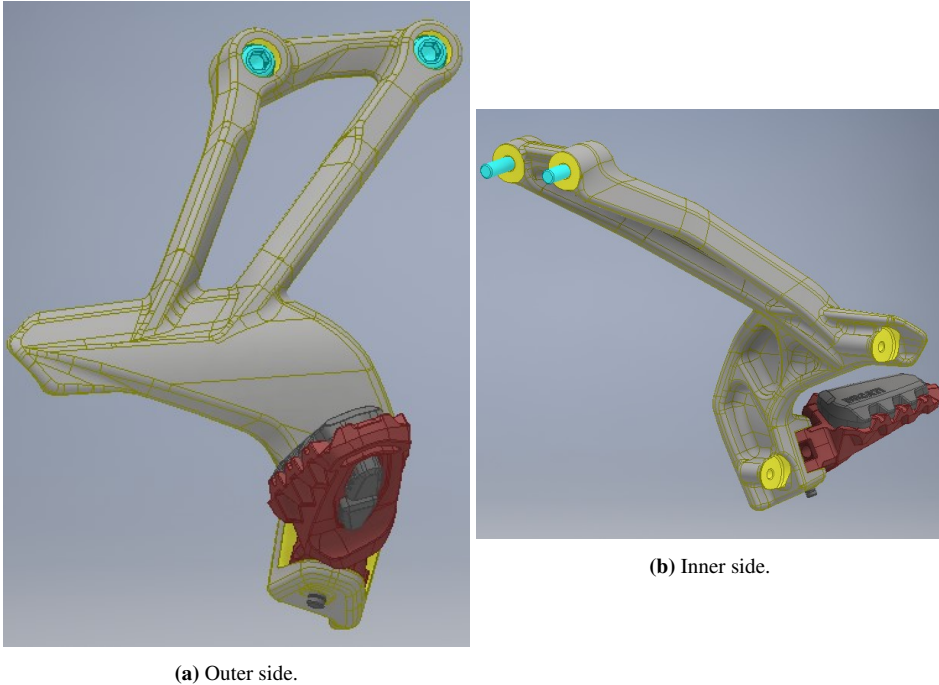
Figure 2.13: CAD model of the current footpeg assembly on the exhaust side of the bike.

The current footpeg assembly, shown in Figure 2.13, consists of a bracket mounted to the bike's subframe with two M8x35 8.8 bolts [Ducati (2019b)]. The bolts are recessed into the bracket. From the mounting points the bracket is formed by a triangle of "bars" going down to a curved piece, which works as the exhaust guard. At the end of this piece is the mounting point of the footpeg itself. The footpeg is mounted by a hinge making it fold-able. On the footpeg (red) one can see the black piece of rubber mounted on the top where the passenger puts their foot. In Figure 2.13b one can also see the mounting points for accessories such as different luggage racks shown in Figure 2.14a and 2.14b respectively. These mounting points are the two yellow circular areas in the lower right corner of Figure 2.13b.

The bracket itself is already a lightweight construction, as one can see by for example the recessing in the back shown in Figure 2.13b, and the weight of 536g (measured in CAD). Therefore weight reduction might not be the biggest potential for optimization this part has. Other examples of things to look into could be advantages of additive manufacturing, such as the previously mentioned easing the assembly by printing it assembled.

(a) Luggage rack mounted on the footpeg bracket [Carpimoto (2019)].

(b) Luggage support mounted on the footpeg bracket [Ducati (2019a)].

Figure 2.14: Different accessories mounted to the footpeg bracket.

2.5   Footpeg Regulations

The Multistrada 1260 is a road approved bike, and therefore some general regulations are relevant. The footpegs, or foot supports, shall according to The European Parliament's regulations be able to freely rotate, fold, bend or flex as a result of contact with other objects [European-Parliament (2016)]. This would for example be in the case of the bike tipping over. The final solution should preferably have this functionality.

Chapter 3

Method

In order to optimize the current design of the footpegs as described in section 1.2, one would need to have a working topology optimization setup. This includes the possibilities of comparing the optimized model to the original design. The new model need to be extracted or reverse engineered into a CAD software where a final design can be created. The final design's structural performance then has to be evaluated. This chapter presents the methods of achieving these objectives.

3.1 Simulation Tools

This section will look into the different pieces of software that were tested during this project, Abaqus Tosca from the pre-master project, and then Siemens NX and Fusion 360 from this master thesis project. Basic description and comparison of setup possibilities, benefits, problem areas and an overlooking diagram of the process in each software will be presented. The final chosen software Siemens NX will be described more in-depth further into this chapter, while Abaqus Tosca and Fusion 360 are described in-depth in Appendix A and C respectively.

3.1.1 Abaqus Tosca

In the pre-master project Abaqus Tosca 2017 edition was chosen as the main contender as TO software, and the final result from its simulations is shown in Figure 3.1. Abaqus has a lot of different features that can be utilized, such as two algorithms for the TO task and complex meshing features. A comparison of these different features were performed with the results of utilizing the sensitivity-based algorithm based on SIMP, from Section 2.1.2, together with a tetra mesh. These comparisons and results are located in Appendix B.
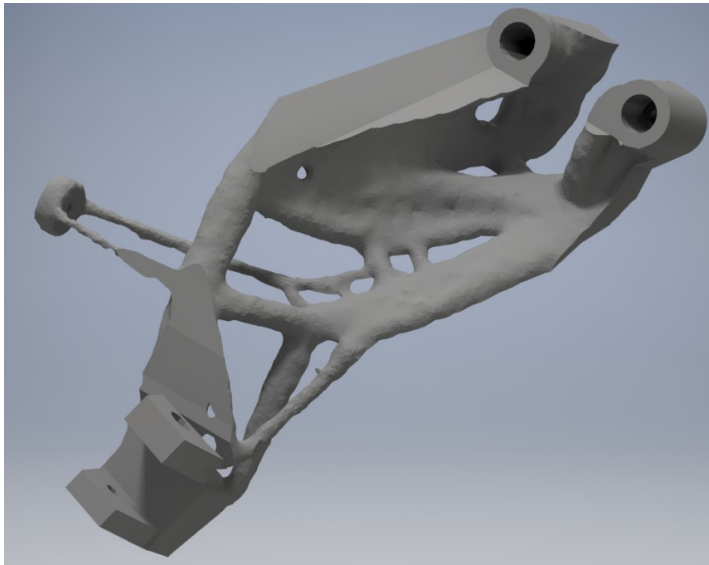
Figure 3.1: Final STL export from Abaqus Tosca in the pre-master project.

Abaqus Tosca is a software with good simulation possibilities, but the modelling part of it leaves things to be desired. It was therefore combined with Autodesk Inventor for modelling purposes, as shown in the workflow diagram in Figure 3.2. The complete process is located in Appendix A, but a short version will be described here. First, a design space was created in Inventor, and then taken into Abaqus Tosca. Load cases, constraints and the rest of the simulation setup in Tosca was added in the order shown in Figure 3.3. Then, the resulting geometry from the TO task in Tosca would have been taken into a FEM verification process in Abaqus. The model would be redesigned in Inventor based on the results of the verification, before the final CAD would be evaluated in Abaqus by a FEM analysis. The final component would then be exported and manufactured.
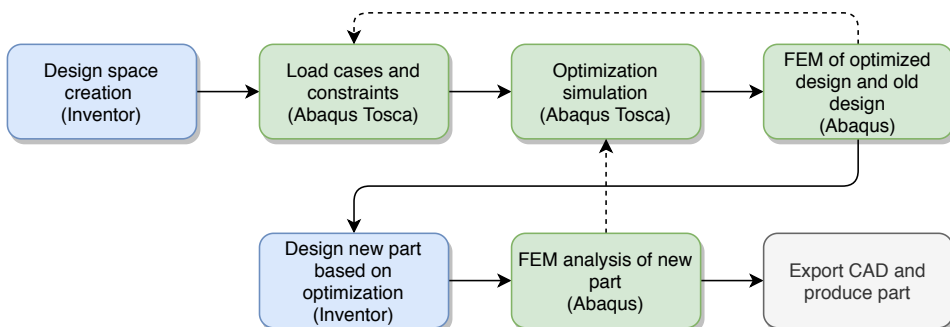
Figure 3.2: The TO workflow with Abaqus Tosca and Autodesk Inventor.
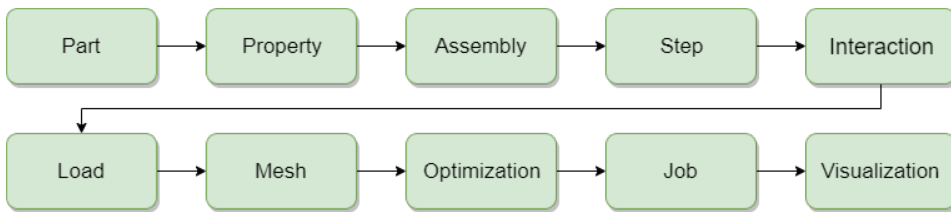
Figure 3.3: Workflow in Abaqus Tosca for the TO in the pre-master project.

Abaqus gives the user a graph of convergence of the different design cycles, and the user can choose which one of the results from the design cycles it wants to use. The final resulting file from the simulation is a mesh based STL file, which are not possible to take directly into a FEM verification process. The smoothing cycles in the STL creation also affected the geometry as shown in Figure 3.4. Here one can see that the higher number of smoothing cycles created a thinner structure, resulting in smaller cross sections. This could potentially reduce stiffness. To avoid big changes in geometry and disconnections the final results were a rather coarse structure. The final file from the Abaqus Tosca simulation would have to be redrawn from scratch to be used further, which could end up being a time consuming solution. This would also come from going between several different pieces of software throughout the process to create the part. The decision from the pre-master were therefore to look into other potential pieces of software as mentioned in Section 1.3.
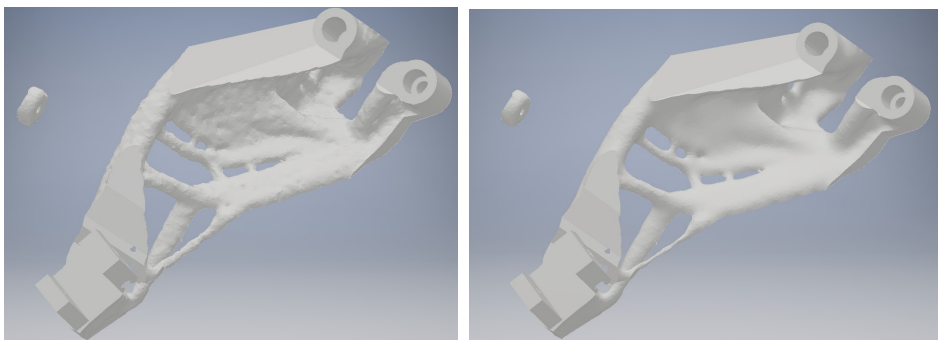
(a) The exported STL with 1 smoothing cycle.   **(b)** The exported STL with 5 smoothing cycles.

Figure 3.4: The STL file with different smoothing cycles.

3.1.2 Siemens NX

The topology optimization feature utilized in Siemens NX was the topology optimization for designers add-on. It had a simpler setup than Abaqus Tosca, by for example using its synchronous modelling tools to partition out some of the faces in the geometry, compared to the partition feature in Abaqus. It also has the possibility to use holes and other features directly in the process if the model have those features in the history tree in NX. It does however not have any controls over the mesh, other than how fine or coarse one wants the simulation to be. A typical workflow with the TO tools in NX is shown in Figure 3.5. This is similar to the workflow in Abaqus, but the main difference being everything is possible to perform in one software, and some differences inside the actual TO setup itself.
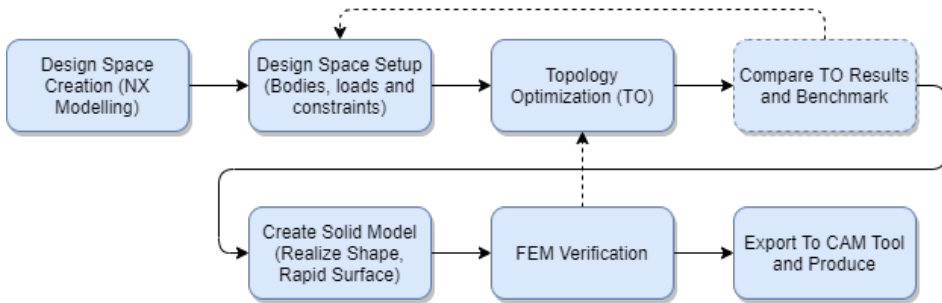
Figure 3.5: Typical workflow when performing topology optimization on parts in NX.

The general idea is to use a design space similarly to Abaqus, and then define different regions of keep-in and keep-out. Keep-out is used in for example mounting holes, and can be chosen to have a certain radius of solid material around the hole for structural purposes. NX's topology optimization tool also has the possibility to add constraints to the actual design space, such as:

- Void fill: avoids internal voids in the structure

- Material spreading: Can be used to force a structure to spread the material in the design space to change the thickness and number of members in the structure.

- Several settings for forcing the part to be symmetrical around certain a plane or axis.

- Overhang and self-supporting structure setting: Relevant when it comes to creating efficient additive manufactured parts, as it can avoid support structure. But first the desired printing direction for the part has to be decided.

Out of these void fill was found to be a good thing to keep on most of the time. The material spread setting can be used to a effect of creating more complex thin structures instead of simpler solid structures, as shown in Figure 3.6. The benefit of the less complex structures is to have thicker cross sections, but higher material spread can also result in failures.
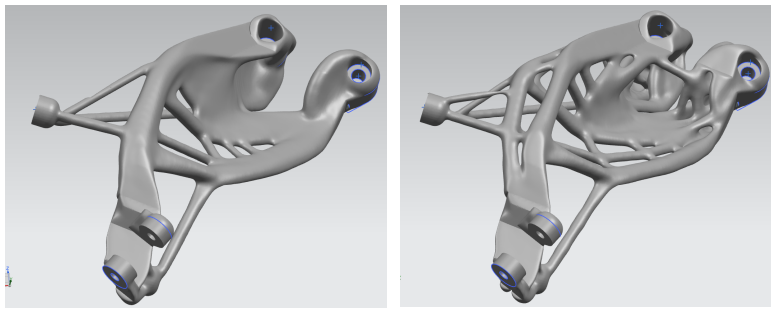
(a) TO with 0% material spread.

(b) TO with 70% material spread.

Figure 3.6: Comparison of material spread settings in Siemens NX.

The possibility of adding manufacturing constraints in accordance to produce the part is also a feature that can be benefited. NX does also have the possibility to check the models for overhang angles and other potential AM issues in its CAM tools after the part is created.

Siemens NX outputs a mesh based file similar to Abaqus, but it has the possibility of creating a convergent body. This convergent body can be taken into tools such as polygon modelling, realize shape and the reverse engineering module. These tools can be used to create models as complex as the results of the TO task more fluently than with traditional modelling. A more in-depth description of this process will be presented in Section 3.3 - CAD Redesign. An example of a solid model created with realize shape is shown in Figure 3.7. This could be further utilized in FEM verification.
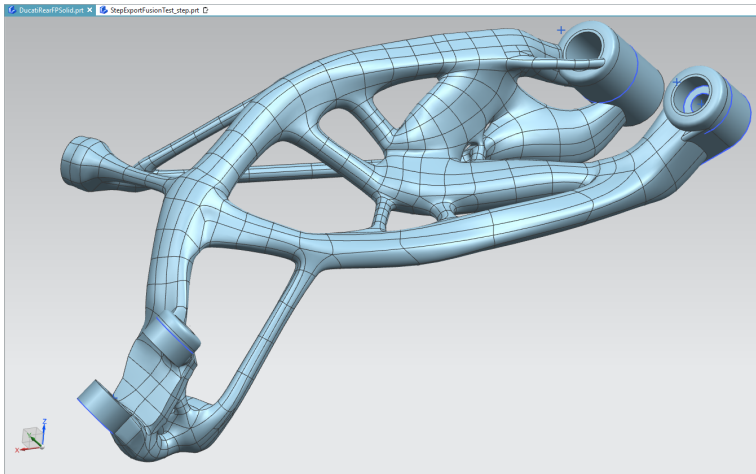
Figure 3.7: Siemens NX solid model created from the convergent model of the TO task.

3.1.3 Autodesk Fusion 360

Autodesk Fusion 360 is utilizing a feature that is different than traditional topology optimization, which they call generative design [Autodesk (2020)]. The typical workflow is however rather similar to the other pieces of software as shown in Figure 3.8. Most of the differences are in the generative design module compared to the traditional TO task, and the workflow of going from this to the solid model.
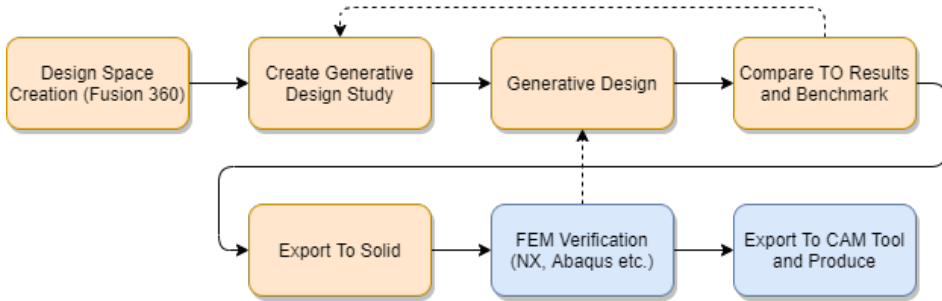
Figure 3.8: Typical workflow of generative design on parts in Fusion 360.

Fusion 360 gives the opportunity to use a defined design space as in the two other pieces of software, but a simulation can be ran without it. Instead one can use a combination of keep-in and keep-out regions to define the most critical constraints. This will let the simulation have more freedom than with a defined design space. The two figures below shows how it fares when it is let to be more free in Figure 3.9, and how it compares if one defines the design space in the more traditional manner in Figure 3.10. A thing to note here is that the part without a defined design space allocated more material outside of the potential design space, which could result in interfering with other parts in the assembly.
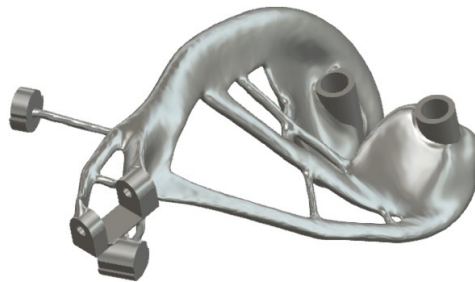
Figure 3.9: TO example from Fusion 360 with just keep-out and keep-in regions.
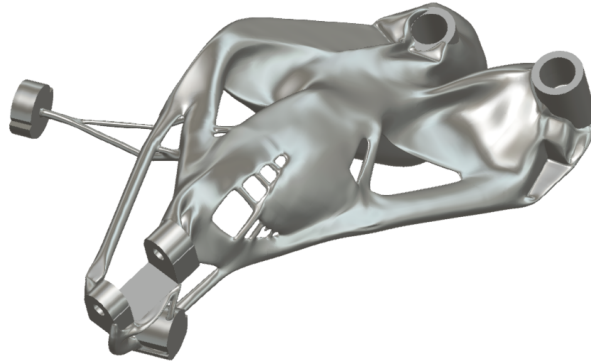
Figure 3.10: TO example from Fusion 360 with a complete design space.

Fusion 360 also has the possibility to run a simulation based on different manufacturing constraints. One of these constraints is the additive manufacturing constraint. This makes the optimization take into account self-supporting and overhang angles in print directions along each of the three Cartesian planes. It is therefore necessary to orient the part along the planes one would want to print it in. The complete simulation setup can be sent to the cloud, and a number of results are returned as shown in Figure 3.11. Getting several results from one study makes it also possible to run multiple load cases or weight targets in parallel, to showcase the difference in the results section. Each of the results has the possibility of choosing which design cycle one want to use further, similarly to Abaqus.
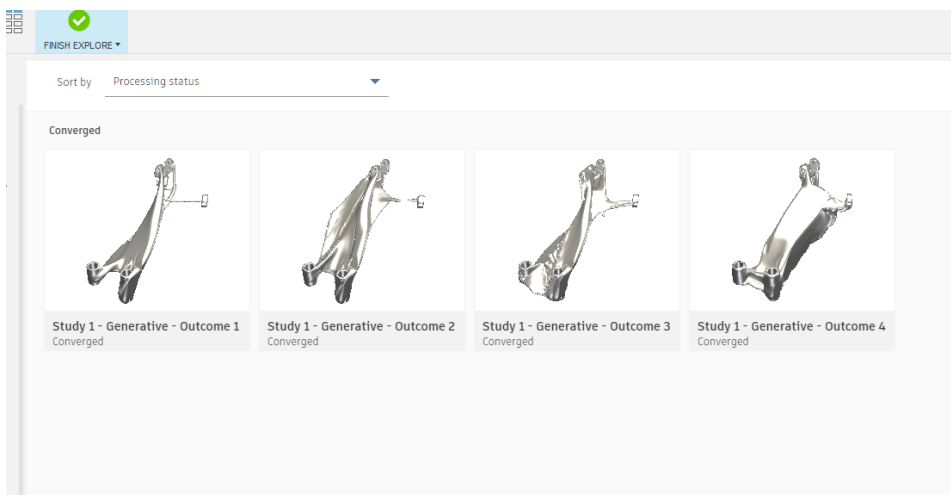
Figure 3.11: Example of multiple results returned from a Fusion 360 simulation.

The major reason for this being a contender is that it has the possibility of creating a solid model directly from the optimization. This would in theory result in skipping the solid from STL creation process altogether. In reality it creates a solid, but the results is a model with complex face structure as shown in Figure 3.12. This could be taken directly into a FEM verification, but some idealizing could be necessary to improve the results of the meshing and simulation process. The direct to solid models were also not the easiest to alter in the redesign and FEM stages, due to them not having a history tree to work with.
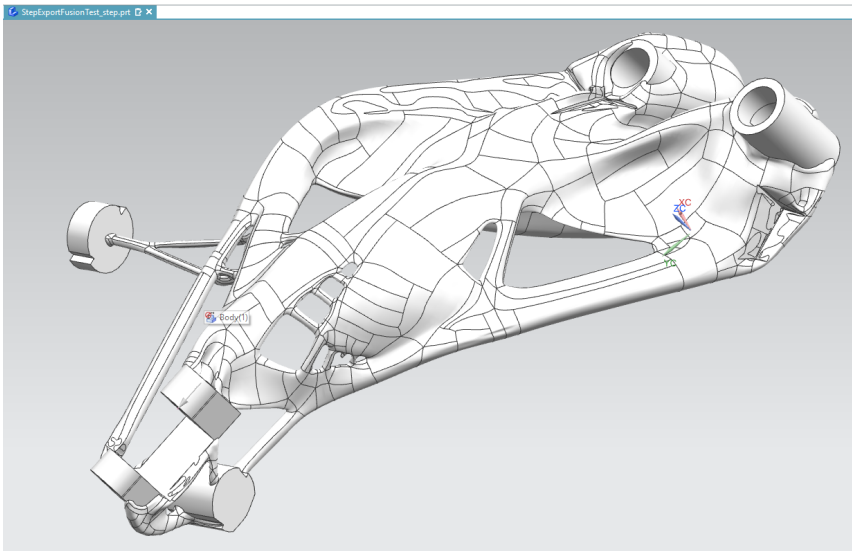
Figure 3.12: Direct to solid from Fusion 360 shown in Siemens NX.

3.1.4 Summary

In general the key points here are:

- NX and Fusion gives the user less control over the mathematics of the simulation by just giving you a coarse to fine accuracy slider for the analysis. Abaqus on the other side give you complete control over different meshes and other settings.

- NX and Abaqus creates STL and other types of facet models, while Fusion can export a solid. The facet model in NX can be directly converted into a convergent model, which makes it possible to use its reverse engineering and solid model creation tools on it. The solid models created in NX were found to be more intuitive to work with after creation, compared to the direct to solid from Fusion. This is however a personal preference as it depends on which modelling tools the user has most knowledge of from before.

- The preserved regions are partitioned out in both Abaqus and Fusion, but are in NX made by the optimization feature setting and included organically in the proposed design result. This can create a more aesthetically pleasing and fluent geometry with less work from the user.

- Both NX and Fusion bring a good amount of settings around manufacturing to the table. The Abaqus version utilized in this project did not. It was however an older version compared to the other two pieces of software. A more current version could potentially be solving these issues, but this was not available for this project.

- Both Fusion and Abaqus gives the user the possibility to choose which design cycle result to return from the TO task, while NX only gives the one that converged or was closest to convergence. This were not seen as a major benefit as the last result typically ended up as the best anyway.

The ultimate point for NX in this project was the possibility to do everything from the start to finish in one software. This made the overall process more streamlined, as it were easier to go back and forth between the different stages of the project. This proved to be especially beneficial in the final benchmarking stages, with iterations back and forth between FEA and CAD redesign.

3.2 Topology optimization setup

This section describes the common components of creating the topology optimization setup, while going more in depth the specific setup used with Siemens NX. Specific descriptions of the setups in Abaqus Tosca and Autodesk Fusion 360 are located in Appendix A and C respectively.

3.2.1 Design space

The design space of the footpegs is depending on several factors:

- Mounting position to subframe.

- Interference with exhaust muffler.

- Interference with swingarm assembly's movement, including chain, brake hoses etc.

- Position of the footpeg itself on the bracket.
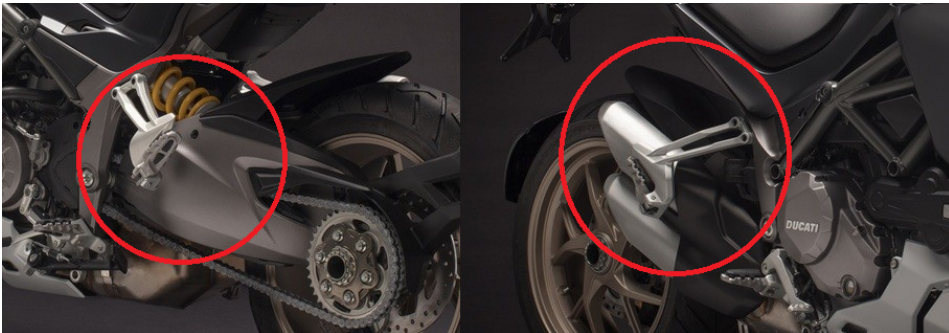
Figure 3.13: The left and right side of the bike, showing the passenger footpeg assemblies highlighted in the red circles [Eker-Performance (2019)].

The footpeg bracket is mounted on the subframe of the Ducati Multistrada 1260, as shown in Figure 3.13. Two M8 bolts are mounting the bracket to the subframe below the seat. The holes and surrounding surface for the bolts need to be kept as non-design areas in the design space to not be removed or altered by the optimization, hence keeping the part a fit to the OEM mounting positions.

The exhaust muffler is mounted on the right side of the bike, neatly slung under the current footpeg solution, shown in the right circle on Figure 3.13. The footpeg bracket has a metal plate that functions as protection for the passenger's foot to not hit the exhaust pipe. This plate also has two mounting points for accessories. The design space need to take this into consideration so that the optimized part has these mounting points, and does not interfere with the muffler in any way. Keeping the mounting points could also potentially ensure enough material in the area, to avoid direct contact between the passenger's foot and the exhaust in the final design.

The single-sided swingarm is mounted on the left side of the bike. It moves closer to the sub-frame when the bike is exposed to weight on the rear part of the frame, or when the shock absorber handles uneven roads. This movement has to be taken into account to avoid interference between the swingarm assembly and the footpegs. An easy way to take this into account is to follow the geometry of the OEM bracket closely for the design space, as the current solution does not interfere with any other parts.

The footpeg itself is mounted at the end of the bracket with a hinge. This has to either have a non-design space in the hinge so that one could mount the footpeg after optimization, or be a part of the assembly. By having the footpeg in the assembly one could have it a non-design space and attach the load to its face.

The design space created in Autodesk Inventor based on the aforementioned cases is shown in Figure 3.14 and 3.15. At this iteration the design space was created along the outermost lines of the OEM bracket's inner side, to overcome the problems of interference with other parts. On the outer side of the bracket the design space goes beyond the OEM part in some places. An example is on the right in Figure 3.14, where the bracket does not have anything that could interfere with it compared to other areas. On the left in Figure 3.15 on the other hand, the design space follows the curves of the OEM component closely. This design space was created in the pre-master specialization project and has been used as basis for all the software testing of topology optimization setups throughout the project. The same design space was used to get an accurate comparison between the pieces of software, and as the final results in the pre-master did not show any issues with it.
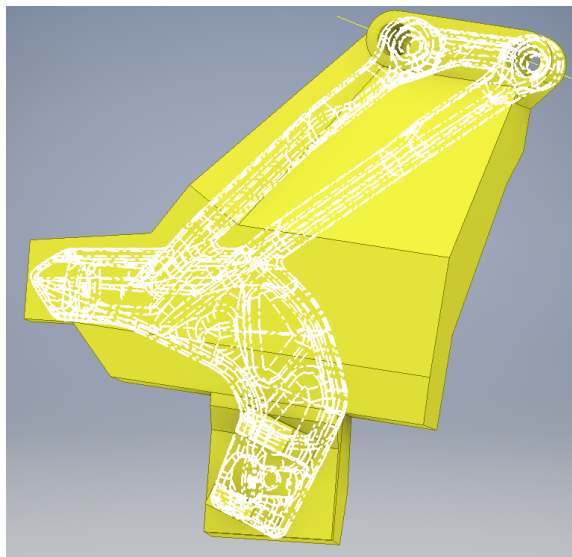
Figure 3.14: The design space seen from the side overlapped with the outline of the OEM structure.
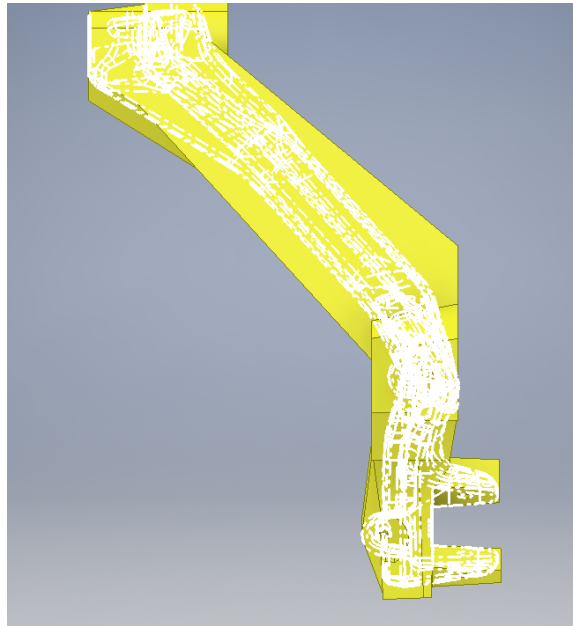
Figure 3.15: The design space seen from the rear overlapped with the outline of the OEM structure.

3.2.2 Load cases
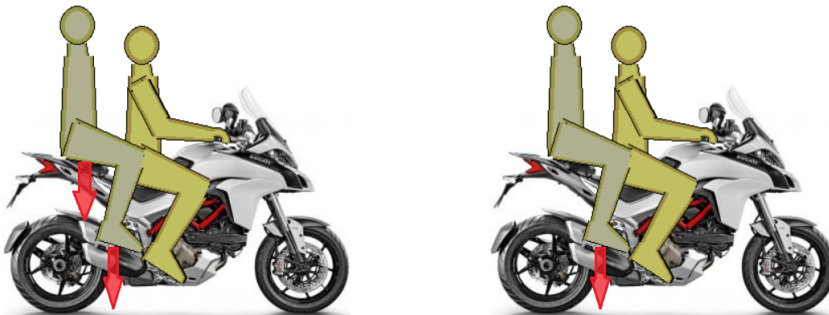
(a) The passenger sitting on the seat distributing their weight between the seat and both footpegs

(b) The passenger lifting themselves from the seat, where all load is then distributed to both footpegs.

Figure 3.16: Load case scenarios for passenger weight on footpegs

The main load case (LC) for the rear footpegs is the weight of the passenger. When seated on the bike the weight is distributed between both left and right footpegs together with the seat, shown in Figure 3.16a. If the passenger lifts itself to change position more of the weight will be put on the pegs itself, shown in Figure 3.16b. The next scenario is when mounting the bike as a passenger. It is then typical to put one foot on one of the footpegs

and then step over the bike. In this scenario most of the person's weight is carried by one of the footpegs alone. The scenario of sitting on the bike will in reality also include potential increases in load when the bike is running over bumps in the road and similar situations.

The specific LC given by Ducati to use in the topology optimization and FEM verification is a load of 1700N in the negative Z-direction, applied at a distance of 15mm from the end of the footpeg's internal side. The negative Z-direction is here parallel with gravity. This were applied as a load in the holes on the bracket where the footpeg is connected in the TO simulations. An optimization with the footpeg itself and the load at the specified point were tested, but this did not work out as will be explained in Section 3.2.4.

An extra LC was added in the form of loads on the luggage rack mounting points shown in Figure 3.17. These loads were added due to the point would almost not have any structure after the TO task without them. This is based on the results of the general TO task, and TO with the OEM bracket as design space in Abaqus, shown in Appendix A.4. The loads are axial loads in each mounting hole of 200N normal to the plane of the mounting point, and a transverse load of 200N along the plane of the bracket in towards the bike, which correlates to the negative Y-direction in the parts global coordinate system. The reasoning behind these loads is that the luggage types mounted in this area can typically store a maximum of 30L to 50L, and carry 10kg to 20kg [Gates (2020)]. The main mounting points for the luggage is however on the frame, and the footpegs accessory points are more for stiffening. The 200N in two directions in each mounting point are therefore an assumption that should give enough structure in the TO task, to ensure a structurally sufficient component.
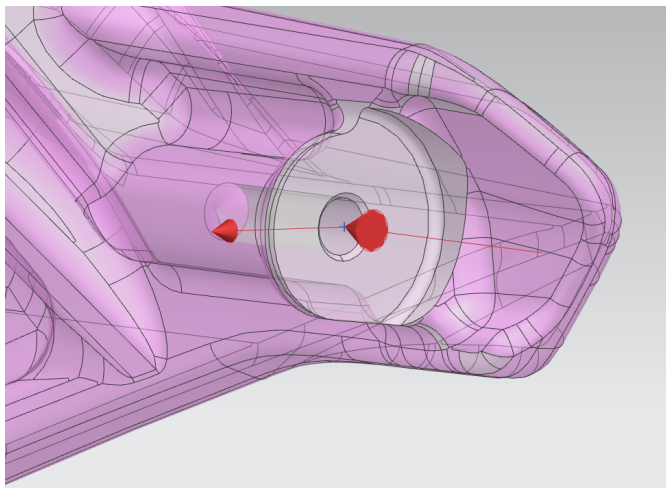
Figure 3.17: Luggage load setup.

3.2.3 Siemens NX TO Setup

The Siemens NX tool used is called topology optimization for designers, and the general workflow for it is shown in Figure 3.18. For this project the main design space was drawn in Inventor during the pre-master, but it could as easily have been drawn in NX as well. The scenery bodies used later in this section were made in NX.
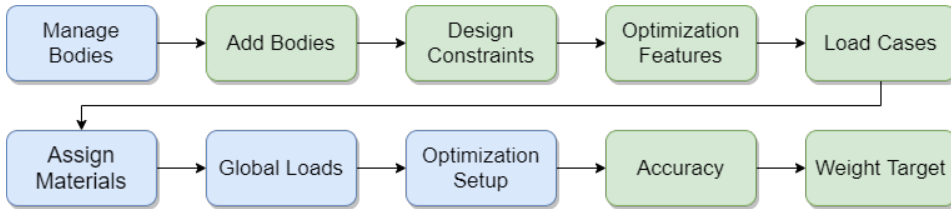
Figure 3.18: Workflow of the NX TO for designers tool. Blue is main commands and green is sub-commands.

The setup begins in the manage bodies tool. This is where the design space is added to the simulation and its constraints and features are assigned. One can import design features if the design space has a NX modelling history tree, to add constraints and loads. If not, one can use synchronous modelling and its copy face function to make the faces of holes and other features available in the history tree. The manage bodies tool does also have the possibility to add several design spaces, and combine them with non design spaces. For this task only a single design space for the footpeg bracket was used, but a combined space of multiple design spaces could be used when trying optimize for multiple components at the same time.

The design constraints used in this setup is:

- Void Fill
- Material Spread
- Self-Supporting

Void fill avoids the creation of internal voids in the geometry by the TO task. It was kept on at all times, which is advised in the description of the tool when working on parts that are made with for example PBF. This is due to excess powder being closed in by the internal voids during production. Self-supporting was used instead of overhang avoidance, due to overhang avoidance being stricter. It is trying to avoid overhangs all together in a certain direction, which can lead to external holes in the geometry being closed and turned solid instead. Self-supporting is on the other hand less strict, and is trying to minimize areas that exceed the overhang angle in a certain direction. This can reduce support structure, but it will not compromise the structural integrity by creating a part with minimal overhang at all cost. The different constraints can also be ordered depending on which one should be top priority. For this project void fill had top priority, and the other two were alternated depending on the case.

Constraints regarding symmetry were not added in this case, as the bracket itself does not have any relevant symmetric features. The only symmetric feature is that there are a mirrored version of the bracket on the other side of the bike. A mirrored version were therefore made after creating the final solution instead.

The design features that are utilized are the mounting holes for attaching to the frame, the luggage accessory holes and the footpeg mounting point. These features are also recognised as keep out areas, with a constraint of a minimum radius of solid material around the holes. The settings are shown in Table 3.1, where one can also see which features have assigned fixed constraints.

Table 3.1: Table of design feature settings in Siemens NX TO task.

Feature	Keep Out/In	Radius	Constraint
Mounting Hole 1	Out	8mm	Fixed
Mounting Hole 2	Out	8mm	Fixed
Upper Pin Hole	Out	6mm	No Constraint
Lower Pin Hole	Out	6mm	No Constraint
Accessory Hole 1	Out	6mm	No Constraint
Accessory Hole 2	Out	6mm	No Constraint

The TO tool assigns its loads, as its constraints, to the different features of the design space. This made it so that the load of 1700N added to the two footpeg mounting holes could not be added to a single node linking the holes. The load were therefore assumed evenly distributed over the two holes. The accessory mounting holes were assigned the two loads presented in the previous section. One normal to the plane of their face, and one in parallel with their face in the negative Y-direction. The complete load setup is shown in Table 3.2.

Table 3.2: Table of load case settings in Siemens NX TO task.

Feature	Load [N]
Upper Pin Hole	850
Lower Pin Hole	850
Accessory Hole 1 (Normal)	200
Accessory Hole 1 (-y)	200
Accessory Hole 2 (Normal)	200
Accessory Hole 2 (-y)	200

Several topology optimization tasks were performed with lowering weight criteria in increments of 50 from 550 to 200g. The results from these were used to decide on a weight target area to focus on. Material spreading and self-support were tested separately for a couple of the cases. Nothing over 70% material spreading was used, due it resulting in errors and non convergence for this specific part. The printing directions tested for the self-support constraints will be further explained in Section 3.5 - DfAM.

The material used was an isotropic version of AlSi10Mg, due to the anisotropy being dependent on the printing direction, and that was not decided at this time. An anisotropic material was applied to the TO tasks that contained self-Supporting as a design constraint. The difference between using anisotropic and isotropic material were not that big for a general case, as shown in Figure 3.19. They seem identical but have a minor thickness difference in some areas. In this example the coordinate system for the material was the same as for the part, meaning the weaker direction, Z, was along the same axis as the main load case at the footpeg area.
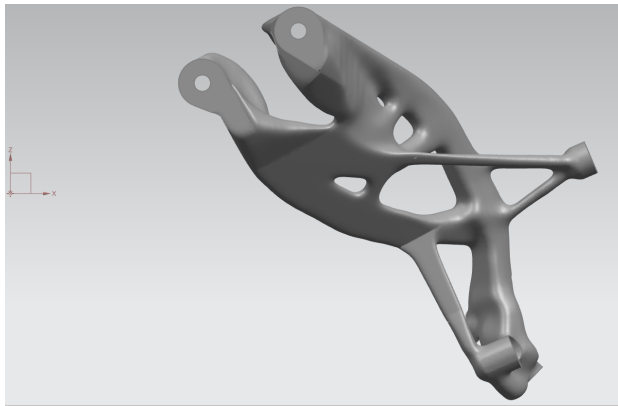
(a) Anisotropic material.
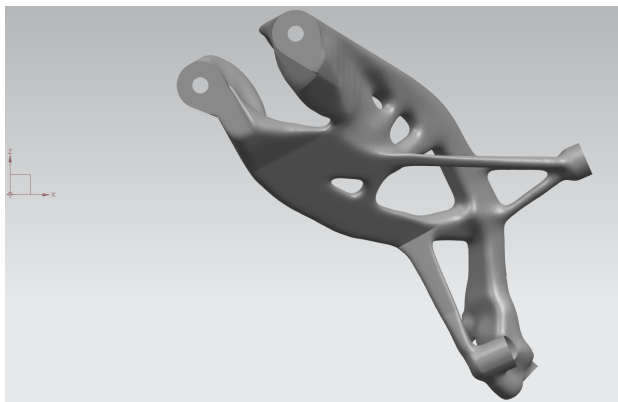
(b) Isotropic material.

Figure 3.19: Comparison of anisotropic and isotropic material.

Table 3.3 shows a complete overview of the settings for the different simulations.

Table 3.3: Complete setup for the topology optimizations in Siemens NX.

Setting:	
Design Constraints	Void Fill "ON"
	Material Spreading 0-70%
	Self Supporting (For some cases)
Optimization Features:	
Load Case	1700 N in the negative Z-direction
	200 N parallel to the accessory mounting point (-Y)
	200 N normal to the accessory mounting points
Geometric Constraints (Design Space)	Fixation to subframe
	Exhaust muffler
	Mounting point for footpeg
	Swing Arm
	Accessory attachment points
Material	AlSi10Mg
E Modulus	70 000 MPa
Poisson Ratio	0.33
Density	2.67e-9 tonne/mm^3
Global Load	Acceleration of 9.81 m/s^2 in the negative Z-direction
Optimization Type	Minimize Strain Energy
Accuracy	9.5 to 6.1mm, increases with lower weight targets
Weight Targets	550-200g (50g intervals)
PC Specs:	
CPU	3.2 Ghz QuadCore (Intel I7-4790S)
RAM	16 Gb with 1600 MHz

3.2.4 Complex Multiple Body TO

A more complex version of the TO task that was closer to the original load case given by Ducati was tested. Two extra scenery bodies were added alongside the design space as shown in Figure 3.20. These two are an idealized version of the footpeg pin from the OEM setup, and a simplified version of the footpeg itself. A comparison of the simplified and the OEM footpeg is shown in Figure 3.21.

The changes the scenery bodies makes to the setup are that one now has to add connections between the scenery bodies and the design space. The TO tool in NX does at the point of this thesis only support glued connections, so those were utilized. The main load case of 1700N was moved to be positioned 15mm from the edge of the footpeg. This is at the edge of the U towards the C in the Ducati logo on the OEM peg, seen in Figure 3.21a.
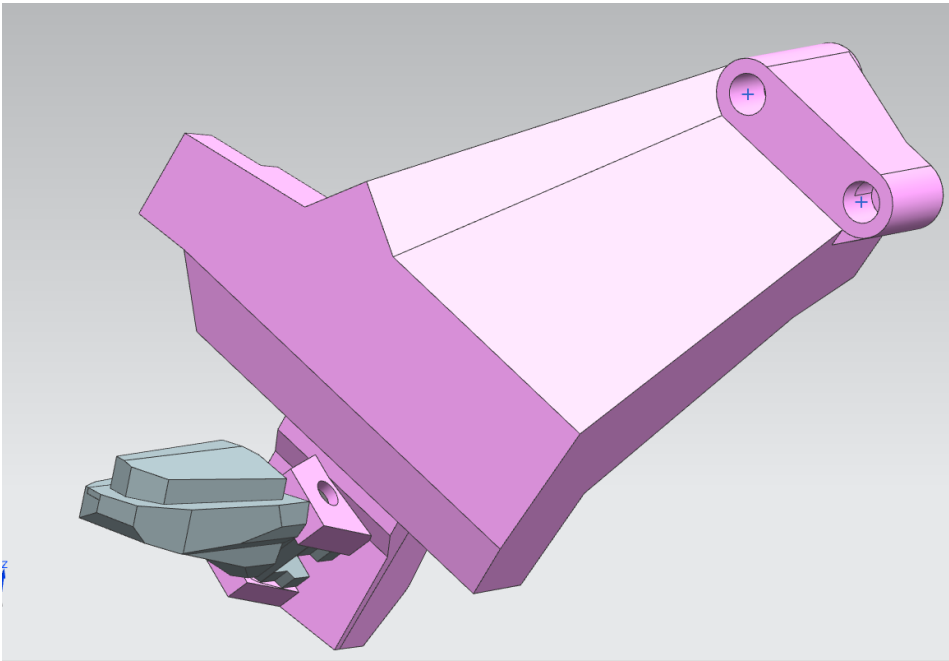
Figure 3.20: The more complex TO setup including the footpeg itself and its pin as scenery bodies.
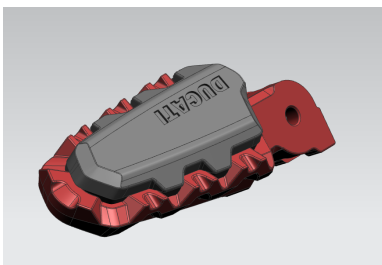
(a) The OEM footpeg model.
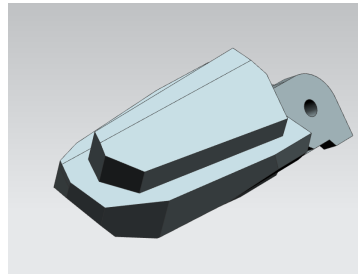
(b) The simplified version of the footpeg.

Figure 3.21: Comparison of the two footpeg models.

This setup did however not converge at any of the tested settings for this project, which were weight targets from 500 to 350g, and with accuracy as low as 6.1mm. The lowest accuracy available for this case were just above 6.0mm. The only difference in setup is the aforementioned connections created by the scenery bodies. These could be the reason for the solution being to malformed and not converging. The simpler TO task was therefore used instead. A setup using the footpeg itself, and the pivot pin, will be used in the FEM verification process.

3.3 CAD Redesign

This section will look into the methods of creating a solid model from the TO results in Siemens NX. These are the same tools that will be utilized in the CAD redesign for the final FEM verification as well. The different tools and commands will be explained together with their respective benefits or issues.

3.3.1 Siemens NX Realize Shape

Siemens NX has some redesigning possibilities with its convergent modelling and realize shape features. From the topology model generated in NX TO one can extract a convergent model that can be used in polygon modelling and realize shape. A polyline can be created along the convergent model in realize shape, by utilizing the point constructor dialog for each point. Trying to make the points stick to the model without this extra dialog is like shooting in the dark. These polylines, shown in Figure 3.22a, can then be used to assign a tube cage that can be formed to create the geometry as a CAD model for further use. Figure 3.22b shows the tube cages before one pulls on the nodes to sculpt the cage to the convergent model, while Figure 3.22c is after sculpting.
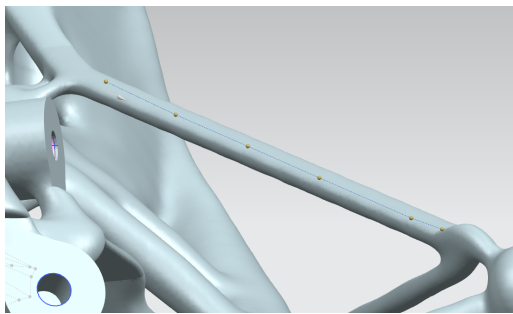
(a) The polylines assigned to the convergent model
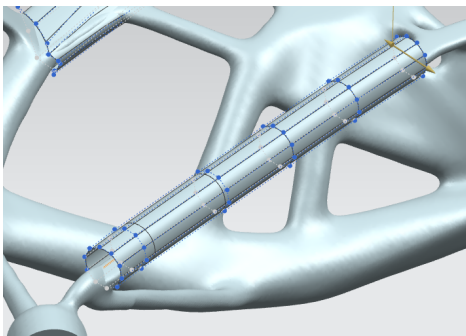
(b) Tube cage before sculpting.
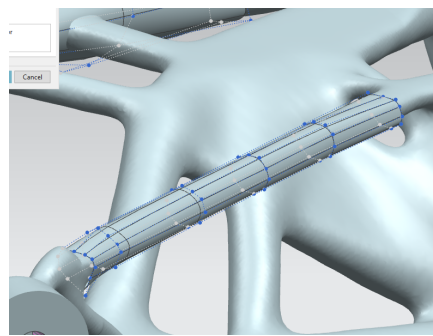
(c) Tube cage after sculpting.

Figure 3.22: Tube cages along polylines.

These tube cages can then be connected using the bridge face command, after the cages have been filled. One can connect as many cages as one wants as long as the adjoining sides have an equal number of nodes. This means one can either connect cages with identical number of end nodes, or one cage to a side faces of a different cage. This can also be performed step-wise. An example of connected tube cages are shown in Figure 3.23.
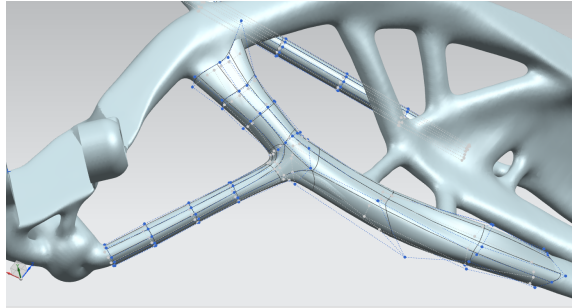
Figure 3.23: Three tube cages joined together.

Several iterations of this results in a complete shell model of the part that can be converted into a solid model, as shown in Figure 3.24. In this particular case the more critical functions, such as mounting holes, where created using traditional modelling methods to keep specific tolerances, and then united with the geometry from realize shape to create a complete solid model. It is easy to alter the thickness by just stretching the nodes of the appropriate tube cage, even after the solid model is made.
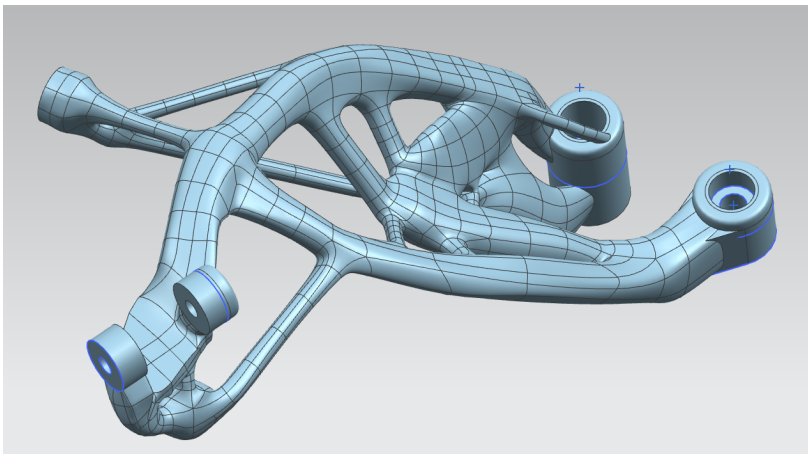
Figure 3.24: NX realize shape solid model example.

3.3.2 Siemens NX Reverse Engineering

Siemens NX does also have a separate reverse engineering module, which has its own features for creating surface models out of a facet model. These can then be converted into a solid model. The first feature is an analyzing tool called detect primitives that analyses which primitive shapes the convergent model could consist of, as shown in Figure 3.25. The colors represent different primitive shapes, and can be used to help with drawing a solid CAD model from the convergent model.
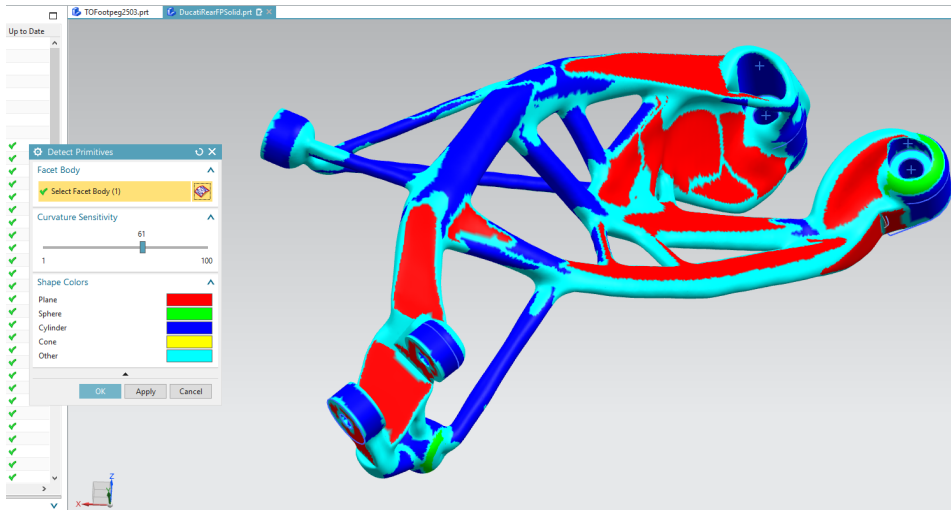
Figure 3.25: Siemens NX Detect Primitives

The main feature utilized here is rapid surface, which lets you draw surfaces based on four lines directly on the convergent model. This is shown in Figure 3.26. The lines can consist of more points to create smooth curves. It is also possible to import lines from the first surface when drawing another surface next to it. A combination of several of these surfaces will result in a shell model similar to the one shown in Figure 3.27. How close it is to the convergent model is dependent on the sizes of the surfaces compared to the curvature of the model. Many smaller surfaces will be closer to the original model, but in several cases a big one is satisfactory. This would especially be the case in the red areas in the detect primitive model shown in Figure 3.25.

An issue with this tool is that one has to be accurate enough with the surfaces drawn to create a watertight model. Meaning the sheet model can not have any gaps between the surfaces. These gaps will cause the model to not be watertight when the sheets are sewn together, resulting in a sewn sheet model and not a solid model. Some of these gaps can be fixed by changing the node tolerance in the sew tool, but it can lead to the sewn faces being warped if the gap problem is sincere enough. This will result in weird geometrical errors.
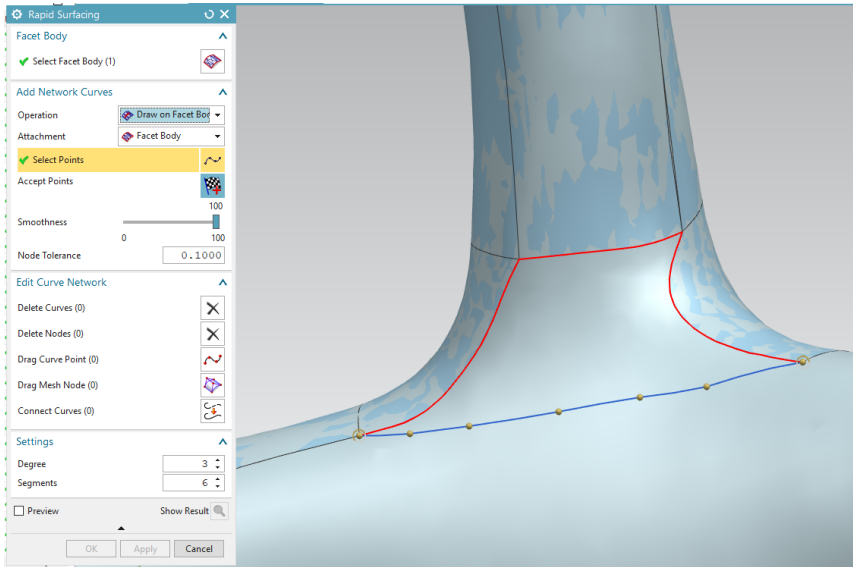
Figure 3.26: Rapid surface tool where one draws on the convergent model.
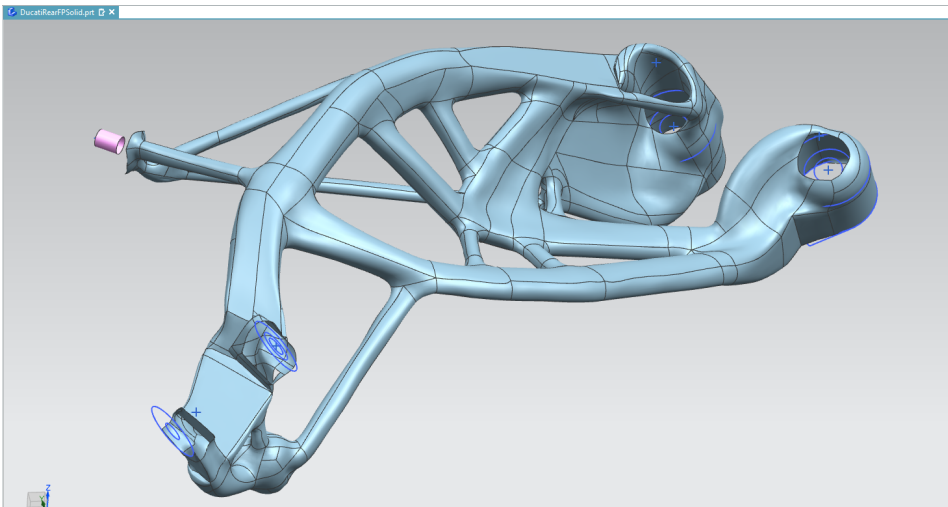
Figure 3.27: Model created with rapid surface, before made into a solid.

Another issue is the geometrical errors that sometimes occur in the convergent model from the TO task, as shown in Figure 3.28. These can lead to the surfaces either not being able to be made or end up warped. The current solution is a case of trial and error with different surface sizes and placement until a decent result is achieved. The polygon modelling environment also have some tools that can clean up the convergent body of some of its errors.
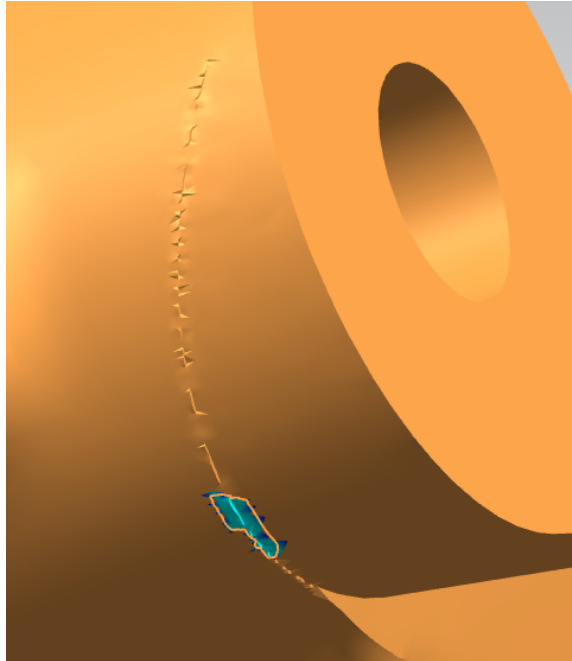
Figure 3.28: Geometrical error that can occur in the convergent model.

The models created with this tool is closer to the original convergent model from the topology optimization than the realize shape sculpted model. This is due to the surfaces being directly linked to the model, compared to just a reference line in the realize shape model. The realize shape model can however be as exact, but this would involve a more time consuming process of sculpting with the nodes.

3.3.3 Realize Shape + Section Tube Command

The aforementioned cases were with an older version of NX that were utilized in the earlier stages of this project. A newer version, more specifically NX 12 build 1911 but anything after build 1872 will suffice, have an extra feature that can be utilized called the Section Tube command. It lets you add the tube cages directly to the surface of the convergent model instead of stretching all the points. This gives in theory the possibility to get the modifiability of the realize shape models, combined with the more directly to the convergent model's surface as rapid surface have. This overall improves the workflow of solid model generation in realize shape.

Figure 3.29 shows the features of the tool, and how the tube cages are directly linked to the convergent model (yellow). The tool lets you specify points on the face similarly to polylines, but avoiding the cumbersome process of sculpting the cages, due to it automatically sectioning the tube cage to the convergent model. It is also possible to choose how many nodes to have around the circumference of the cage. How many faces/sections that is on the length of the cage is chosen by adding more points. The more points, the closer it comes to the underlying structure, but trying to have similar size on the cages is important for bridging them together more easily.
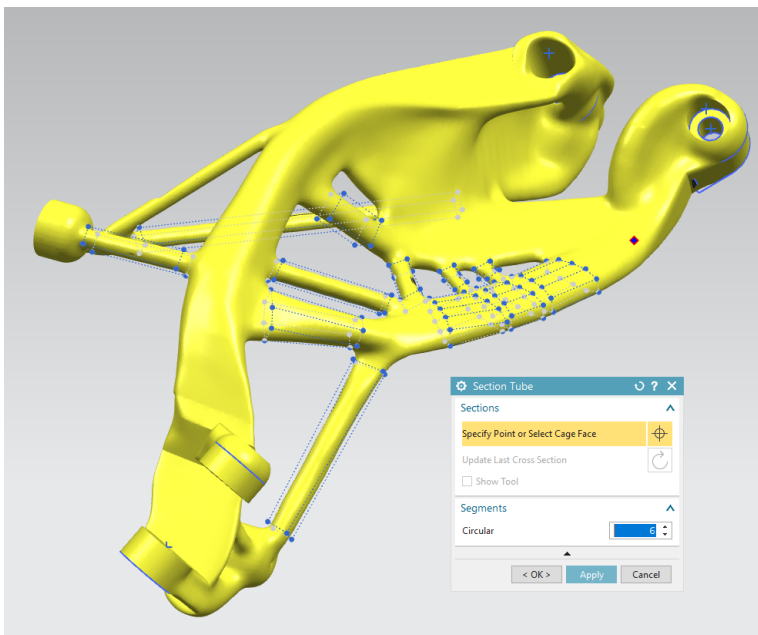
Figure 3.29: NX Section Tube command.

A technique for deciding on how many nodes to use, is to see how the cross section looks compared to the convergent models structure. This is shown in Figure 3.30, were Figure 3.30a shows a lower number of nodes and Figure 3.30b shows a higher number of nodes. The higher number is of course closer to the structure. This view can however be used to find a high enough number that is usable, while still being in the area that is easy to connect to other tube cages.
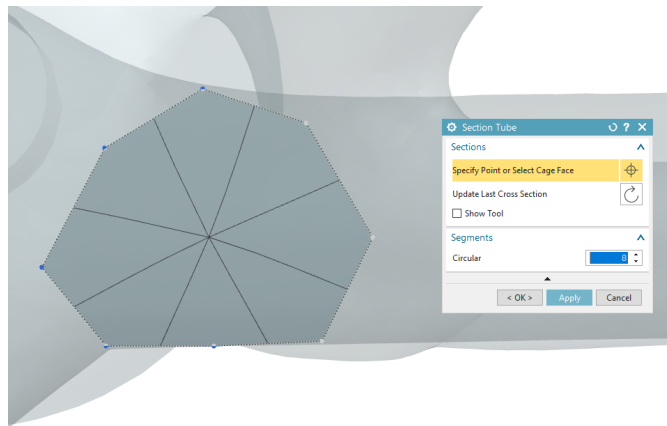
(a) 8 nodes.
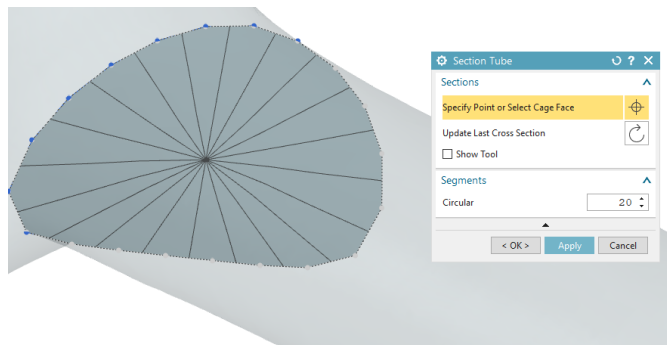
(b) 20 nodes

Figure 3.30: NX section tube number of nodes examples.

A general number used for this project was four, six or eight nodes for the cylindrical connecting rods, and then eight to ten for the more complex shapes. Four were used for the small cylindrical ones since four is easy to connect to one single side face of the bigger ones, as one single face has four nodes. Six would be used for connecting to two faces, since two faces have two shared nodes, resulting in six in total. Eight would be for connecting three faces and so on.

3.4 FEM Verification

The FEM setup in Siemens NX was used to test and benchmark the old design vs the new proposed one, and to validate the final design. As the specific material of the OEM bracket was unknown, it were assumed to be similar to Al6061-T6. The same material were used on the footpeg itself, while the footpeg pin were assumed to be similar to the NX library AISI SS 304 Annealed. The properties of these materials are shown in Table 3.4. A linear structural static analysis similar to the TO setup, and a linear contact analysis including the footpeg were performed. This section will present ideas around the meshing used and then each of the simulation setups.

Table 3.4: The materials applied to the OEM parts in the analyses [ASM (2020), and NX built in library].

Material:	Al6061-T6	AISI SS304 Annealed
Young's Modulus [MPa]	68 980	190 000
Yield Strength [MPa]	275	276
Ultimate tensile Strength [MPa]	310	572
Density [kg/mm^3]	2.71e-6	7.90e-6
Poisson's Ratio [ ]	0.33	0.29
Fatigue Strength [MPa]	96.5	N/A

3.4.1 Mesh

The OEM bracket had some tiny radiuses that interfered with the meshing. It was therefore idealized by the use of synchronous modelling before being meshed. The mesh settings used are shown in Figure 3.31. CTETRA(10) elements were used with 2mm element size. The surface curvature based size variation and small feature tolerance were set to lower values than default, due to this making the mesh skip some of the details in the geometry that were not possible to idealize for ease of calculations. Internal mesh graduation is a setting that lets you choose how much the mesh grows throughout the internals of the models volume. A low value was used as this makes the mesh size stay closer to constant throughout the model. A too low value were however not used as it makes the calculations more computationally heavy. Minimum two elements through thickness is generally advised to use to secure that the mesh calculates values efficiently through different thicknesses. Auto fix failed elements was used as this makes NX try to re-mesh bad element areas itself. It does this by reducing the element size and re-meshing until it is satisfied with the resulting mesh.

The bracket was assigned two RBE2 elements in the mounting holes connecting the surface of the screw head area to the rear where the bracket is fixed against the sub-frame. A similar element is applied to the footpegs mounting holes to apply the load similarly to the case used in the TO task. A RBE2 element were also applied to each of the luggage mount holes to distribute the loads across the faces of these mounting points.
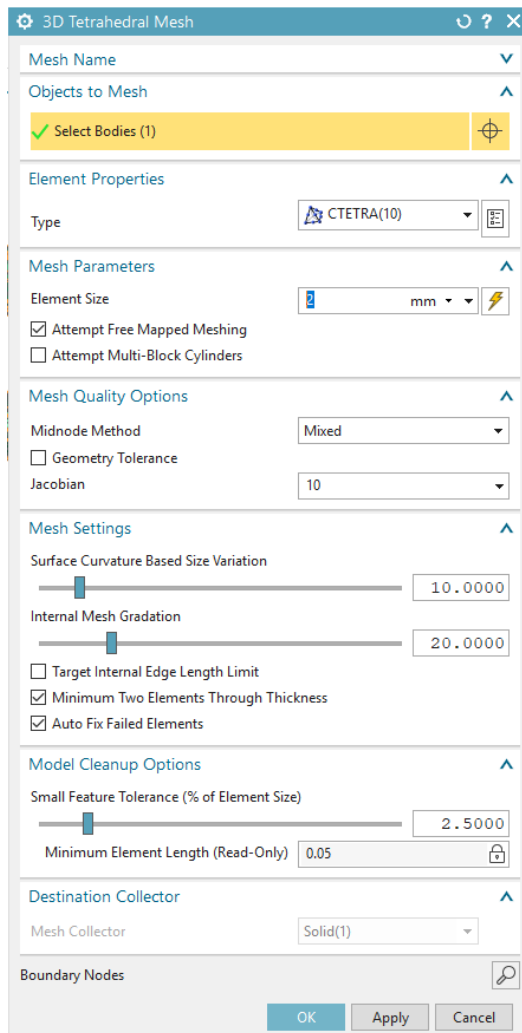
Figure 3.31: Mesh settings for the OEM bracket.

3.4.2 Structural Static Analysis - NX SOL101

The basic structural analysis was performed with the load case used in the TO tasks, as shown in Figure 3.32. The original load given by Ducati, being 1700N in the negative Z-direction, and the luggage loads of 200N. The 1700N load was in this case applied to the RBE2 element connected to the footpeg mounting holes. General FEM task settings are shown in Table 3.5. This type of setup were applied to the TO designed parts as well, with the goal of verifying the assumptions taken from the direct stress results of the TO task. The TO bracket used the AlSi10Mg material as it had in the TO task, previously shown in Table 2.2.
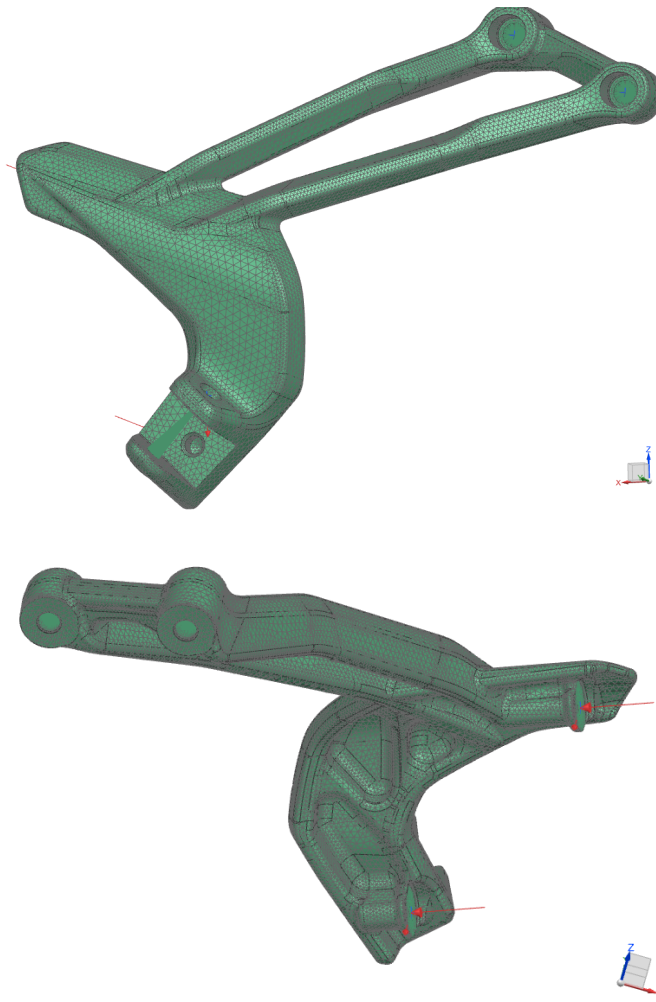
Figure 3.32: NX SOL101 setup with TO style loads.

Table 3.5: Settings for the structural static analysis of OEM bracket in SOL101.

Settings:	
Material	Al6061-T6
E Modulus	68.9 GPa
Poisson Ratio	0.33
Density	2.71e-9 tonne/mm^3
Element Type	CTETRA(10)
Element Size	2 mm
Load Case 1	1700 N in the negative z-direction applied in footpeg hinge
Load Case 2	200 N normal and parallel to the luggage mounting holes
Constraints	Fixed in mounting holes

3.4.3 Linear Contact Analysis - NX SOL101

A linear contact analysis was set up in NX SOL101 to simulate the assembly of the footpeg bracket, footpeg itself and the pivot pin connecting them. This analysis made it possible to have the load on the actual footpeg, as per the original load case given by Ducati. The setup applied to the OEM footpeg bracket is shown in Figure 3.33a. The meshes for the OEM bracket and the footpeg had identical settings as the OEM bracket in the previous analysis. The pivot pin had a mesh with smaller element size, due to the component being a much smaller component than the others, as shown in Figure 3.33b. The friction coefficients used in the surface-to-surface contacts are shown in Table 3.6. Zero gaps and penetration were chosen for the initial parameter. The load of 1700N in the negative Z-direction was assigned to a mesh point on the footpeg 15mm from the inside of it. A fixed constraint was set in the mounting points, as in the previous analysis.

Table 3.6: Friction coefficients used in the linear contact analysis [Engineering-Toolbox (2004)].

Material Combination	Friction Coefficient []
Aluminium - Aluminium	1.1
Aluminium - Steel	0.61
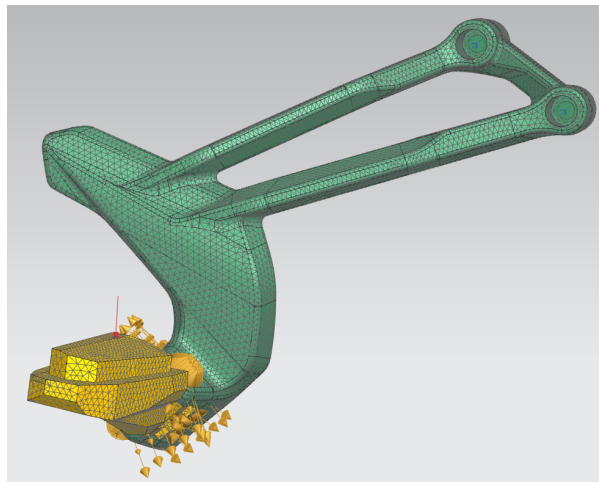
(a) Setup.
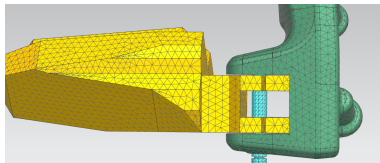
(b) Side view of the three different meshed components at connection point.

Figure 3.33: The NX SOL101 contact analysis setup.

3.5 DfAM

Siemens NX CAM tools for AM were used to check how the model would fare when it comes to overhang angles and support structure. These were also combined with Autodesk Netfabb to get an example of how the part looks with support structure. This section presents the print directions used for the self-supporting constraints, and how they were found.

3.5.1 Print Direction

An important factor for optimizing for additive manufacturing is finding an optimal print direction. There was also a need to decide on a printing direction, since the topology optimization can take it into account when optimizing the design. If one looks at the design space, some printing directions can seem logical. Two examples are shown in Figure 3.34.

(b) Frame mounting point.

(a) Footpeg mounting point area.
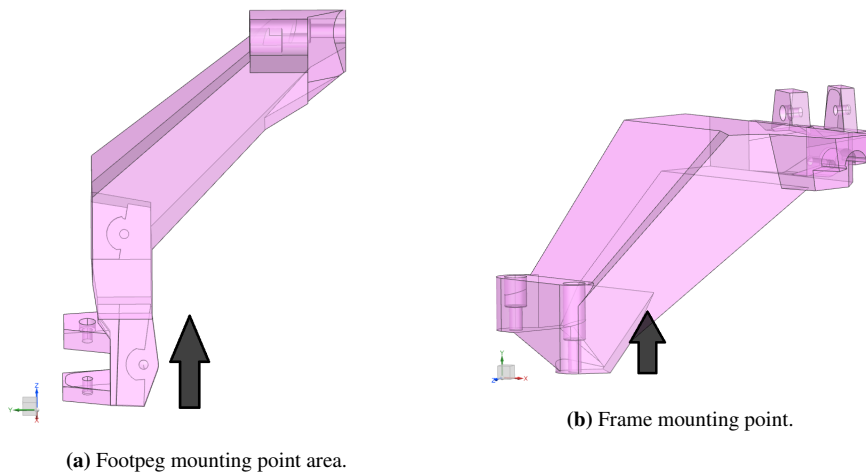
Figure 3.34: Two different printing directions based on design space.

Figure 3.34a shows an example that could be a decent approach based on the design space, but the smallest section of the part is now the base of the print. The overhang with the two mounting points are not a big problem angle wise, but the potential weight of the overhanging parts could cause support structure to be needed anyhow, due to the size of the base. This orientation would also cause the part to have its weakest axis, Z, close to parallel with the load direction.

The example in Figure 3.34b would have issues with overhang angle between the two mounting holes being under $45°$ as shown in Figure 3.35. This angle is $25°$ and would need support structure. A fix for this could be to alter the mounting points to the frame so that they lay in the same plane, but this would also need modifications to the frame of the bike. For this project the main focus was to create a part that fits the current Multistrada

1260. The overhanging of the structure could also end up with its center of gravity far enough out from the base, for it to not be able to make the structure self supporting.
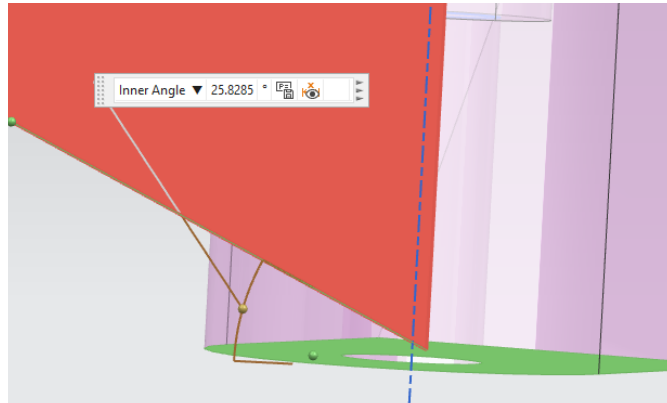
Figure 3.35: The angle between the two frame mounting points.

Siemens NX has an additive manufacturing direction command that tries to find the optimized printing direction for a part. It was applied to the final TO results from the weight target comparison, optimizing for minimal support structure and print time. The optimization returned several different resulting directions with different weightings, with two of the top-weighted orientations being shown in Figure 3.36. These two orientations will be used in self-support criteria on the weight target area that is chosen in the next chapter. The resulting geometries from it will be used to create the final design. The printing directions will be referenced as SS1 for Figure 3.36a and SS2 for Figure 3.36b.

(a) The first printing direction (SS1).

(b) The second printing direction (SS2).
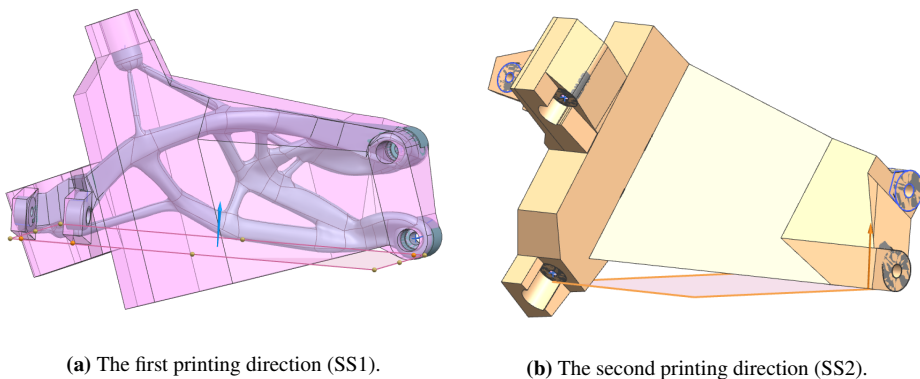
Figure 3.36: Printing directions used for the self-supporting constraints.

3.5.2 Printing Entire Assembly VS Bracket Alone

The printing of the entire assembly as one was a feature that could potentially optimize the part related to DfA. Hinges are possible to produce directly in AM, but the clearance around the rod have to be within 0.3-0.5mm. This were not found to be sufficient for this case when looking deeper into the tolerances of a lock pin setup. A typical pivot pin that is used to mount the footpeg has diameter clearence tolerances at a tenth of this [Misumi (2014)]. This means that the clearance needed to print the footpeg setup as a complete assembly with a functional hinge, would not be vial for the current footpeg pin setup. If the clearance between the footpeg and the pin is high, the fitment of the part might not be up to par of what is expected by the user from a brand such as Ducati. Leaving the hinge out all together were also an option, but this would cause the bike to not conform with the EU regulation about the footpeg being able to freely rotate or fold. The decision was therefore to focus on printing the bracket alone for this project.

Chapter 4

Results

This chapter presents the results of the simulations, CAD redesigning and FEM verification. It also has some discussions through the iterations based on the first results regarding choice of convergent model, solid model generation and redesign after FEM verification.

4.1 Topology Optimization

This section will first present graphs and tables of the different TO tasks and their results. These values will be used to argument for which weight target area to go for and other settings. Afterwards, the geometry of the models from the TO task will be analyzed, and the final model and design ideas chosen for further analysis will be presented.

4.1.1 Settings Comparison and Weight Targets

The results from the Siemens NX TO tasks are located in Table 4.1, and some of the data will be presented in graphs further down. Here the direct results of max displacement and Von Mises stress from the TO tasks were gathered to use as a guide of performance. These results are not entirely correct, which will be seen in later sections, but accurate enough to find areas of potential limits of weight reduction. These TO tasks had all the same material, AlSi10Mg, and no material spread or self-support constraints.

The graph of the displacement from the TO results related to the weight reduction shown in Figure 4.1, shows a high increase in displacement after the 300g mark. This increase is especially noticeable between 250g and 200g. The displacement values themselves are all below 2mm, and therefore not of the biggest concern for the bracket in this case.

A similar increase can also be seen at the 300g mark in the stress graph shown in Figure 4.2. The weight targets of 250g and 200g are also getting close to the yield stress of AlSi10Mg, shown with the orange line. The 200g result ended up having lower max stress than the 250g, but these max values have some inaccuracies as will be shown.

Table 4.1: Table of TO results with weight targets from 550g to 200g.

Weight Target [g]	Accuracy [mm]	Max Stress [MPa]	Displacement [mm]	Weight Result [g]
550	9.66	111	0.665	555.0
500	9.50	115	0.701	508.1
450	7.00	144	0.746	458.3
400	7.50	179	0.838	405.1
350	6.50	188	0.956	353.5
300	6.20	192	1.110	303.9
250	6.10	232	1.410	251.8
200	6.05	217	1.970	197.3
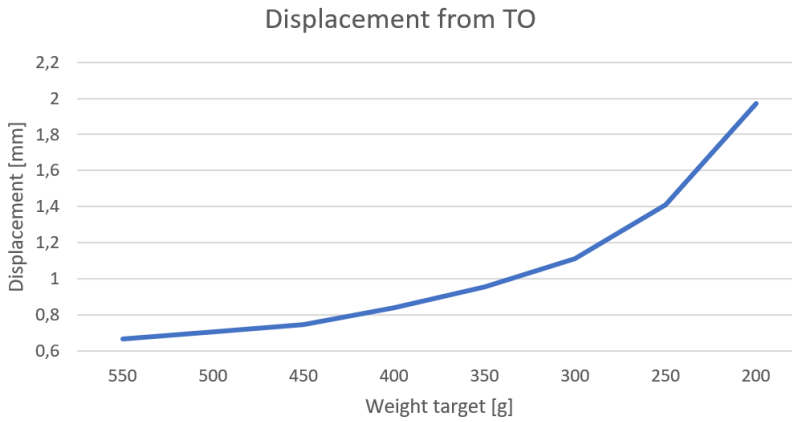
Figure 4.1: Max displacement from the different weight targets in the TO task.
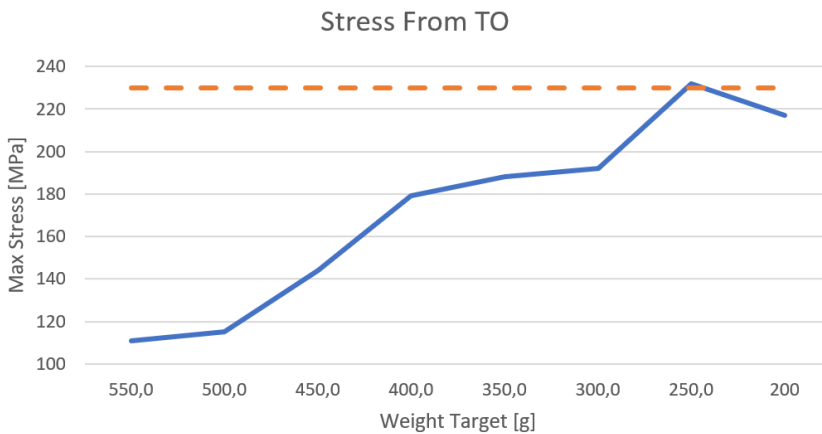
Figure 4.2: Max stress from different weight targets in the TO task and orange yield limit.

Figure 4.2 also has a high increase in max stress from 500g to 400g, but this was still not close to the yield stress. The stress is however not consistent in these higher weight targets, as can be seen in Figure 4.3. It shows the max stress changing with the accuracy. The lower accuracy simulations are the ones from Table 4.1, while the higher accuracy ones are using an accuracy of 6.5mm. The high accuracy simulations had a higher maximum stress value compared to the lower ones, except for the 400g weight target. Figure 4.4 shows the max stress values plotted with the high accuracy settings, showing that the stress increase is more even until the 300g weight target, compared to Figure 4.2.
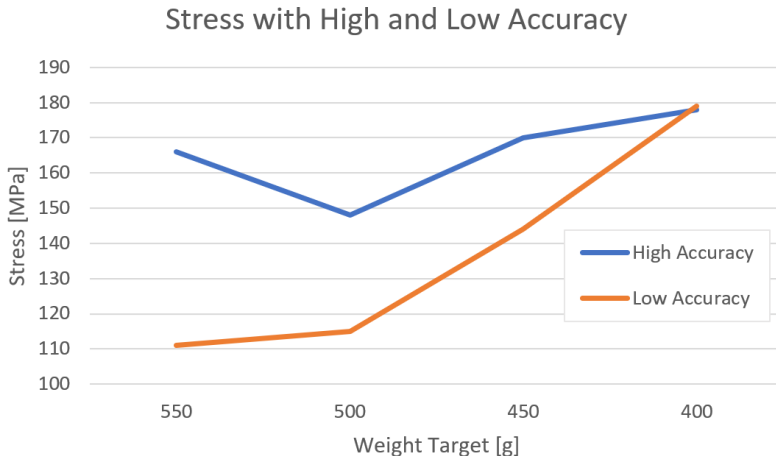
Figure 4.3: Comparison of stress of different weight targets with high and low accuracy.

Figure 4.4: Max stress from different weight targets with high accuracy settings and orange yield limit.

The displacement stayed almost the same for high and low accuracy, as one can see in Figure 4.5. The same were true for the weight which all were within 5g between high and low accuracy. This were expected as the TO task is optimizing the component for a specific weight target while minimizing strain energy, which in turn also is about minimizing displacement. The weight targets lower than 400g were not used in this accuracy comparison, due to them already being high accuracy simulations. They would also not converge and return results with low accuracy settings.
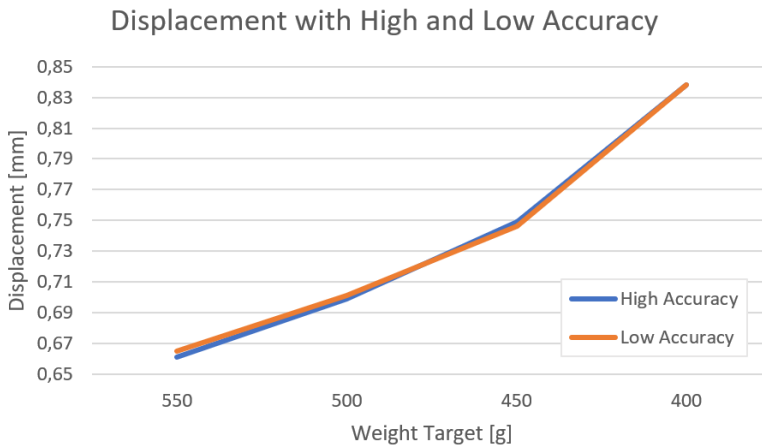
Figure 4.5: Comparison of displacement of different weight targets with high and low accuracy.

The inaccuracy in the stresses is difficult to find an exact reason to based on the direct TO results. It is however a reoccurring theme in all the TO results that the highest stress region is located in the mounting point to the frame as shown in Figure 4.6. The rest of the stress results are only described by the colored scale on the model without specific numbers.
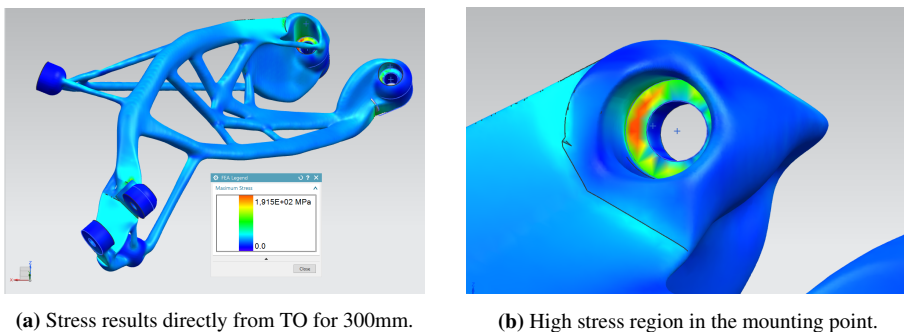
(a) Stress results directly from TO for 300mm.

(b) High stress region in the mounting point.

Figure 4.6: High stress region and point shown in a two weight target result.

Other things that were found is how the simulation time increases with the increased accuracy, as shown in graph 4.7. It changes linearly, but the time increase per mm accuracy is rather big.
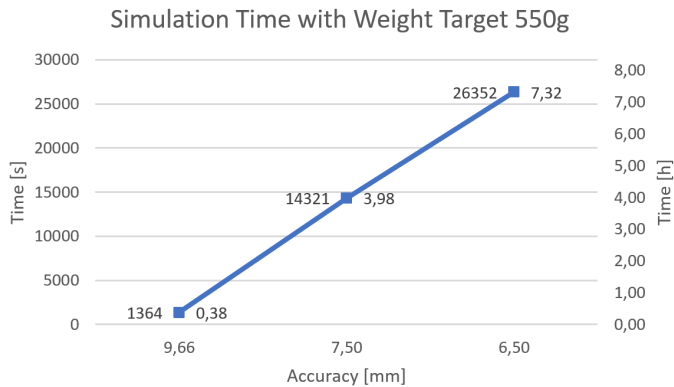
Figure 4.7: TO simulation time with different levels of accuracy.

The time increase caused the material spreading test located in Table 4.2 to be tested using a high weight target of 550g, since it was then possible to have a lower accuracy, and hence lower simulation time. Four different levels of material spreading were tested, 0%, 35%, 50% and 70%. The results from 50% were discounted, due to the optimization returning a model with a discontinuity that resulted in 3.68km of displacement. The only thing drawn from these results was that material spreading itself do not seem to give any significant performance increase for this case. The complex structures could also be harder to manufacture. For this project material spreading were therefore not used further on.

Table 4.2: Table of Material spread test in NX TO with 550g weight target.

Material Spread [%]	Accuracy [mm]	Stress [MPa]	Displacement [mm]	Weight Target [g]
0	7.5	166	0.661	558.6
35	6.5	140	0.662	564.7
70	6.5	151	0.717	549.4

Self-Supporting was applied to the weight target of 350g. Table 4.3 shows the comparison of the results from with and without self-supporting in different directions. SS1 and SS2 are the print directions from Section 3.5.1. The self-supporting results had lower max stress, and a tiny increase in weight. The physical results are of bigger importance in this case, and will be looked further into in the end of the following section.

Table 4.3: Table of TO results with different self-support settings.

Weight Target [g]	Self-Support []	Accuracy [mm]	Max Stress [MPa]	Displacement [mm]	Weight Result [g]
350	No	6.50	188	0.956	353.5
350	SS1	6.50	158	0.957	358.9
350	SS2	6.50	164	0.967	358.1

4.1.2 Convergent Models

In this section the actual models from the TO tasks will be analyzed. This is to further investigate the decisions taken from the previous section, and to find the common structural elements in the different results. They will be compared by doing low and high accuracy for the weight targets from 500g to 400g, and then comparing one weight target to the next for the lower weight targets. At last the self-supporting geometries will be analyzed.

500g: 9.5mm vs 7.5mm (Figure 4.8): The main difference between these two is thickness related. 7.5 mm is thicker in the footpeg mounting area, while 9.5mm is generally thicker in the cylindrical members in the geometry. The structure is so close to identical in this case that not much is to draw from the differences.

(a) 9.5mm accuracy.   **(b)** 7.5mm accuracy.
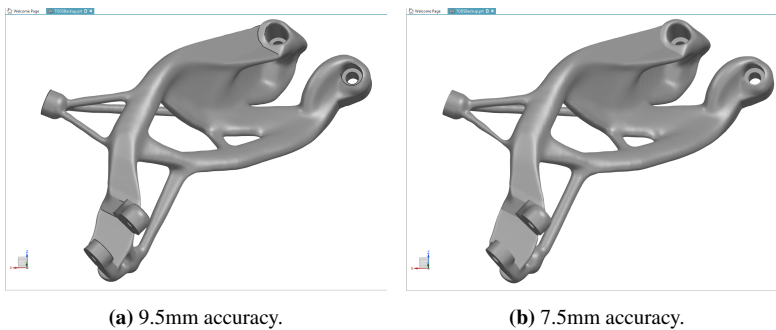
Figure 4.8: 500g convergent models with different accuracy.

450g: 7mm vs 6.2mm (Figure 4.9): Both these follow up on the general structure of the 500g simulations. The structure has more holes in its main section for both results, with bigger holes in the 7mm compared to the 6.2mm. The 6.2mm one has a thinner structure in general. The structure has a uniqueness with the rod connecting the two mounting points. In the 6.2mm one can also see the beginning of two more rods. They have almost identical weight and displacement, and the stress is higher for the 6.2mm one when compared with the numbers from previous section.

(a) 7.0mm accuracy.   **(b)** 6.2mm accuracy.
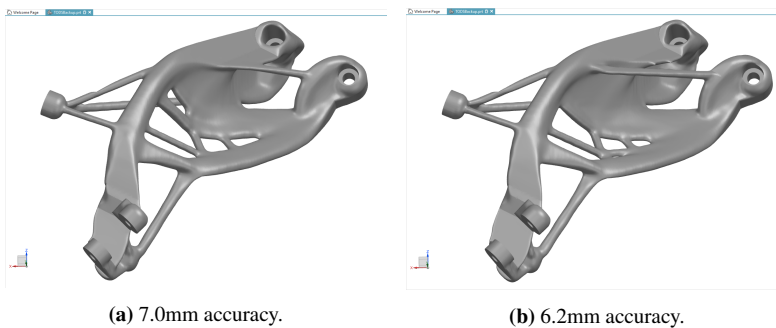
Figure 4.9: 450g convergent models with different accuracy.

400g: 7.5mm vs 6.5mm: The weight target of 400g shown in Figure 4.10 yielded a little bit different results than the earlier comparisons. The 6.5mm created two main rods from the upper mounting point to the footpeg mounting point. The rest of the structure is therefore thinner since they are aiming for the same weight target.

(a) 7.5mm accuracy.
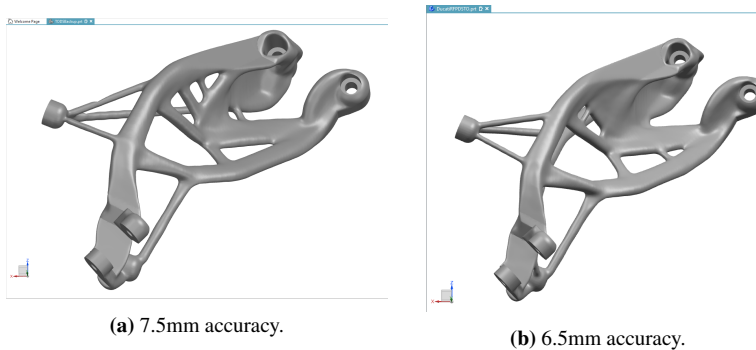
(b) 6.5mm accuracy.

Figure 4.10: 400g convergent models with different accuracy.

350g (6.5mm) vs 300g (6.2mm): The tasks are only performed at one accuracy for each weight target at this point. Therefore, the two following weight targets are compared instead. The 350g and 300g weight targets, shown in Figure 4.11, are very similar. The 300g result is in general thinner, and has two extra holes created in the center. It also created an extra rib in one of the holed out sections.

(a) 350g with 6.5mm accuracy.

(b) 300g with 6.2mm accuracy.
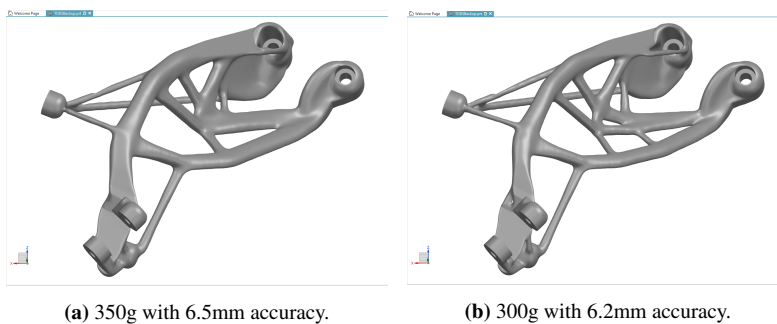
Figure 4.11: 350 and 300g convergent models.

250g (6.1mm) vs 200g (6.05mm): 250g and 200g were the last weight targets used in the weight target simulations, mainly due to them getting close to the yield stress. This were also due to further decreases in weight resulting in non-convergence with the accuracy limit of 6mm. They clearly have a lot of similarities to the 300g result when comparing these to the earlier results. The 250g result has a more strut like structure around the upper mounting point, and the geometry of the rear accessory mount's rods has shifted it's position slightly higher up on the bracket. The 200g result goes further into the strut like appearance and has an unique design for the rear accessory mount.

(a) 250g convergent model with 6.1mm accuracy.

(b) 200g with 6.05mm accuracy.
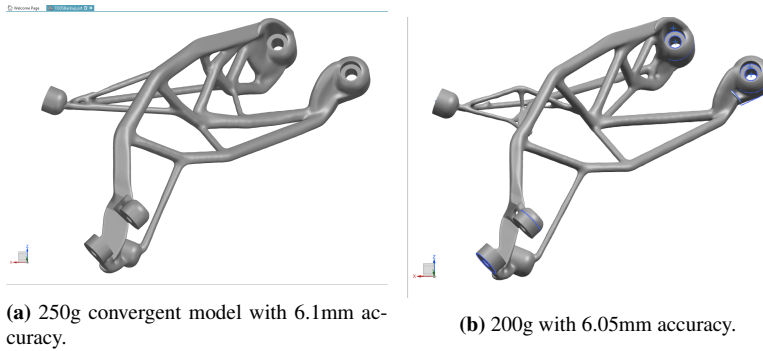
Figure 4.12: 250 and 200g convergent models.

Stress results: The stress results for 200g vs 300g are shown in Figure 4.13. It shows that the 200g one has averagely higher stress in the entire model compared to the one with 300g. This is to be expected, but one could try to estimate the stress values for these models. NX TO does not give exact values for anything but max stress directly. Based on max being 217MPa for the 200g one, and by assuming a linear increase, would put most of this structure up under the 100MPa area. That is the area of the fatigue stress at 97MPa from Section 2.2.7. The 300g result would for the most parts lay lower than this at around 70MPa, since the max stress here is 192MPa and the coloring is in the darker blue regions. These are coarse estimates, but work as an argument towards staying in the 400g to 300g range for the final model. The stress results directly from the TO task can also be optimistic. Especially, since the load case is simplified by not having the load on the actual footpeg.

(a) 300g with 6.2mm accuracy.

(b) 200g with 6.05mm accuracy.
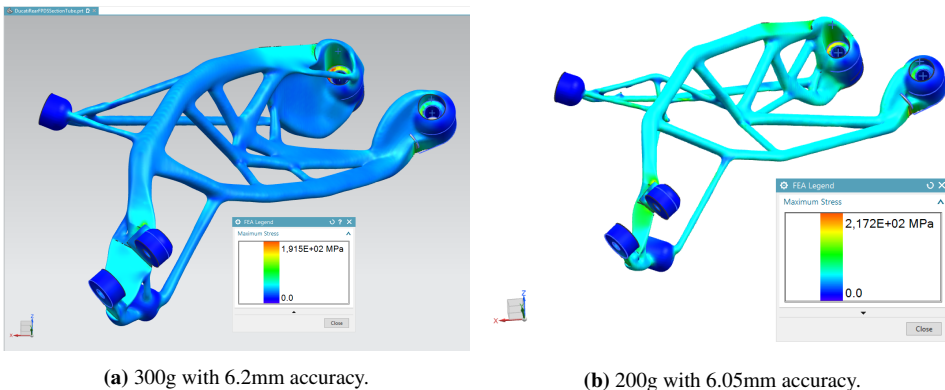
Figure 4.13: 300 and 200g convergent models showing stress.

Self-Supporting: The results of the simulations with self-supporting constraints for the final weight target of 350g are shown in Figure 4.14 and 4.15. The datum planes in Figure 4.15 are illustrating the planes that were set as the build plates for the self-support constraints. A big difference in both, compared to the ones without self-supporting, is that the structure going from the left mounting point of the frame, to the footpeg is now split into two main rods. This could potentially stiffen the model in these areas. Figure 4.14a does also have a more gridlike structure close to the frame mounting point compared to the other results. This area were in previous results one piece of solid material for most weight targets. A potential issue especially noticeable in Figure 4.15a, is that one of the rods going to the accessory mounting point in the upper left of the figure has a thin structure.

(a) Self-supporting constraint 1.

(b) Self-supporting constraint 2.
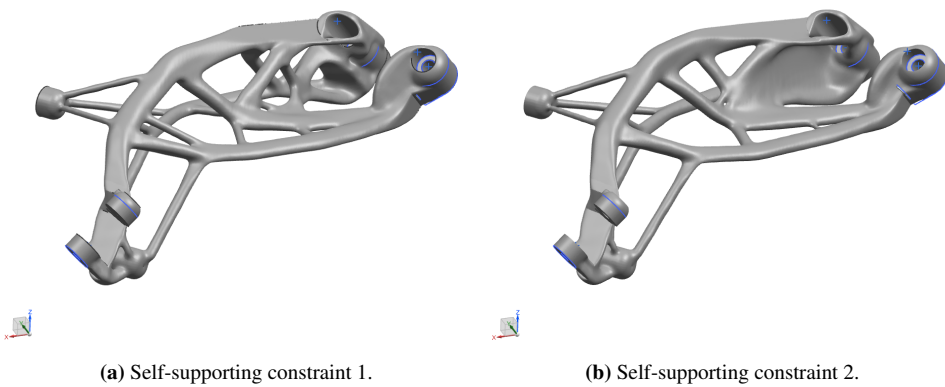
Figure 4.14: The two self-supporting constraint 350g models from an isometric view.

(a) Self-supporting constraint 1.

(b) Self-supporting constraint 2.
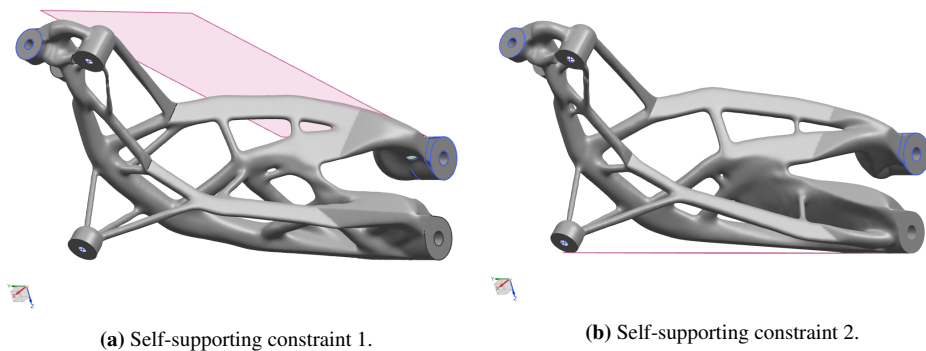
Figure 4.15: The two self-supporting constraint 350g models from a rear view.

4.1.3   Final Design Proposal

A definite final model was not chosen for this step based on the results in previous section. Instead, the decision was to go for the 350g one from the 400g to 300g interval. This one should then be combined with ideas from the other ones to create an overall best model in the CAD Redesign phase. The 350g weight target also contained most of the general structure that was present in the different TO tasks. This were found by overlaying the different weight target results with each other, and a simple illustration shown with blue lines can be seen in Figure 4.16.
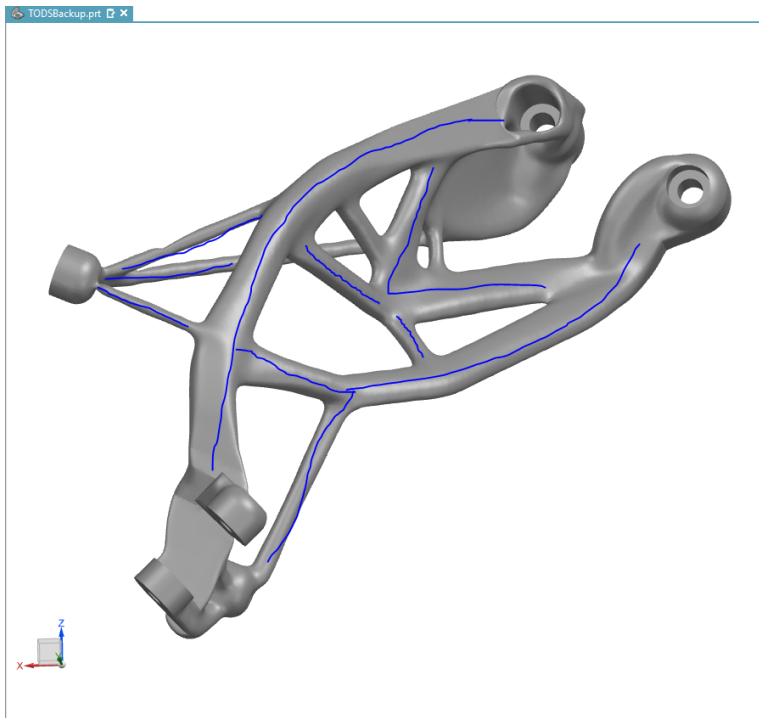
Figure 4.16: The general reoccurring structure illustrated with blue lines on the 350g weight target.

A static analysis, as per Section 3.4.2, was performed on a solid model of the 350g weight target, before comparing it with the self-support constraint results. The stress results are shown in Figure 4.17. This model is within the yield stress, but it has a stressed region that is above the fatigue stress towards the mounting point of the footpeg, shown with green/yellow in the figure. The same area is where the part's displacement starts to increase. This area could potentially need stiffening to further improve the part.

350SolidModel_sim1 : Solution 1 Result
Subcase - Static Loads 1, Static Step 1
Stress - Elemental, Von-Mises
Min : 0.06, Max : 183.76, Units = MPa
Deformation : Displacement - Nodal Magnitude

183.76
168.45
153.14
137.84
122.53
107.22
91.91
76.60
61.29
45.98
30.67
15.37
0.06

[MPa]
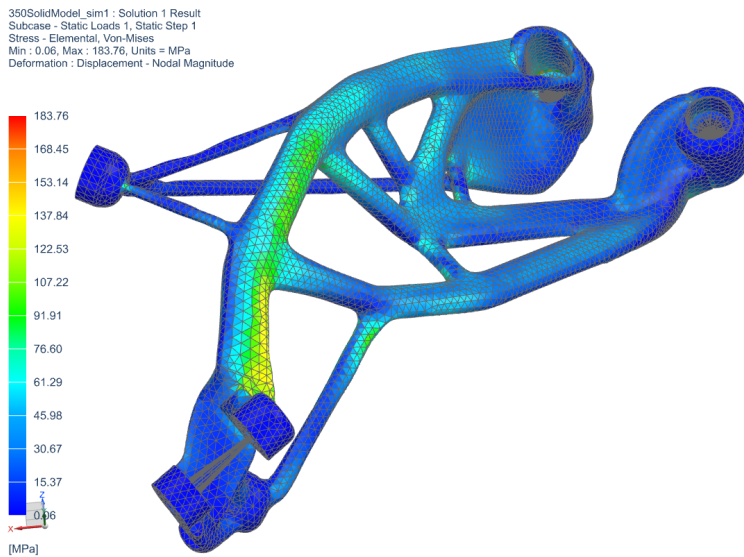
Figure 4.17: Stress result of the 350g weight target without self-support constraint.

A potential solution can be seen when comparing the backside of this area with the results from the self-supporting constraint, as seen in Figure 4.18. It shows that the design idea from the self-supporting constraint in Figure 4.18b, could potentially improve the stiffness in this area compared to the other. The extra material added here seems to come from removal of material in the section along the left mounting point, where the component had little displacement and stress.

(a) No self-support constraint.

(b) Self-supporting constraint 1.
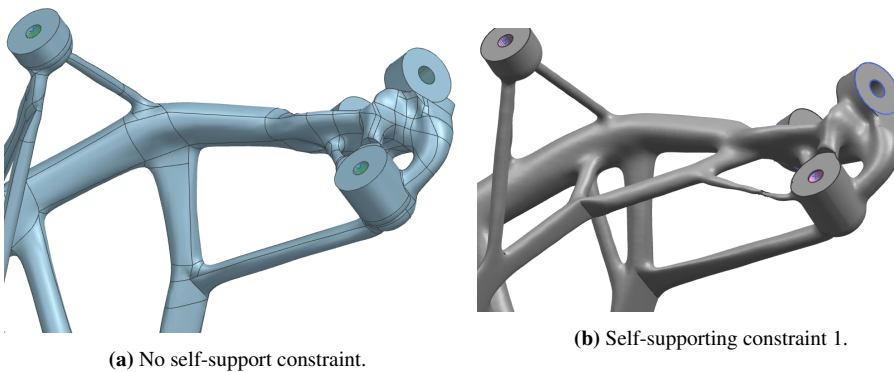
Figure 4.18: Structure comparison between self-support constraint and not.

4.2 CAD Solid Model

The creation of a solid model in NX from the convergent model outputted by the TO task can be performed in several ways, as shown in Section 3.3. This section will contain a comparison of the results of the realize shape and rapid surface model of the 350g weight target. The chosen method were further used on the CAD redesign results of the SS1 constrained model.

4.2.1 Realize Shape VS Rapid Surface

Figure 4.19a is the model created with realize shape. It has some differences to the direct TO results, due to bridging of tube cages not taking the convergent model into account. The weight of this model is 349.3g, compared to 353.5g of the convergent TO result. The model created with rapid surface ended up as shown in Figure 4.19b. This model had a final weight of 357.4g. It kept some of the thin geometry created in the TO task, resulting in stress concentrations as shown in Figure 4.20. This had to be fixed by using realize shape to unite a bigger tube cage to the rapid surface model.

(a) Realize Shape
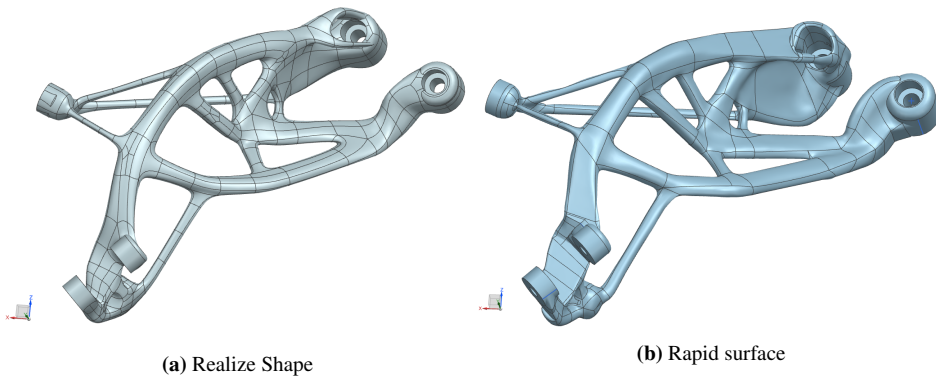
(b) Rapid surface

Figure 4.19: Comparison of solid model of 350g weight target with rapid surface and realize shape.
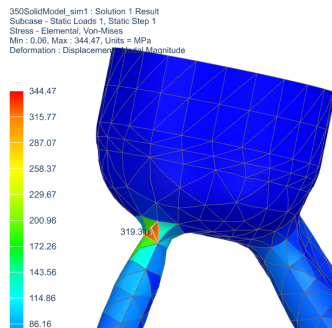
Figure 4.20: High stress region due to low thickness in the rapid surface model.

The realize shape model were made in a fraction of the time of the rapid surface model. Rapid surface had similar modifiability as the direct results from Fusion, while realize shape is more intuitive to modify. The realize shape tools were chosen for further CAD creation, as modification of the models is to be expected in the following stages. Rapid surface is however a brilliant tool for accurately converting facet geometry to solid geometry.

4.2.2 CAD Redesign - Design 1.0

The next model created in the CAD redesign phase, shown in Figure 4.21, is based on the SS1 constrained model. This model have some minor changes compared to the direct TO result. The material above the screw hole area in Figure 4.22a originally had some interference with the mounting screw. It were altered so that the screw should be a drop in fit without problems. A plate for the footpeg to rest against, and thickness on the previously mentioned thin member were altered in the footpeg mounting point, as shown in Figure 4.22b. Figure 4.22c shows how the footpeg rest against the plate.
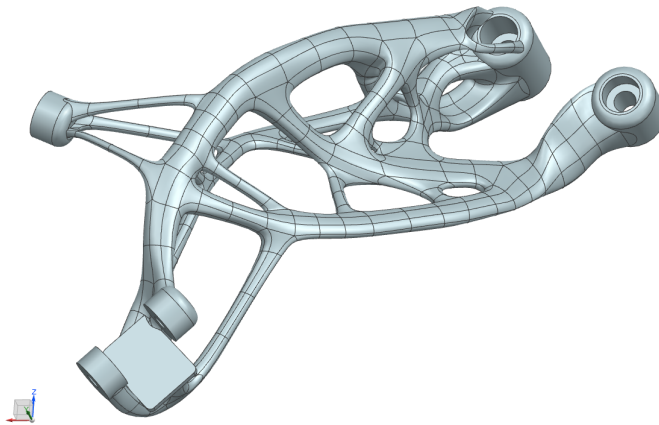
Figure 4.21: Solid model of 350g SS1 constrained result.
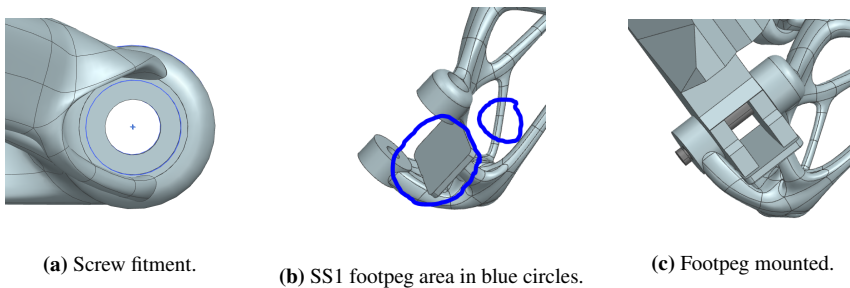
(a) Screw fitment.   **(b)** SS1 footpeg area in blue circles.   **(c)** Footpeg mounted.

Figure 4.22: Design changes to the SS1 solid model.

4.3 OEM Benchmark and FEM Verification

4.3.1 Singularity Checks

This section will present the singularity check method used throughout the following results. Some of the results from the structural static analysis had concentrated high stress zones, as for example the OEM component shown in Figure 4.23. It shows that the highest stress of 524MPa is located in an element along the edge in the mounting hole. This could come from a singularity, and a finer mesh was assigned with mesh control in this local area to check for potential singularities.
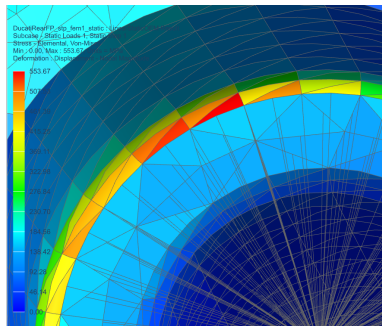
Figure 4.23: The potential singularity area around the mounting point.

A new analysis was performed with the finer mesh shown in Figure 4.24a. The resulting stress has a max stress of 881MPa, as shown in Figure 4.24b. The shown high increase is concentrated in one element, compared to the lower stressed elements around it. Another iteration with even finer mesh could help support this being a singularity. This type of singularity check have been used throughout this project, and it will not be as documented as in this case every time. A thing to note about this singularity is that it is in the same area as the high stressed region in the TO results from Figure 4.6b.
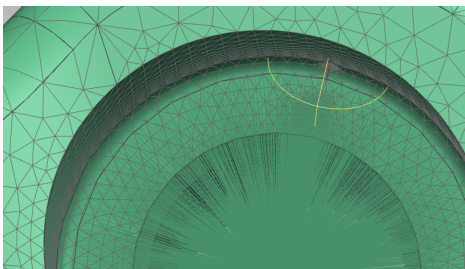
(a) The finer mesh applied to check for singularity.
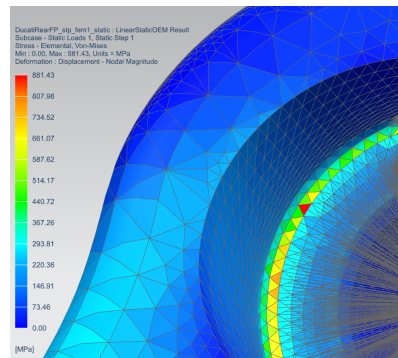
(b) The single high stressed element with finer mesh.

Figure 4.24: Singularity check by adding finer mesh.

4.3.2 Structural Static Analysis - OEM

The results of the structural static analysis of the OEM bracket with TO load setup is shown in Figure 4.25 and Figure 4.26, showing stress and displacement respectively. The max displacement in this case had a value of 5.785mm. The stress results had a singularity in the mounting point, and the max stress without it was the red section close to the mounting point. It exceeded yield with a max stress of 320MPa.
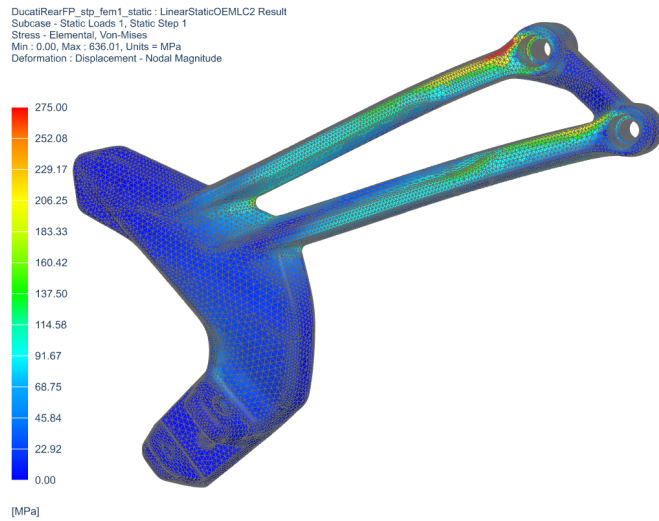
Figure 4.25: Stress from structural static analysis with TO loads and yield limit of 275MPa.
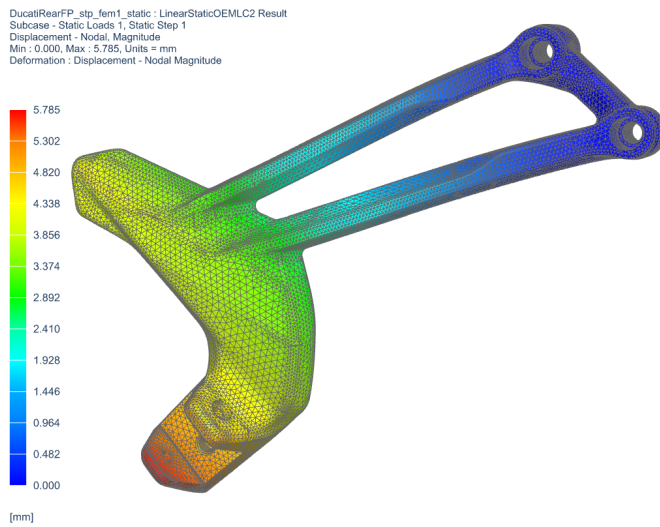
Figure 4.26: Displacement from structural static analysis with TO loads.

4.3.3 Structural Static Analysis - CAD Redesign

This section shows the results from the static analysis of design 1.0 with TO load setup. The stress and displacement results can be seen in Figure 4.27 and 4.28 respectively. It has a max stress of 385.5MPa, located in one element under the left mounting point to the frame. The following high stress elements shown in red exceeds yield with a values of up to 303MPa. The max displacement was 2.431mm, which is lower than the OEM bracket's 5.785mm from Section 4.3.2.
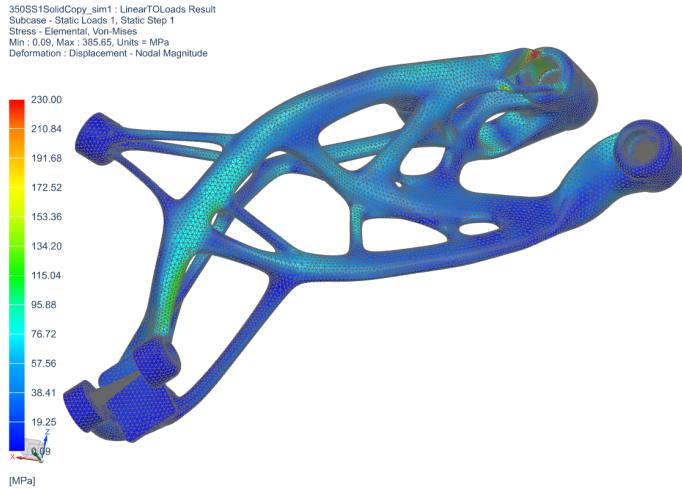
Figure 4.27: Stress results of the CAD redesign with 230MPa yield limit.
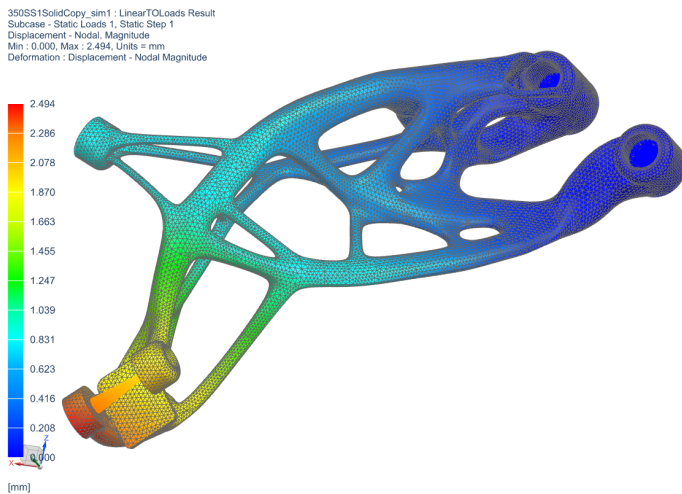
Figure 4.28: Displacement results of the CAD redesign.

4.3.4 Linear Contact Analysis - OEM

Figure 4.29 shows the stress results of the linear contact analysis of the OEM bracket with a yield limit of 275MPa. The high max value of 427MPa comes from a single element at the backside of the left mounting point. The OEM bracket has a section of yield on the upper side seen in red, maxing out at 303MPa. Figure 4.30 shows the displacement of the same analysis, maxing out at 6.95mm. The contact results are shown without the other components to avoid the displacement being shifted higher. A small displacement in the footpeg mounting point would come out as a higher displacement on the tip of the footpeg.
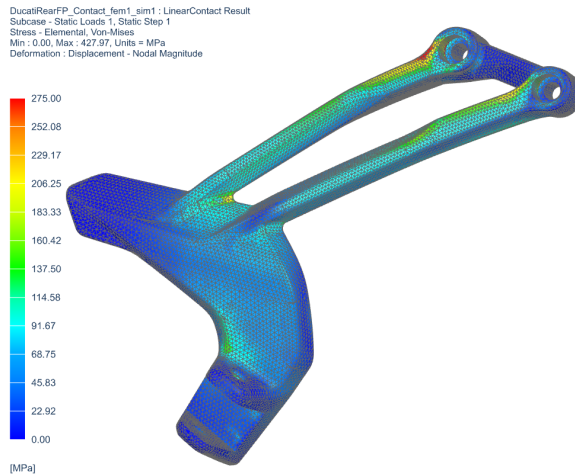
Figure 4.29: SOL101 linear contact analysis stress results of OEM bracket with 275MPa yield.
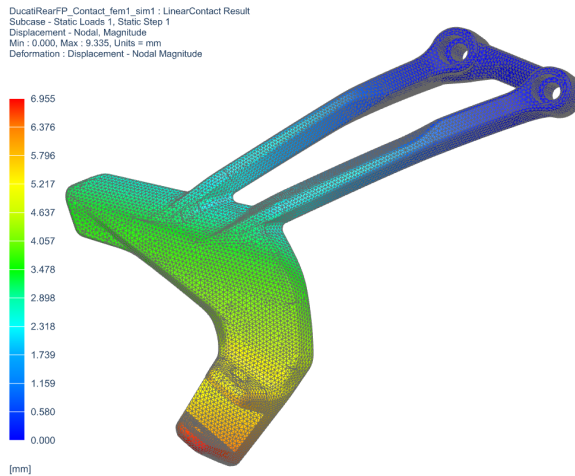
Figure 4.30: SOL101 linear contact analysis displacement result of OEM bracket.

4.3.5 Linear Contact Analysis - CAD Redesign

Figure 4.31 shows the stress results of the linear contact analysis of the design 1.0 bracket. It has several areas that are above the yield stress shown with red. It also has a lot of areas that exceed the fatigue stress. The OEM component did also exceed fatigue stress in certain areas, but not to the degree of these results. The displacement shown in Figure 4.32 is however with a max value of 5.208mm, which is lower than the OEM bracket.
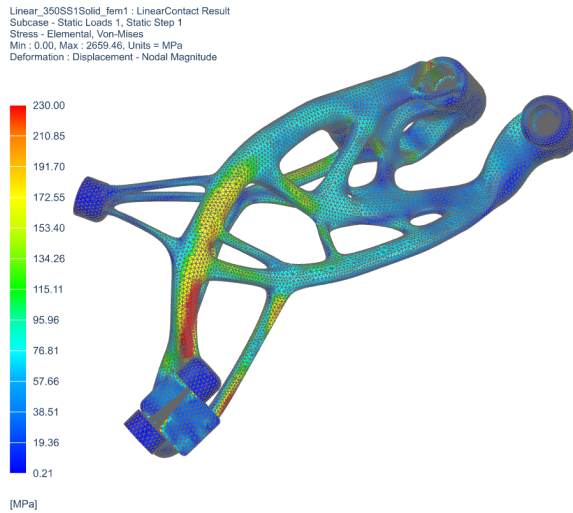
Figure 4.31: SOL101 linear contact analysis displacement result of CAD redesign bracket.
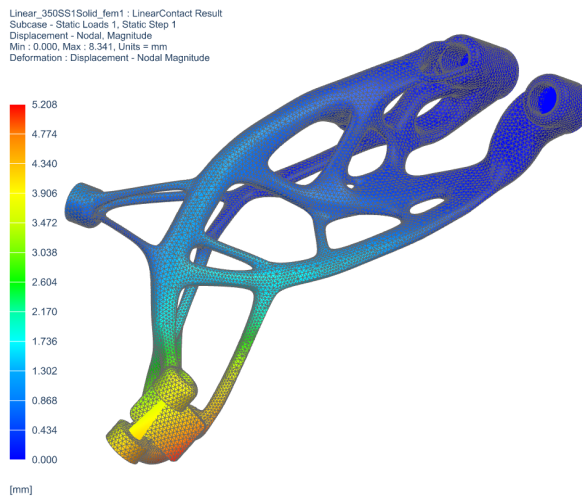
Figure 4.32: SOL101 linear contact analysis displacement result of CAD redesign bracket.

4.4   Post FEA - Design 2.0

The previous stress and displacement results of the TO designed part, proved that it needed further enhancements to lower its stresses. Several iterations of adjusting the cross sections were performed to improve the stress results. The footpeg mounting area's plate was made bigger, and the transitions from it to the mounting points were made less steep, as shown in Figure 4.33a. Fillets were also added to several of the areas where the subdivision body from realize shape unites to other solid geometry, as seen in Figure 4.33b and 4.33c. This was to ensure smooth connections, and avoid stress concentrations by sharp corners. The resulting geometry is shown in Figure 4.34.

(a) Adjusted footpeg mount area.

(b) Fillets on united geometry.

(c) Fillets added to mounting point.
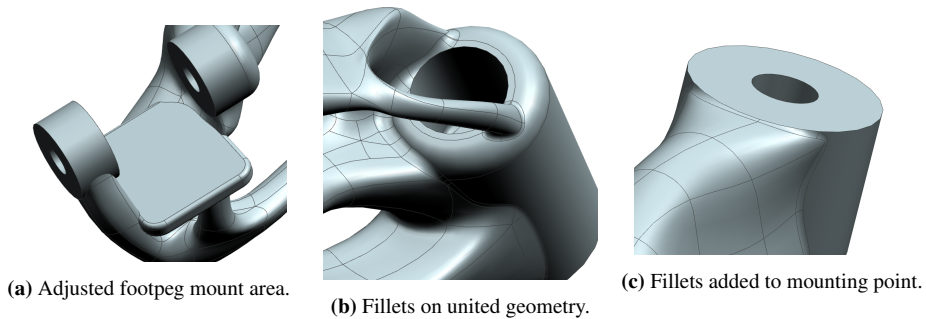
Figure 4.33: Design changes to the SS1 solid model.
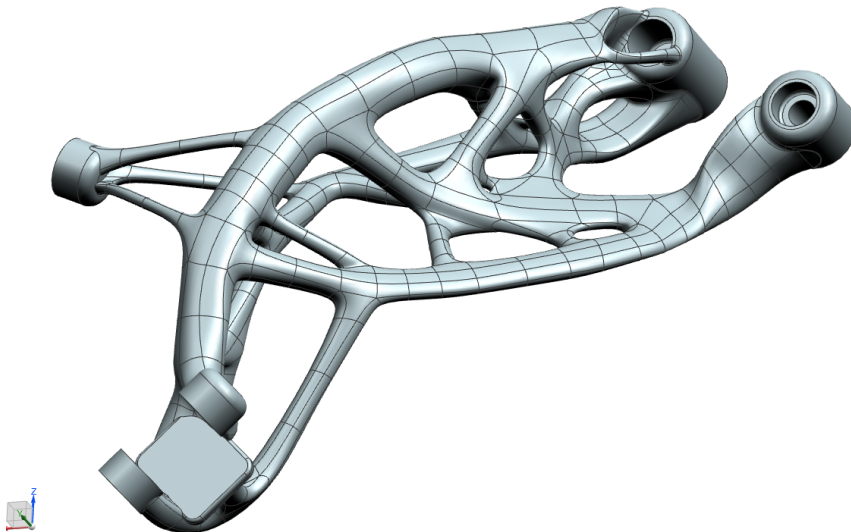
Figure 4.34: The final iteration of the solid model, Design 2.0.

4.5 Final FEM Validation

This section presents the FEA results of the final design in this project, after the design changes in the previous section.

4.5.1 Structural Static Analysis - TO Setup

The structural analysis with load similarly to the TO task gave the stress results shown in Figure 4.35. It has a tiny strip of elements above the yield stress in the upper mounting point, but the rest of the model is below the fatigue stress. This stress distribution is similar to the direct from TO result, aside from a higher max stress at 257MPa. The displacement result shown in Figure 4.36 shows a max displacement of 1.706mm, which is almost twice the amount of the direct from TO result of 0.957mm. It is however lower than the max of 2.431mm from the design 1.0 model.
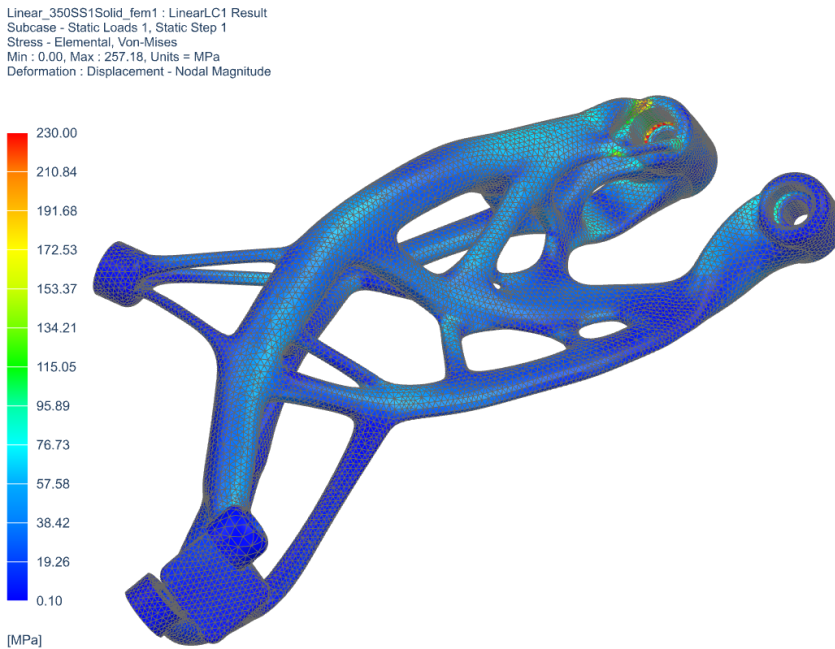
Figure 4.35: Stress results of the structural static analysis of the final design.
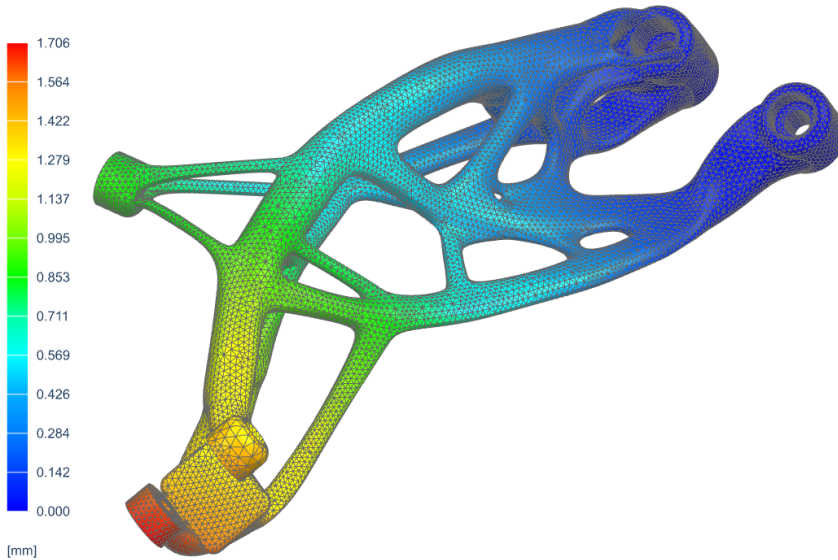
Figure 4.36: Displacement results of the structural static analysis of the final design.

4.5.2 Linear Contact Analysis

The linear contact analysis of design 2.0 gave the stress result shown in Figure 4.37. It has a similar max stress area in the upper mounting point, but is averagely higher stressed than the TO style load case. Most of the model is in the higher light blue area which is just below the fatigue stress. This is a major improvement over design 1.0, which had several areas of yield and lots of sections above the fatigue stress. Some of the areas are above fatigue stress, but the load case used is more of a worst case load case as will be discussed in the next chapter. The displacement result shown in Figure 4.38 shows a max displacement of 2.749mm. This is almost half of the design 1.0 at 5.208mm, and even lower compared to the OEM's 6.955mm.
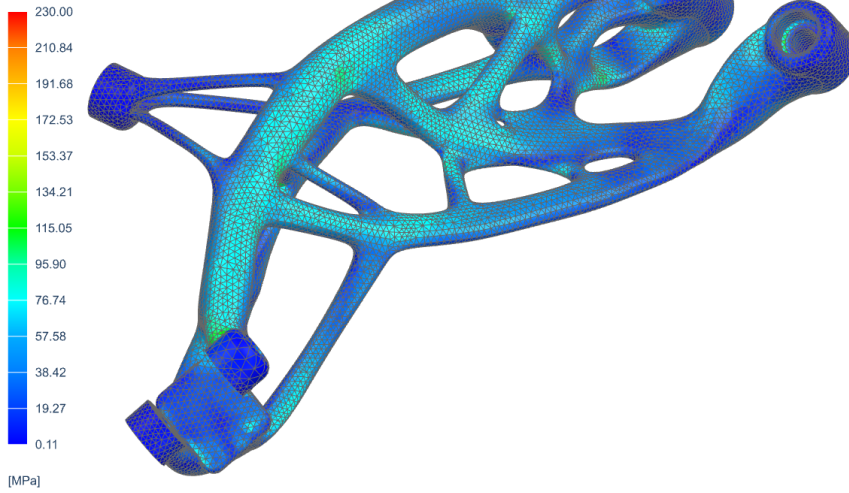
Figure 4.37: Stress results of the linear contact analysis of the final design.
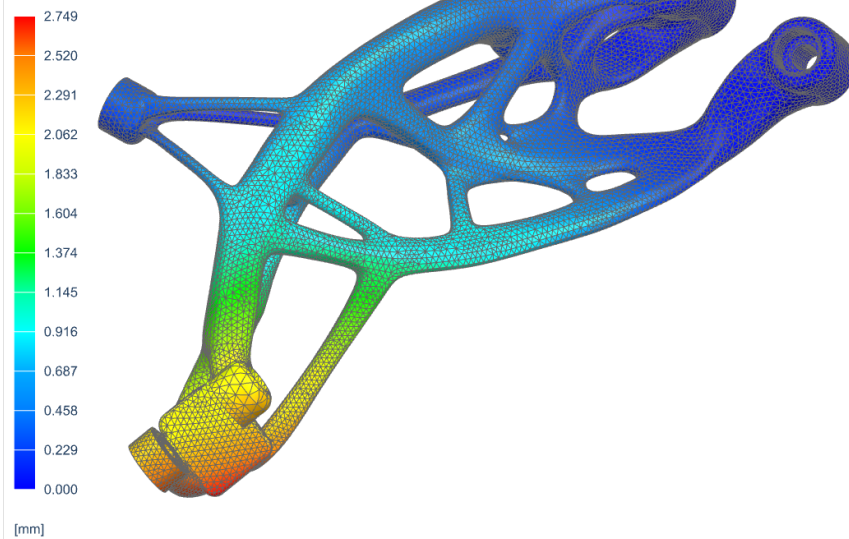
Figure 4.38: Displacement results of the linear contact analysis of the final design.

4.6   DfAM

The final model were ran through Autodesk Netfabb's scripts for printing directions and support structure generation for an EOS M280 SLM machine with AlSi10Mg. This script proposed a new printing direction as the optimal, shown in Figure 4.39a. The SS1 direction was also set up in the software, as shown in Figure 4.39b. Table 4.4 shows the values for these directions used in the printing direction ranking in the software. A reason for the new printing direction in Netfabb, compared to the SS1 from NX, could come from the SS1 direction utilizing a large area that are close to the limits of the printer bed. It does also use almost twice as much support material, but creates a component with lower center of gravity (CG) in the print and shorter print time. The support material is a gridlike structure to minimize the material used. In this case the support volumes of 15.55cm^2 and 26.40cm^2, would actually be 125.4cm^2 and 213.4cm^2 instead, if the supports had been completely solid.

(a) Netfabb optimal.

(b) SS1.
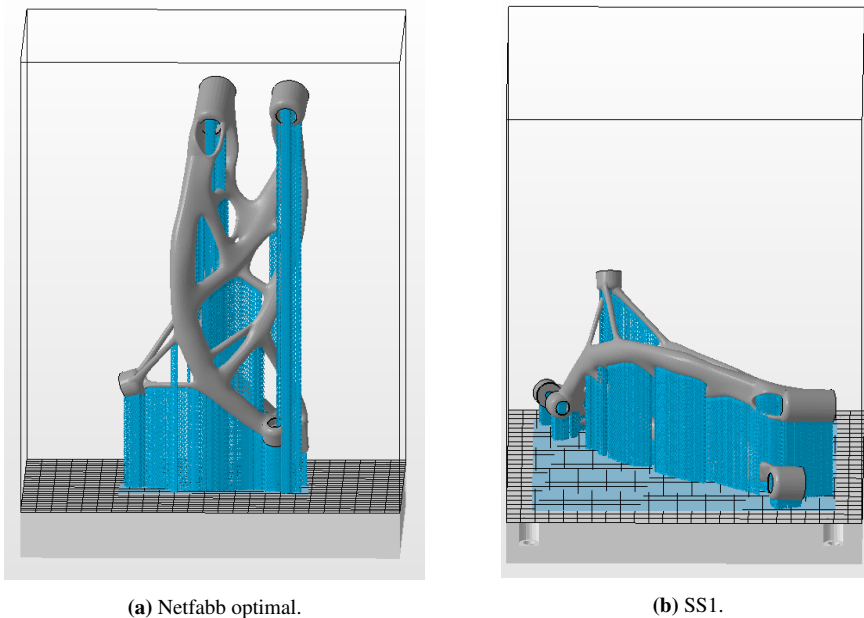
Figure 4.39: Netfabb results of its optimal printing direction and the original SS1 direction.

Table 4.4: Print direction optimization results in Netfabb.

	Build Volume [cm^2]	Support Area [cm^2]	Support Volume [cm^3]	Height [mm]	Height CG [mm]	Print Time [h:min:s]
Netfabb	142.88	29.279	15.55	270.2	143.0	46:57:28
SS1	142.90	73.668	26.40	124.9	48.5	40:48:11

4.7 Renders of the Final Design

Figure 4.40 are renders of the final design together with the other parts of the assembly. These were rendered using Siemens NX ray traced studio.
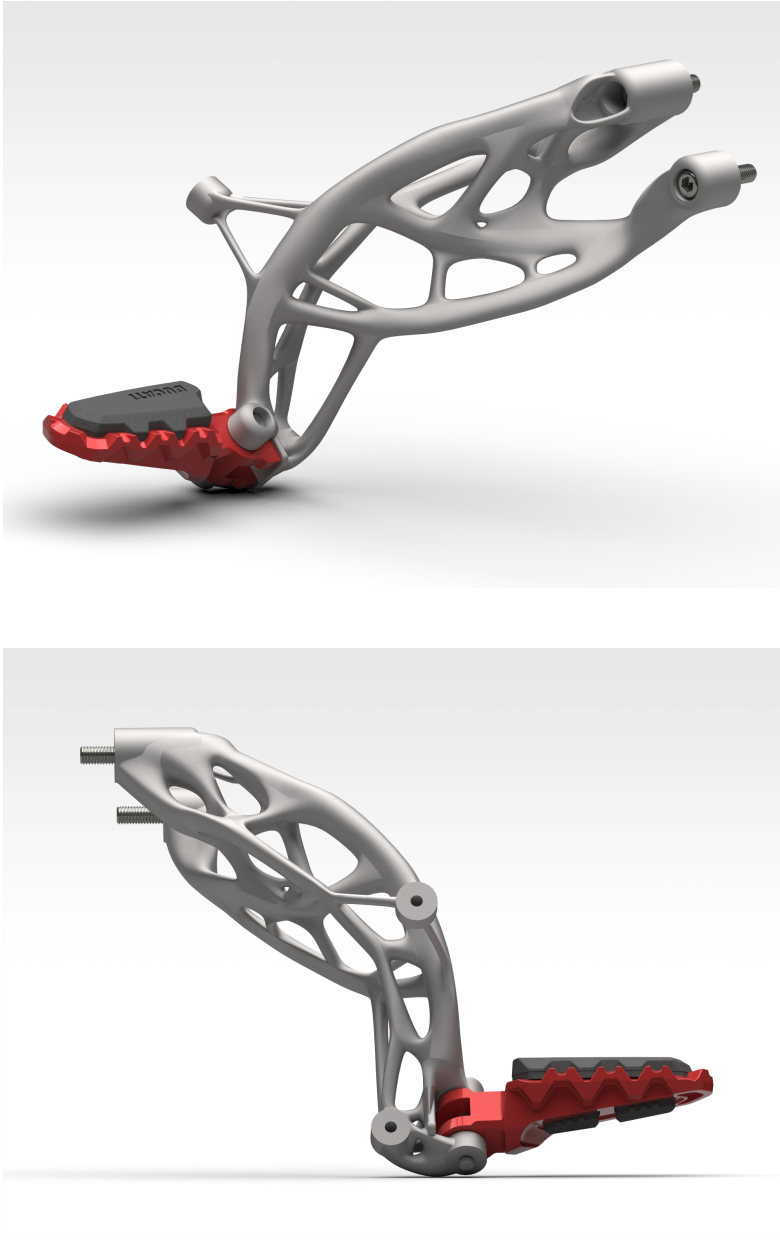
Figure 4.40: Renders of the final design.

Chapter 5

Discussion and Conclusion

In this chapter the results and theory research in this project will be discussed, and used as a basis for drawing conclusions and deciding on potential further work.

5.1 Topology optimization

5.1.1 Simulation Tools

A part of this project was to evaluate and choose a simulation tool. Siemens NX was chosen based on the comparison between it, Fusion 360 and Abaqus Tosca. The main reason was the possibility of doing everything in one software. This decision showed its benefits several times throughout this project. Especially, in the CAD redesign and FEM sections. Design 1.0 had its shortcomings in comparison with the OEM bracket. The following iterations of the design by going back and altering it in realize shape, then back through re-meshing and into a new simulation to check for improvements, were an efficient workflow. A manual re-meshing update had to be performed in some cases, due to the previous mesh settings not fitting the new design. The workflow did however still not involve the importing and exporting of files, as a flow with utilizing several software tools would do. A justification of the software choice could almost be made by the workflow alone, but NX also showed to be beneficial in recreating the TO results, by the ease of accurately creating convergent models and modifying them.

One important point to make is however that the choice of software tools are a field where personal preference is a big factor. The optimal choice of software could therefore be completely different for a different project or person. All the pieces of software could in the end probably end up with similar results, but the road to those results would be different.

5.1.2 Design Space

The design space utilized in this project worked sufficiently. There was however a common trend that the resulting geometries had some areas they never filled with material. These areas could potentially have been removed when the trend was found, to reduce the simulation time. The simulation time were however not that long, with the longest TO tasks being just below ten hours on the desktop PC used.

The contact area for the footpeg where a plate were added in Section 4.2.2 - CAD redesign, should potentially have been part of the design space from the beginning. This were found in the later stages of this project, and therefore added in the CAD redesign phase instead. The process would however be faster if it had been there from the beginning.

5.1.3 Setup and Results

The TO setup achieved resulting geometries that were not that far off the final design, but the load assumption could potentially have been better. The TO results had lower stress and displacement compared to the final contact analysis. They had however closer stress and displacement results with similar load setup as in the TO task. The stress results of the TO task were found to vary with simulation accuracy, but the displacement results did not. The difference between the TO results and FEM verification could therefore potentially come from the simplified load case of the TO task. Better direct results could maybe have been achieved if a setup similar to the one checked out in Section 3.2.4 - Complex TO, had been able to converge. This could also reduce the iterations of CAD redesign needed for stress adjustment. It did not converge for this project, even with weight targets way above the final weight achieved in the end, as previously mentioned. Further work on this matter would be to look deeper into the multiple body TO tasks, and the differences in stress values with simulation accuracy.

The increments between the weight targets could in retrospect have started out bigger, and then been lowered as one got closer to a high stress or deformation result. For example could it have started at 100g and then been lowered to 25g. This would result in more design proposals close to the final weight target, in the same time as the analysis with fixed increments of 50g used in this project. This would be advisable if one want to get to the final weight target more efficiently, or have more results close to it to take inspiration from in the redesign phase. The fixed increments were however good for seeing the continuous change between the different weight targets, as were investigated in the results section in this project.

5.2 FEA comparison

5.2.1 Structural Analysis

The structural analysis of design 1.0 proved to have small amounts of yield, with the SOL101 solver and the simplified load case utilized in the TO tasks. This proved to not be the case when doing the linear contact analysis in SOL101. The stress results from these were used as a guide for iterations of changing the design by adjusting the cross sections of the component to reduce the stresses. This were the moment where the benefits of utilizing NX as a software tool really came into play.

The final stress results of design 2.0 were lower than the OEM component, but some of them still had stresses over the fatigue limit. However, the load case used in the analyses are assumed to be a worst case load scenario. This is backed up by the OEM bracket also having high stress regions that are above fatigue limit, and in some areas yield limit. Another point supporting this assumption is that the load used would correlate to almost 170kg of weight on one footpeg. If one assumes an average person to weigh around 85kg, and this weight would be distributed between both the footpegs and the seat. The load on the footpeg could then be safe to assume to be lower in most driving situations, than the one used in the simulations in this project. A load would also only be applied to the rear footpegs in cases of driving with a passenger. The final design in this project should therefore be within the limits of a decent fatigue life, based on the worst case load not having too many stress areas above the fatigue limit. The fatigue limit given in the material sheet was 5 million cycles at 97MPa [EOS (2014)], and the part could therefore be estimated to have close to infinite life.

A further work on this point could be to produce the part and get actual loads from usage of the bike. These could then be used to even further optimize the part, or get a more accurate definition of the parts fatigue life.

5.3 Weight Reduction

The final component had a weight of 382g compared to the OEM bracket's weight of 536g. It corresponds to a weight reduction of about 30%. This is however a weight that is higher than the 350g TO result it was based on. The direct result had a reduction of 34%, and the first solid model based on it had 40% reduction. The lower weight reduction in the end comes from higher stresses occurring in the FEM verification with the footpeg, compared to the simplified load case used in the TO task.

A part that could potentially improve the weight reduction was to add new structural geometry to the TO design, instead of just altering the cross sections of the existing geometry in the design 2.0 creation. For this project this was avoided to try and not change the actual structure that was optimized for a certain printing direction in the TO task.

5.4 Additive Manufacturing

5.4.1 Method

Several additive metal manufacturing methods for metal were researched in this project. SLM and EBM are methods of powder bed fusion, and LMD is a method of direct energy deposition. SLM and EBM have potential benefits in their creation of dense structures with complex features. The hinges and joints that could be made with these were not utilized in this project anyway as previously mentioned. A dense structure is however important to avoid potential porosity that could compromise mechanical properties. LMD on the other hand has the advantage of overcoming some overhang constraints, which were a big challenge with the footpeg bracket. The main overhang angle of the footpeg's shape could potentially be avoided with a tilting printer bed. However, many of the features in the final design is in different directions, due to its gridlike structure. This could result in overhangs in other directions even with a tilting printer bed trying to the avoid the main overhang.

Surface Roughness can be better in LMD (Section 2.2.6), but hand SLM and EBM have on the other a bigger potential for dimensional accuracy with 0.04mm to 0.2mm compared to 0.5mm to 1.0mm for LMD [DebRoy et al. (2018)]. This is a feature that can be important for creating complex parts with tight tolerances. When comparing EBM and SLM, they are rather similar, but SLM have been around for longer and is a more established method.

The final decision for this project is to advice the part to be produced with SLM. It is however important to note that a deeper analysis of manufacturing costs is needed before deciding on producing all the 10 000 components a year with only AM, or by utilizing it to potentially create for example casting molds instead.

5.4.2 Support Structure

The general support structure generator used in Netfabb utilized a grid structure to reduce the volume of the support structure. It is at this iteration using the standard values for the holes in the grid structure, but these could potentially be altered to further reduce the amount of support structure.

The mounting holes of the bracket are currently using M8 bolts, which are bigger than the recommended maximum of 6mm holes found in the research into AM. This means that these holes would need support structure to avoid a potential collapse. The potential risk of rough surfaces means that the holes will most likely need to be re-drilled after manufacturing anyway. A solution could therefore be to decrease the size of the holes to a small enough diameter to avoid support structure, and then use them as a center hole for re-drilling them up to the recommended clearance for M8, which is 9mm [Tingstad (2019)], afterwards.

Extra material should be added on the surfaces where the part interacts with other parts, such as the mounting points to the frame and the footpeg mounting area. This is to make it possible to machine down the surface roughness from printing of the part. Both of the

final printing directions have these areas located at angles that could result in the staircase effect. By machining down the areas to the correct size one would ensure a tight fit and smooth finish of the component.

5.5   Conclusion and Further Work

The main thing to take from this thesis is that topology optimization combined with the possibilities of additive manufacturing is a good solution for weight reduction of parts. It is however important to note that the direct results from the topology optimization are design proposals that need to be verified and potentially altered. The final part had a weight of 382g, which is about 30% lower than the OEM part, while still keeping the displacement lower as well. It did also perform fine structurally when it came to stresses, compared to the OEM part. The tools tested proved to have their advantages and disadvantages, and while NX became the contender in this project might not mean it would be the best for other projects. There is also much of the software choice that comes down to personal preference.

Things that can be improved on in future work could be divided into the topic of the topology optimization method and the footpeg bracket itself. For the bracket itself the further work would be getting load data from real life usage of the bike, to potentially further improve the design regarding weight reduction and fatigue life. It would also be to look deeper into the cost of manufacturing, and if the part would be beneficial to make with additive manufacturing alone. Other solutions like casting molds made with the help of additive manufacturing could potentially be beneficial for creation of bigger volumes.

The further work would for the case of topology optimization be to look deeper into the setup and results of the simulations. The direct stress results were shown to depend on the accuracy of the analysis. A deeper investigation to find the exact reasons for this could be performed. The topology optimization with the usage of glue connections between scenery bodies that did not converge, could also be researched further. This could potentially improve the accuracy of the direct design proposals from the topology optimization.

Bibliography

ASM, 2020. Al6061-t6 material properties. `http://asm.matweb.com/search/SpecificMaterial.asp?bassnum=MA6061T6`. Last accessed 20.05.20.

Autodesk, 2020. Generative design. `https://www.autodesk.com/solutions/generative-design`. Last accessed 11.05.20.

Bandyopadhyay, A., 2015. Additive Manufacturing. Taylor and Francis, Hoboken.

Bendsoe, M.P., 2004. Topology Optimization : Theory, Methods, and Applications. Second edition, corrected printing. ed., Springer, Berlin, Heidelberg.

Carpimoto, 2019. Ducati multistrada - givi engine guard. `https://www.carpimoto.com/EN/Bike_Ducati_Multistrada-1260-Pikes-Peak/Specific/Brand_Givi/Accessories/Guards/50819_TN7406B-GIVI-Engine-Guard-for-Ducati-Multistrada-1200-15-17.htm`. Last accessed 18.11.19.

Christensen, P.W., 2009. An introduction to structural optimization. volume vol. 153 of *Solid mechanics and its applications*. Springer, S.l.

Crucible-Design-Ltd, 2015. Laser metal deposition manufacturing (lmd). `https://www.crucibledesign.co.uk/images/uploaded/guides/bs7000-part-2-a-management-guide-download-original.pdf`. Last accessed 10.10.19.

Dassault-Systemes, 2014. Abaqus 6.14 documentation. `http://ivt-abaqusdoc.ivt.ntnu.no:2080/v6.14/index.html`. Last accessed 11.10.19.

DebRoy, T., Wei, H., Zuback, J., Mukherjee, T., Elmer, J., Milewski, J., Beese, A., Wilson-Heid, A., De, A., Zhang, W., 2018. Additive manufacturing of metallic components – process, structure and properties. Progress in Materials Science 92, 112 – 224. URL: `http://www.sciencedirect.com/science/article/pii/S0079642517301172`, doi:`https://doi.org/10.1016/j.pmatsci.2017.10.001`.

Ducati, 2019a. Ducati multistrada 1260. `https://www.ducati.com/ww/en/bikes/multistrada/multistrada-1260/make-it-yours-multistrada-1260-s`. Last accessed 18.11.19.

Ducati, 2019b. Ducati spare parts catalogue. `https://www.ducati.com/ww/en/service-maintenance/spare-parts-catalogs`. Last accessed 04.12.19.

Durakovic, B., 2018. Design for additive manufacturing: Benefits, trends and challengess. Periodicals of Engineering and Natural Sciences 6, 179–191.

Eastman, C.M., 2012. Design for X: concurrent engineering imperatives. Springer Science & Business Media.

Eker-Performance, 2019. Ducati multistrada 1260. `https://ekerperformance.com/produkt/ducati-multistrada-1260-pikes-peak/`. Last accessed 26.09.19.

Engineering-Toolbox, 2004. Friction coefficients for some common materials and materials combinations. `https://www.engineeringtoolbox.com/friction-coefficients-d_778.html`. Last accessed 25.05.20.

EOS, 2014. Eos alsi10mg material sheet. `https://cdn0.scrvt.com/eos/public/8837de942d78d3b3/4e099c3a857fdddca4be9d59fbb1cd74/EOS_Aluminium_AlSi10Mg_en.pdf`. Last accessed 22.04.20.

European-Parliament, 2016. Commission delegated regulation (eu) 2016/1824s. `https://eur-lex.europa.eu/legal-content/EN/TXT/?uri=CELEX:02016R1824-20161015`. Last accessed 17.10.19.

Gates, M., 2020. Top motorcycle panniers 2020. `https://autoquarterly.com/best-motorcycle-panniers/`. Last accessed 10.05.20.

Gaynor, A.T., Guest, J.K., 2016. Topology optimization considering overhang constraints: Eliminating sacrificial support material in additive manufacturing through design. Structural and Multidisciplinary Optimization 54, 1157–1172. URL: `https://doi.org/10.1007/s00158-016-1551-x`, doi:`10.1007/s00158-016-1551-x`.

Gebhardt, 2012. Understanding Additive Manufacturing : Rapid Prototyping - Rapid Tooling - Rapid Manufacturing. Hanser.

Hoffarth, M., Gerzen, N., Pedersen, C., 2017. Alm overhang constraint in topology optimization for industrial applications .

Huang, X., Xie, M., 2010. Evolutionary topology optimization of continuum structures: methods and applications. John Wiley & Sons.

Irgens, F., 1992. Formelsamling i mekanikk : statikk, fasthetslære, dynamikk, fluidmekanikk.

Langelaar, M., 2017. An additive manufacturing filter for topology optimization of print-ready designs. Structural and Multidisciplinary Optimization 55, 871–883. URL: `https://doi.org/10.1007/s00158-016-1522-2`, doi:`10.1007/s00158-016-1522-2`.

Lim, S., Buswell, R., Valentine, P., Piker, D., Austin, S., De Kestelier, X., 2016. Modelling curved-layered printing paths for fabricating large-scale construction components. Additive Manufacturing doi:`10.1016/j.addma.2016.06.004`.

Mahamood, R.M., 2018. Laser Metal Deposition Process of Metals, Alloys, and Composite Materials. Engineering Materials and Processes. 1st ed. 2018. ed., Springer, Cham.

McKnight, M., 2017. Generative design: What it is? how is it being used? why it'sa game changer. KnE Engineering , 176–181.

Misumi, 2014. Pivot pin tolerances. `https://my.misumi-ec.com/vona2/detail/110300098460/`. Last accessed 10.05.20.

Plattner, H., 2018. Design Thinking Bootleg. Institute of Design at Stanford.

Redwood, B., 2019. Am map. `https://www.3dhubs.com/knowledge-base/additive-manufacturing-technologies-overview/`. Last accessed 02.10.19.

Tingstad, 2019. Gjenge- og frihullsdiametre. `http://www.tingstad.no/upload_images/3BCAAB409548472FBEB17D7EB7E49D9E.pdf`. Last accessed 08.12.19.

TWI-Ltd, 2014. Laser metal deposition manufacturing (lmd). `https://www.youtube.com/watch?v=yKnlmfuMSgo`. Last accessed 09.10.19.

Ulrich, K.T., Eppinger, S.D., 2011. Product design and development, 2012. McGraw-Hill, New York.

Varotsis, A.B., 2019. Introduction to sls 3d printing. `https://www.3dhubs.com/knowledge-base/introduction-sls-3d-printing/`. Last accessed 09.10.19.

Wong, K., 2012. K.v. wong, a.hernandez, "a review of additive manufacturing," isrn mechanical engineering, vol 2012 (2012), article id 208760, 10 pages. ISRN Mechanical Engineering 2012. doi:`10.5402/2012/208760`.

Yap, C.Y., Chua, C.K., Dong, Z.L., Liu, Z.H., Zhang, D.Q., Loh, L.E., Sing, S.L., 2015. Review of selective laser melting: Materials and applications. Applied physics reviews 2, 041101.

Zare, 2019. Metal sintering dmls/slm. `https://www.zare.it/en/technologies/metal-sintering-dmls-slm`. Last accessed 20.11.19.

Zegard, T., Paulino, G., 2016. Bridging topology optimization and additive manufacturing .

Appendix A

Abaqus Tosca Setup + Results

A.1 Topology Optimization

An optimization task in Abaqus with Tosca is performed by going through the modules as shown in the workflow diagram in Figure A.1. In this section the process in each of the different modules is presented in detail for this project.
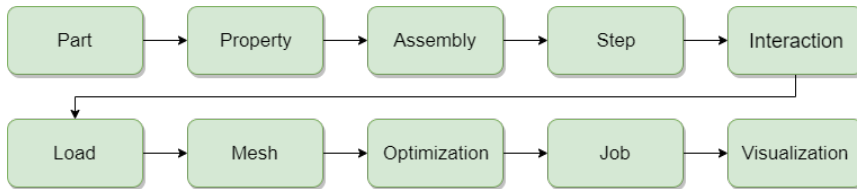
Figure A.1: Workflow in Abaqus Tosca for the topology optimization in this project.

The setup in Abaqus Tosca is first based on the design space created in Inventor. This setup is imported into Abaqus' **part** environment where one creates partitions of the part. For the bracket the hinge area for the peg and its pin, the mounting points to the frame and the accessory points were partitioned.

In the **property** module, material properties for AlSi10Mg shown in Table A.1 were assigned. The property module does also have the possibility of creating sections in the model. The sectioning that is relevant to apply is defining the design and the non-design spaces. The bracket's main part was chosen to be a design space, while the mounting point for the footpeg was set as is. The mounting points to the subframe and the accessory points were also set as non-design space.

After this an **assembly** was created in its respective module. This is done by just inserting the instance of the part as it is already complete from modelling in Inventor.

Table A.1: Material properties for AlSi10Mg [Zare (2019), DebRoy et al. (2018)]

AlSi10Mg:		
Young's modulus [MPa]	Density [tonne/mm^3]	Poisson's ratio [ ]
70 000	2.67e-9	0.33

The next the **step** module, where two static general steps were created using default settings for incrementation and linearity. The two steps are to split when the boundary conditions and load are applied, to easier see if one of them is applied wrong if the simulation crashes.

Interaction was used to create couplings for applying the load as shown in Figure A.2a. One coupling was applied to the upper mounting point of the footpeg hinge, and the other to the lower point. The couplings are used to apply the load to a specific point and then distribute it over the coupled surfaces. **Load** cases and constraints were then assigned to the model as shown in Figure A.2. The constraints were set as the two mounting holes having fixed translation in all directions. The load was set as 1700N in the two holes where the footpeg is attached to the bracket. The load was set at an angle compared to the hole so that it represents the load on the actual footpeg as it is offset with an angle of 36.2° compared to the pin.

(a) Coupling to distribute load.   **(b)** Load applied at coupling.   **(c)** Boundary conditions.
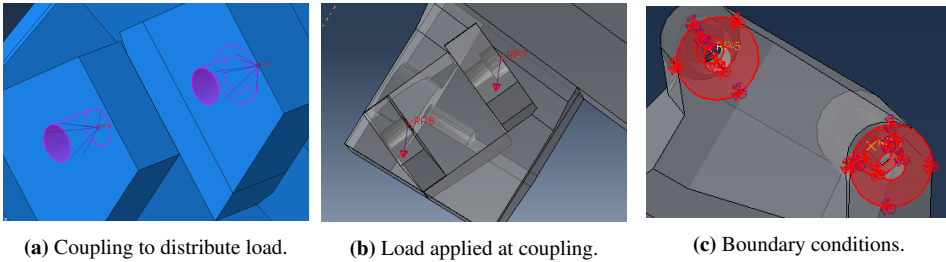
Figure A.2: Steps in the interaction and load modules.

The next module is the **mesh** module. The global seed size was set to 2.5 with a C3D4 tetrahedral mesh. Some of the areas around the mounting holes were however not meshable with this setting. To overcome the problem a combination of virtual topology where one tries to smooth out some of the geometry, and a finer local seed where used. A more thorough description of mesh choice is located in Appendix B.

At last the **optimization** setup was created and the objective function, state variable and design variable were set. First an optimization task is created for the defined design space section. The algorithm chosen were the sensitivity-based, as a result of the comparison in Appendix B. Two design responses were created, one based on weight, and one based on strain energy. The strain energy (U) was then set as the objective function with the goal to minimize U. The weight/mass (m) was set as the behavioral constraint with a target of

450g, being around 17% lower than the OEM component's weight of 536g. The design constraints (x) are the material being AlSi10Mg and the geometrical shape of the design space. Equation A.1 shows these constraints applied to the mathematical formulation for topology optimization presented in equation 2.2.

$$\mathbb{TO} = \begin{cases} \text{minimize } U \text{ with respect to } x \text{ and } m \\ \text{subject to} \begin{cases} \text{behavioral constraints on } m \\ \text{AlSi10Mg and shape of design space } (x) \\ \text{equilibrium constraint} \end{cases} \end{cases} \tag{A.1}$$

This setup was then applied to a **job** and the simulation was submitted. During the simulation one can continuously plot the design response from the simulation.

The **visualization** window showed an animation of the design cycle steps from the simulation, and it could also display direct stress and deformation results. A summary of the setup specs is shown in Table A.2.

Table A.2: Setup for the topology optimizations in Abaqus Tosca.

| Setting:	
Material	AlSi10Mg
E Modulus	70 000 MPa
Poisson Ratio	0.33
Density	2.67e-9 tonne/mm^3
Element Type	Linear Tetrahedron
Mesh Size (seed)	2.5 global, and 1 local in mounting points to frame
Number of Nodes	147 310
Number of Elements	809 211
Load Case	1700 N in the negative z-direction
Design Responses	Weight and Strain Energy
Objective Function	Minimize Strain Energy
Constraint (weight)	0.0005 tonnes
Geometric Constraints	Fixation to subframe
	Exhaust muffler
	Mounting point for footpeg
	Swing Arm
	Accessory attachement points
Optimization Algorithm	Sensitivity-Based (SIMP, penalization = 3)
Design Cycles	45
Paralellization	4
PC Specs:	
CPU	3.2 Ghz QuadCore (Intel I7-4790S)
RAM	16 Gb with 1600 MHz

A.2 Abaqus STL Export

The optimized model was first exported out of Abaqus as an STL file. The complete settings used for exporting the STL file is shown in Table A.3, and the following explanations of their functions are based on the Abaqus manual's description [Dassault-Systemes (2014)]. Default values were used where none else is specified.

- The design cycle chosen was the last one, but an earlier one could have been chosen if needed.

- Iso-value is used to decide how deep into the model the smoothing cycle is going to "cut". A higher value will reduce the model and can potentially cause disconnections.

- Reduction percentage and angle is used to decide how many percent of the faces of the model should be reduced, and the maximum angle between two faces that should be removed.

- The number of iterative smoothing cycles were used with a low value of one as higher values from experience result in loss of important geometrical features and structure. A comparison of one and five cycles is shown in Figure A.3, where one can see that the higher value resulted in some of the structure being really thin. The part was however more smooth on the surfaces.

- Target volume is the ratio between the isosurface and original volume.

- Filtering is used to remove irregularities before the smoothing process is made, one can have zero, one or five filtering cycles. The cycles did not do anything major to the file at this point.

The smoothed component should be taken into Inventor to redesign the proposed design from the optimization. In this project the part was only smoothed out and not reverse engineered and redesigned. This will however be something to come back to in further work.

Table A.3: Export setting of TO in Abaqus.

Settings:	
Format	STL
Design Cycle	41
Iso Value	0.3
Reduction Percentage	0
Reduction Angle	15
Smoothing Cycles	1
Target Volume	0
Filtering	None
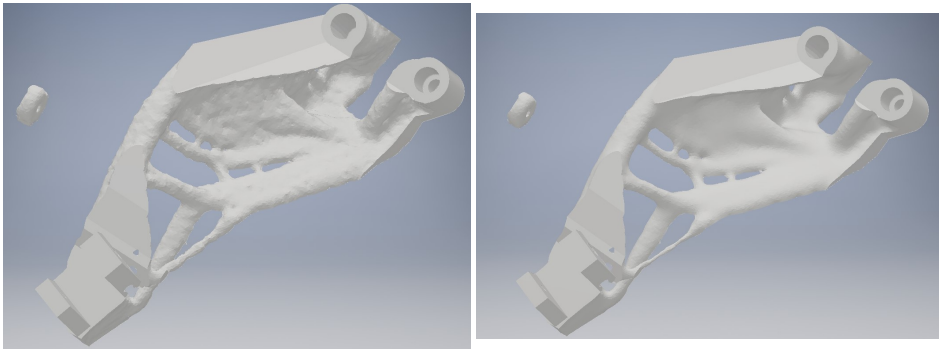
(a) The exported STL with 1 smoothing cycle.

(b) The exported STL with 5 smoothing cycles.

Figure A.3: The STL file with different smoothing cycles showing how the smoother model has thinner structures.

A.3 Results

A.4 Topology Optimization

The final result from the TO in Abaqus is shown in Figure A.4a. It had a strain energy of 1935Nmm and a weight og 449g. This had also applied the load of 200N for fixing problems with the accessory mount not attaching to the main structure. It ended up having some disconnected members, as seen in for example Figure A.4b.
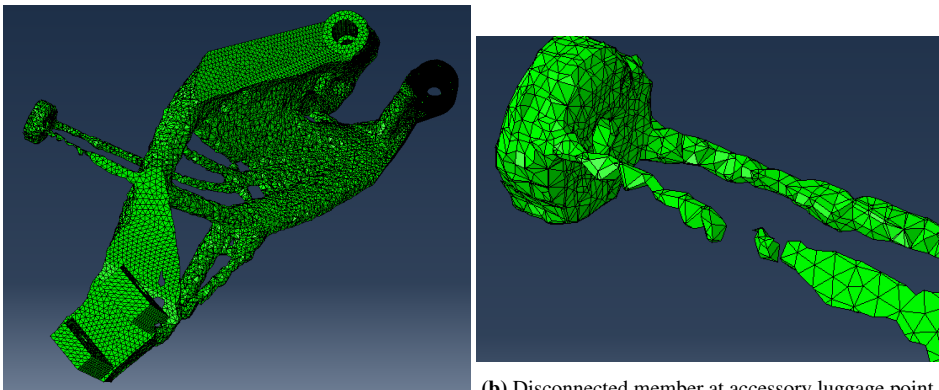
(a) Final structure.

(b) Disconnected member at accessory luggage point.

Figure A.4: The final TO results in Abaqus.

As a test a topology optimization were also executed using the OEM part itself as a design space, with the goal to reduce the volume of 20% and 15 design cycles. The results of this is shown in Figure A.5. The results show that the first parts to be removed where the accessory point/exhaust guard, and the bar between the mounting points.
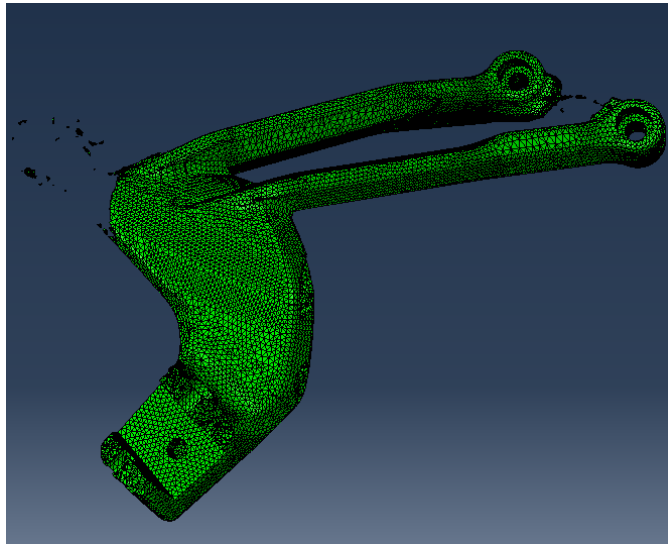
Figure A.5: Resulting geometry of a TO with the OEM part as a design space.

B | Appendix

Tosca Mesh and Algorithm Choice

B.1 Mesh choice:

The meshes available in Abaqus are hexahedra, tetrahedra and wedge mesh, as shown in Figure B.1. Each of them have different number of nodes available, like for example 4 or 10 for tetrahedral. Out of these free meshing is only available with the tetrahedral mesh, the two others need bottom-up or other mesh techniques to work. Hexahedral elements need less elements to represent the same geometry as a tetrahedral element, but tetrahedral on the other hand is better at going around complex structures due to the geometrical shape. The procedure of assigning a hexahedral me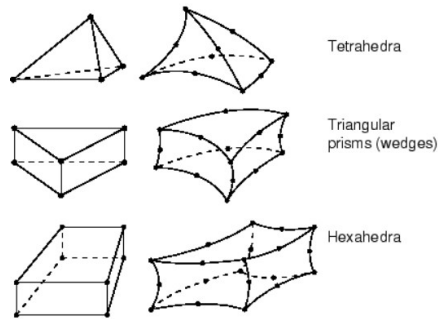sh to a complex structure as the OEM footpeg bracket would need bottom up meshing which from experience can be a time consuming process. A decent result could be acquired with a tetrahedral mesh with more elements. The final decision was to go for the tetrahedral.

Figure B.1: The different 3D meshes available in Abaqus [Dassault-Systemes (2014)].

When it came to the **number of nodes** for the topology optimization 4-node tetrahedral were chosen over 10-node tetrahedral for the reason of reducing the simulation time. The proposed design from the TO is just a design proposal and will need to be redesigned and checked afterwards anyway.

B.2   Condition-based vs general/sensitivity-based:

Abaqus Tosca features two types of algorithms for topology optimization, the condition-based (CB) and the general/sensitivity-based (SB) algorithm. From the Abaqus manual [Dassault-Systemes (2014)] it is noted that the SB algorithm, which is the default, is applicable to more problems due to having a higher variety of variables to use as objective function and constraints. The CB algorithm have less variety by only having volume and strain energy as variables, but is more efficient when calculating as it typically converges from a lower number of design cycles.

Table B.1: Setup for SB VS CB experiment, differences are emphasised by use of **Bold Text**.

Setting:	
Material	AlSi10Mg
E Modulus	70 GPa
Poisson Ratio	0.33
Density	2.67e-9 tonne/mm^3
Element Type	Linear Tetrahedron
Mesh Size (seed)	2.5 global, and 1 local in mounting points to frame
Number of Nodes	147 310
Number of Elements	809 211
Load Case	1700 N in the negative z-direction
Design Responses	Volume and Strain Energy
Objective Function	Minimize Strain Energy
Constraint (Volume Fraction)	0.25 (of design space)
Geometric Constraints	Fixation to subframe
	Exhaust muffler
	Mounting point for footpeg
	Swing Arm
	Accessory attachement points
Optimization Algorithm	One simulation each with **SB and CB**
Design Cycles	**50 for SB** and **15 for CB**
Paralellization	4
PC Specs:	
CPU	3.2 Ghz QuadCore (Intel I7-4790S)
RAM	16 Gb with 1600 MHz

To figure out which algorithm would be better for this project, a test of both were performed. The same setup are used for both algorithms, shown in Table B.1. The only differences being the algorithm itself and the number of design cycles as these are different in the default settings of the two algorithms. SB has a default number of 50, and CB has a default of 15 [Dassault-Systemes (2014)].

Two sets of comparison simulations resulted in the values shown in Table B.2. It shows that the CB algorithm came to convergence in almost one third of the time of the SB with a volume fraction of 0.25, and half the time with a volume fraction of 0.5. It is interesting

to see that CB's simulation time did not increase that much between the change in volume fraction. It did just have one more design cycle to go on before reaching its limit of 15, while SB were only just past halfway with 0.5 volume fraction, and still converged before its roof of 50 with 0.25 volume fraction. SB got closest to the weight targets in both cases.

Table B.2: Results of the 0.25 Volume simulation of SB vs CB algorithm. Some values from 0.5 Volume is shown in parenthesis for comparison.

	SB	CB
Simulation Time [hour/min]	2h45m (1h58m)	55m (49m)
Design Cycles Converging [#]	42 (29)	15 (14)
Strain Energy [Nmm]	1224.5 (918.8)	1176.5 (909.3)
Deformation [mm]	1.31	1.29
Volume Fraction Target [%]	0.25 (0.5)	0.25 (0.5)
Volume Fraction [%]	0.249 (0.449)	0.261 (0.508)

The resulting geometries are shown in Figure B.2a for SB and Figure B.2b for CB. These geometries are rather similar. Both have removed material in close to the same areas, and ended up with a geometry that is somewhat following the lines of the OEM part.
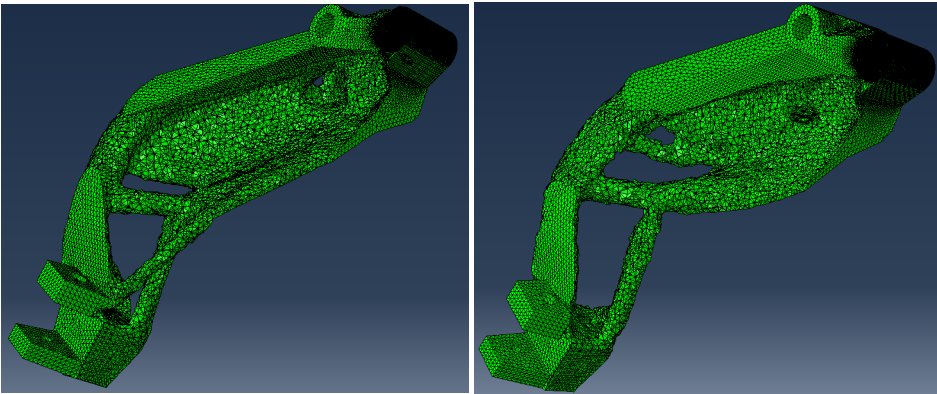
(a) The resulting part after 42 cycles of TO with SB algorithm.

(b) The resulting part after 15 cycles of TO with CB algorithm.

Figure B.2: CB vs SB comparison.

To conclude on one of the two options one have to look at the case at hand, for this project the main thing is reducing weight and increasing stiffness. This can be done by both by using volume to reduce weight. In a direct comparison between the two using volume and strain energy CB has a noticeable advantage in simulation time. However, with SB one could use weight directly in the simulation, and also have the possibility of optimizing for other cases. The conclusion were to mainly use the SB algorithm, but in the cases of strain energy vs volume the CB algorithm will be utilized.

Appendix C

# Fusion 360 Generative Design Setup

C.1 Generative Design

The generative design setup in Autodesk Fusion 360 consist of several commands, typically performed in the order shown in Figure C.1. It begins by setting up a study and deciding on the synthesis of the study. This is in practice the accuracy of the study, and it is set on a simple slider scale from coarse to fine.
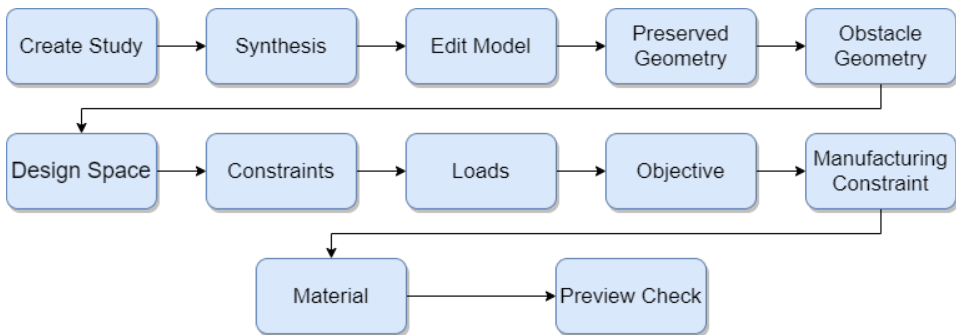
Figure C.1: Typical workflow within the generative design setup of Fusion 360.

The next step is to add and potentially edit the model. Here the later preserved and obstacle geometry were created. These are then assigned to the model in each of their respective tools. The preserved regions (green/blue) were partitioned parts of the design space such as mounting holes, and it is used to have them be kept as-is in the optimization. Obstacle geometry (red) were assigned around the footpeg location and screw holes to have these areas be kept free from material that could interfere with other parts. Some of this were

added to the top of design space as well as Fusion is not always keeping within the limits of the design space. The design space (yellow) were added based on the design space created from the OEM bracket. The model with all these settings applied is shown in Figure C.2.
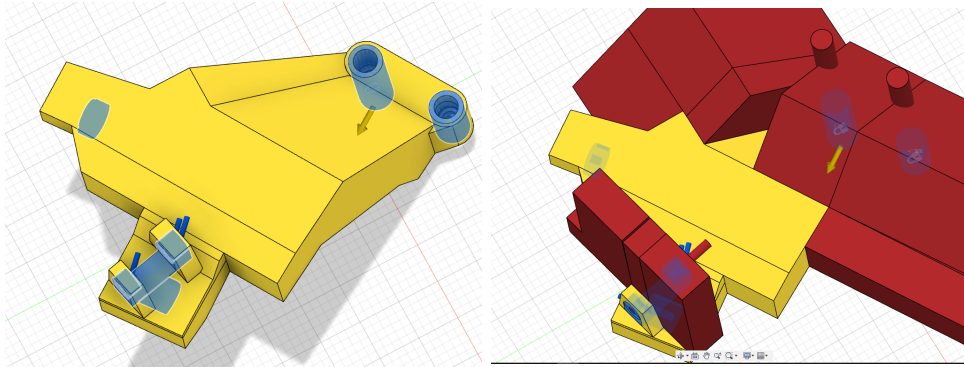
(a) Design space (yellow) + preserved geometry (green/blue).

(b) Design space (yellow) + preserved geometry (blue) + Obstacle geometry (red).

Figure C.2: The design space showed with different parts of the preserved and obstacle geometry.

The next step is adding constraints and loads. These are applied to the preserved geometry, meaning the mounting holes to the frame were fixed, and loads were added to the footpeg mounting area and the accessory mounting points. The loads were as shown in Table C.1.

Table C.1: Table of load case settings used in Fusion Generative Design.

Feature	Load [N]
Footpeg Pin Holes	1700
Accessory Hole 1 (Normal)	200
Accessory Hole 1 (-y)	200
Accessory Hole 2 (Normal)	200
Accessory Hole 2 (-y)	200

Then it is the study's objective which is either to minimize mass or maximize stiffness. Both have the possibility of adding a wanted safety factor, and maximize stiffness also lets you choose a weight target. Maximize stiffness were utilized with a weight target of 450g and a safety factor of 1. The safety factor were set this low, due to the software not reaching wanted weight target with higher safety factors. It is exaggerating the factor, and parts with 1 in safety factor still showed to be within limits of yield.

Manufacturing constraints can then be added for anything from traditional milling to casting and additive manufacturing. Additive manufacturing were used with a overhang angle of 45°. this makes the optimization look at printing the part based on each of the model's

Cartesian coordinate system planes (XY, XZ and YZ). A setting of unrestricted were also assigned. This will in total give four resulting geometries from the optimization.

The final setting is to add material, and here AlSi10Mg were assigned from Fusion's AM material library. It's values are shown in Table C.2. After this it is possible to do a pre-check to see if everything is assigned, and then do a short preview of the first cycles to look for any immediate problems with the setup.

Table C.2: Material properties for AlSi10Mg in Fusion 360.

AlSi10Mg:	
Young's modulus [MPa]	71 000
Density [tonne/mm^3]	2.67e-9
Poisson's ratio [ ]	0.33
Yield Strength [MPa]	240
UTS [MPa]	460

After the optimization is complete the results are shown as in Figure C.3. Here one can look further into each of the proposed designs and each of the design cycles they have been through. When one finds the one that one wants to go with it is possible to export it as STL or solid.
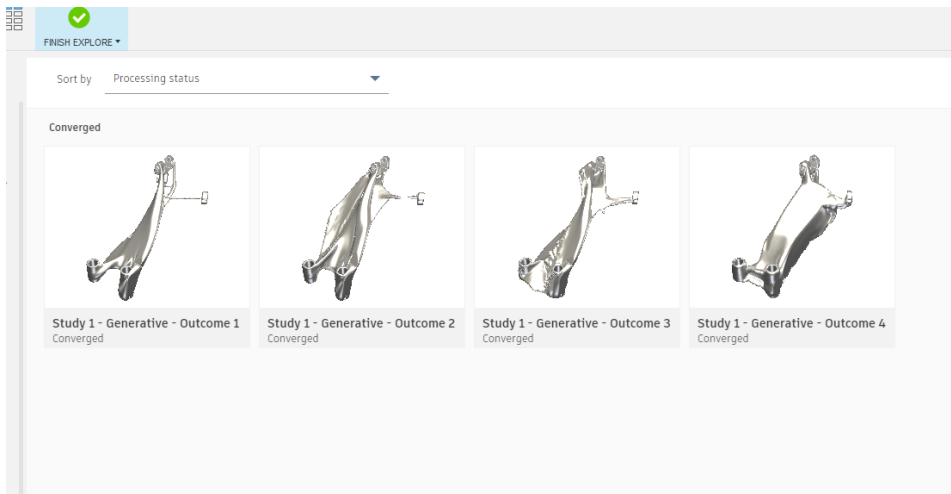

Figure C.3: Example of multiple results returned from a Fusion 360 simulation.

C.2 Fusion 360 export to solid

In Fusion 360 one has the possibility to export the resulting geometry of the generative design directly into a solid file. This file can then be used for further redesign and FEM verification. An example of a solid export is shown in Figure C.4. This is an intuitive process, but the final solid has some weird looking faces and could end up with needing to be idealized before further use.
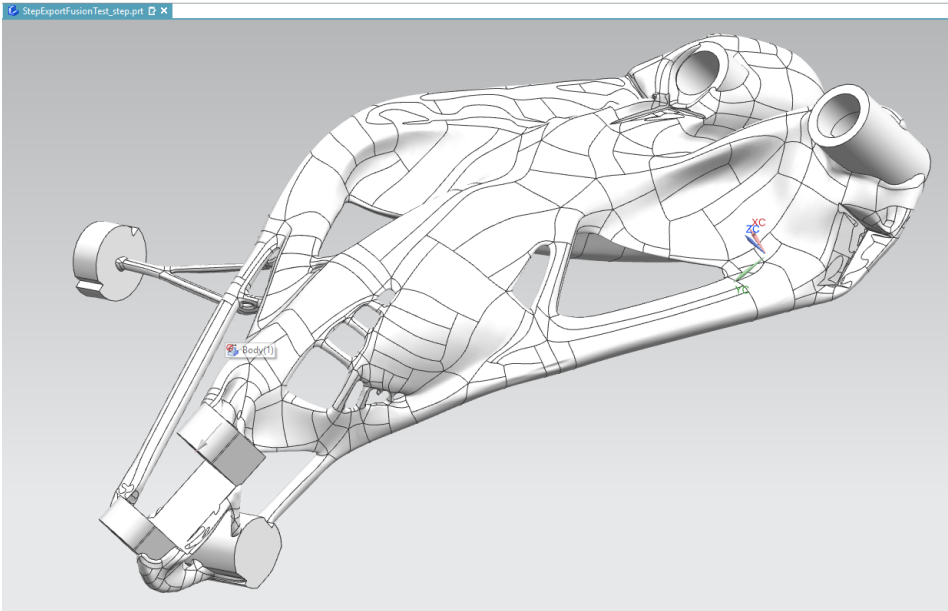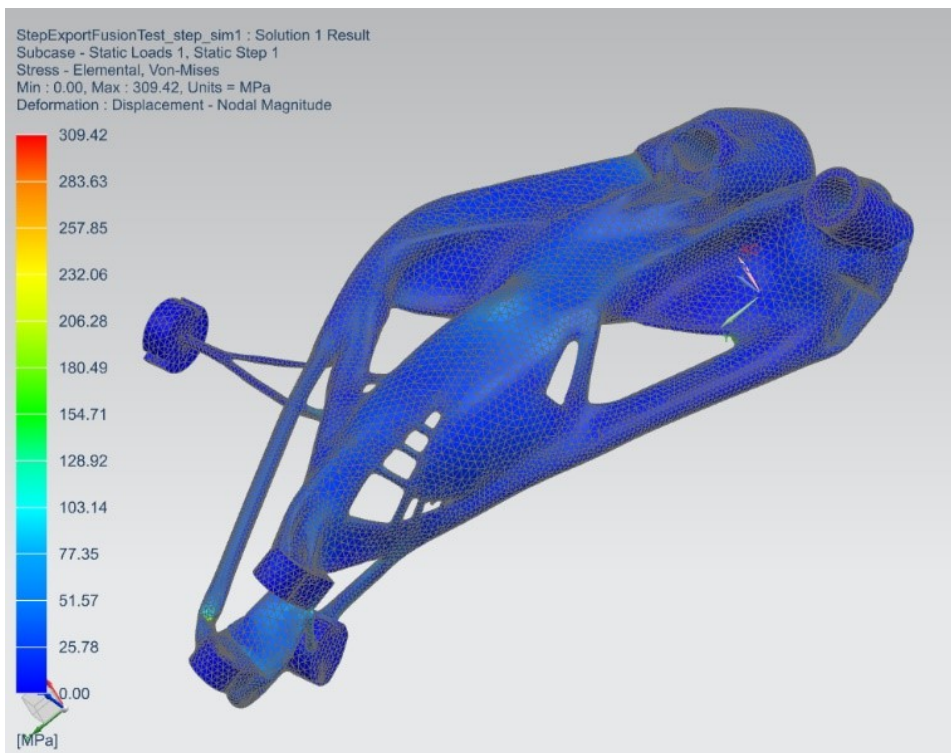

Figure C.4: Direct to solid from Fusion 360 shown in Siemens NX.

C.3 Idealization and further FEM analysis in Siemens NX

The solid models exported directly from Fusion were taken into Siemens NX for further idealization, meshing and then FEA verification. The solid models contained some disjoint faces, resulting in idealization being necessary for efficiency later on. Some of the problems found here were that the model contained double faces in some locations. The stress result of a solid model taken through a FEM analysis is shown in Figure C.5. this was a fast setup simulation and it contains some tiny high stress regions, but as one can clearly see, most of the model's stress is well within the yield stress. This model would have to have been looked further into had it been utilized further in the project.

Figure C.5: FEM verification of direct to solid from Fusion 360 performed in NX.

Per Kristian Moe Garnes

Design and Optimization for Additive Manufacturing of Rear Footpeg Bracket

NTNU

Norwegian University of
Science and Technology